CHEMICAL REVIEWS

pubs.acs.org/CR Review

Self-Regulating Hydrogel Actuators

Published as part of Chemical Reviews special issue "Tough Gels".

Taehun Chung,[§] Jaewon Choi,[§] Takafumi Enomoto, Soyeon Park, Saehyun Kim, and Youn Soo Kim*

Cite This: https://doi.org/10.1021/acs.chemrev.5c00358 Read Online

ACCESS | Metrics & More | Article Recommendations

ABSTRACT: Self-regulating hydrogels represent the next generation in the development of soft materials with active, adaptive, autonomous, and intelligent behavior inspired by sophisticated biological systems. Nature provides exemplary demonstrations of such self-regulating behaviors, including muscle tissue's precise biochemical and mechanical feedback mechanisms, and coordinated cellular chemotaxis driven by dynamic biochemical signaling. Building upon these natural examples, self-regulating hydrogels are capable of spontaneously modulating their structural and functional states through integrated negative feedback loops. In this review, the key design principles and implementation strategies for self-regulating hydrogel actuators are comprehensively summarized. We first systematically classify self-regulating hydrogels into sustained regulation, involving continuous modulation cycles under constant stimuli and one-cycle regulation, characterized by transient transitions driven by specific chemical fuels. Thereafter, the underlying mechanisms, types of hydrogels used, fuels, oscillation periods, amplitudes, and potential applications are highlighted. Finally, current scientific challenges and future opportunities for enhancing the robustness, modularity, and practical applicability of self-regulating hydrogel actuators are discussed. This review aims to provide structured guidelines and inspire interdisciplinary research to further develop advanced hydrogel-based regulatory systems for applications such as soft robotics, autonomous sensors, responsive biomedical devices, and adaptive functional materials.

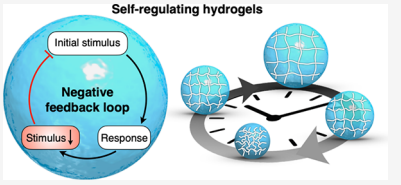

CONTENTS

1. INTRODUCTION

Self-regulation refers to the ability of living systems to autonomously sense, respond, and adapt to external stimuli, and it is a defining feature across all biological scales.[1,2] Self-regulating actuation, in particular, is ubiquitously observed in biological systems,[3−9] where organisms generate cyclic motion across a wide range of length scales in response to changing environmental conditions through tightly coupled feedback mechanisms.

Received: April 30, 2025
Revised: August 6, 2025
Accepted: August 22, 2025

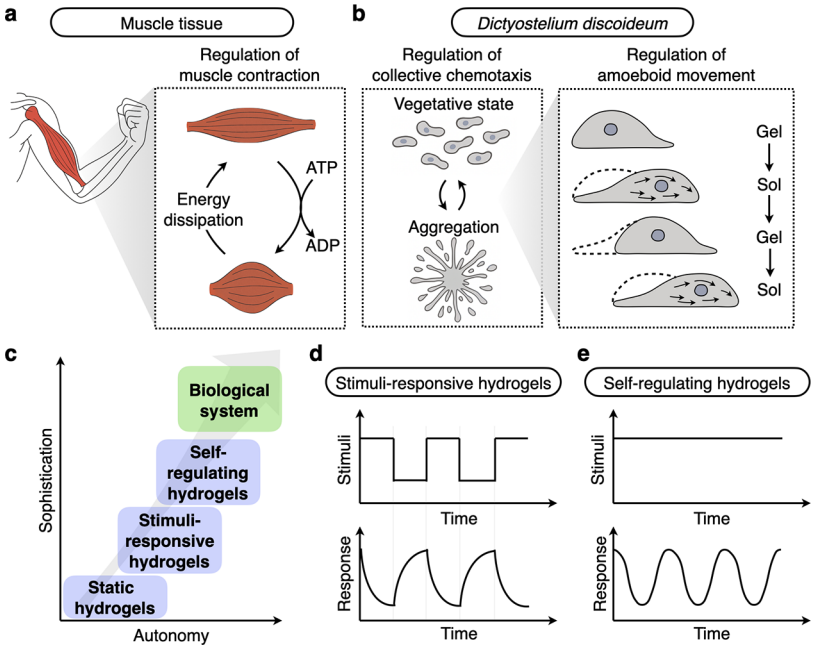

Figure 1. General description of the field. (a) Self-regulated actuation in muscle tissue, where ATP-driven contraction and relaxation are tightly controlled through biochemical feedback and energy dissipation. (b) Schematic representation of the self-regulated aggregation of *Dictyostelium discoideum* triggered by starvation-induced cyclic adenosine monophosphate (cAMP) signaling. Collective chemotaxis is achieved through gel−sol−gel transitions that underlie amoeboid movement. (c) Correlation from static hydrogels to complex biological systems in terms of autonomy and sophistication. (d) Schematic graph of stimuli-responsive hydrogel deformation according to external stimulus variation. (e) Schematic graph of self-regulating hydrogel deformation under a constant stimulus.

A representative example is muscle tissue (Figure 1a), which functions as a self-regulating actuator through tightly controlled biochemical and mechanical feedback loops.[10−12] Contraction is initiated by calcium ion signaling and regulated via the troponin−tropomyosin complex, enabling precise and reversible force generation. This process is sustained by ATP hydrolysis, during which ATP is converted to ADP with concomitant dissipation of the chemical energy. Feedback mechanisms modulating calcium dynamics allow for coordinated transitions between contraction and relaxation, thereby enabling rhythmic and adaptive muscular function. Other prominent examples are found in *Dictyostelium discoideum* (Figure 1b), which transitions from a vegetative state to aggregation through collective chemotaxis.[13−15] When nutrients are scarce, individual cells begin to move in a coordinated manner by sensing and secreting cyclic adenosine monophosphate (cAMP), creating a positive feedback loop that amplifies the signal. Importantly, this signaling is controlled by a delayed negative feedback mechanism, which temporarily reduces the cells' sensitivity to cAMP. This prevents continuous activation and allows the signal to pause periodically. Collective chemotaxis proceeds through amoeboid locomotion, which relies on sol−gel transitions driven by the dynamic interplay between actin polymerization and depolymerization. At the leading edge, monomeric G-actin assembles into filamentous F-actin, while disassembly at the rear facilitates cytoskeletal turnover.[16−18] Crucially, these polymerization−depolymerization dynamics are tightly regulated through biochemical and mechanical feedback mechanisms, enabling the system to autonomously adapt its cytoskeletal structure in response to environmental cues. These coordinated, self-regulated mechanical changes enable directional migration.

Inspired by such biological systems, researchers have pursued the development of artificial materials capable of mimicking self-regulated actuation. Among various platforms, hydrogels—cross-linked polymer networks swollen with water—are particularly advantageous owing to their intrinsic flexibility, enabling significant deformation.[19−21] Furthermore, their open system facilitates efficient transport and exchange of substances between the internal hydrogel matrix and the surrounding environment.[22−24] Due to these characteristics, hydrogels can effectively function as reaction media, facilitating chemical reactions by allowing species to diffuse into their internal matrix.[25,26] These reactions can drive water transport in and out, leading to structural deformation.[27] Moreover, if the cross-linked polymers within the gel spontaneously undergo dissociation or depolymerization, this can mimic the polymerization−depolymerization dynamics observed between actin monomeric subunits (G-actin) and filamentous actin (F-actin), driving sol−gel transitions reminiscent of the fundamental processes underlying various forms of cell motility.[28]

Among these, stimuli-responsive hydrogels are particularly notable for their ability to undergo significant and reversible changes in shape,[29−31] stiffness,[32] viscoelasticity[33] or turbidity[34] in response to external stimuli. However, stimuli-responsive systems require external stimuli or fuels for each transition. Specifically, these systems rely on one external input for deformation and another independent external input or on−off switching to revert to the original state. By embedding feedback mechanisms within their polymer network, hydrogels can overcome this limitation and achieve self-regulating transitions exhibiting swelling−shrinking behaviors, sol−gel phase transitions, assembly−disassembly processes, and transparent−opaque changes under constant stimulation. These hydrogels are termed "self-regulating hydrogels". Their ability

https://doi.org/10.1021/acs.chemrev.5c00358
Chem. Rev. XXXX, XXX, XXX−XXX

Table 1. Comparison Table between Stimuli-Responsive Hydrogels and Self-Regulating Hydrogels

Aspect	Stimuli-responsive hydrogels	Self-regulating hydrogels
Trigger for cyclic actuation	On−off switching of external stimuli	A single stimulus or constant environment
Operation condition	Simply exposed to external stimuli	Coexistence of activating factors (chemical or light fuels) and inhibiting factors (light/diffusion blocking, or chemical deactivators)
Feedback loop origin	None	Intrinsic (embedded within the hydrogel)
Thermodynamic state	Toward an equilibrium	Nonequilibrium
Autonomy	No (passive actuation)	Yes (autonomous actuation)
Intelligence	Low	High (memory, programmability, decision-making)
Energy efficiency	Low (requires alternating stimuli for sustained motion)	High (utilizes internal feedback loops for autonomous actuation under constant input)
Applications	Externally controlled actuators, drug delivery, sensors	Autonomous actuators, power generation, transient information storage

to spontaneously transduce chemical fuels into mechanical output aligns closely with the core principles of biological self-regulation. Recent advances in materials chemistry and dynamic network design have advanced these systems toward increasingly complex and adaptive behaviors.

The evolution from static hydrogels to self-regulating hydrogels and ultimately to biological systems represents an increasing gradient of autonomy and sophistication (Figure 1c). Here, autonomy refers to the hydrogel's capability to undergo actuation independently without continuous external stimulus control, while sophistication denotes the complexity of internal structural design and the number of integrated feedback mechanisms. Static hydrogels maintain equilibrium states defined by the balance between osmotic pressure and elastic pressure within the gel network.[22,35−37] In contrast, stimuli-responsive hydrogels seek new equilibrium states in response to external chemical (e.g., pH,[38−41] ionic strength[42,43]), physical (e.g., temperature,[44−46] light,[47,48] magnetic field,[49] electric field[50]), or biological (e.g., enzyme,[51,52] DNA[53,54]) stimuli. Their operating conditions are simply exposed to the aforementioned stimuli. During this process, mechanical deformation or morphological transitions—collectively termed "actuation"—occur (Figure 1d).[55−57] However, once altered, the hydrogel maintains its changed state and ultimately reaches equilibrium as long as the external stimulus remains constant, highlighting the absence of intrinsic intelligence. Consequently, to achieve oscillatory actuation characterized by repetitive deformation and recovery cycles, external stimuli must be periodically switched on and off. From the perspective of energy efficiency, this approach is considered low due to the continuous requirement for alternating stimuli to sustain motion. By contrast, self-regulating hydrogels embed internal feedback loops within their polymer network,[58−63] enabling them to autonomously exhibit deformation and recovery in response to a single or constant stimulus (Figure 1e).[57,64,65] This intrinsic integration of feedback loops provides self-regulating hydrogels with physical intelligence (including memory, programmability, decision-making capabilities),[66,67] inherently maintaining a nonequilibrium state without additional external stimuli. Consequently, they exhibit high energy efficiency as they utilize internal feedback loops for autonomous actuation under constant input, enabling long-term and repeatable operation without the need for repeated external interventions. These distinguishing aspects between stimuli-responsive hydrogels and self-regulating hydrogels are systematically summarized in Table 1. Thus, the intrinsic capability of self-regulating hydrogels to autonomously modulate their structure bridges the gap between engineered materials and biological systems, offering significant potential for applications requiring autonomous adaptive behaviors without continuous external intervention. While traditional stimuli-responsive hydrogels have been widely explored as externally controlled actuators, drug delivery systems, and sensors, self-regulating hydrogels provide advanced functionalities, such as autonomous actuators for soft robotics, self-sustaining power generation, and transient information storage. These unique capabilities position self-regulating hydrogels as promising next-generation intelligent materials with broad applicability in diverse fields.

This review explores the fundamental principles, synthetic strategies, and emerging applications of self-regulating hydrogel actuators. We first discuss the underlying mechanisms governing these actuators followed by an in-depth examination of their material properties, feedback mechanisms, and regulatory capabilities. Subsequently, we review recent advances, address current limitations, and identify key challenges in the achievement of self-regulating motion. Finally, we highlight future perspectives and opportunities to advance self-regulating hydrogels toward practical applications in adaptive functional materials and soft robotics.

2. DESIGN PRINCIPLES OF SELF-REGULATING HYDROGEL ACTUATORS

Feedback loops play a crucial role in regulating dynamic systems by influencing the system's response based on its own output. Positive feedback loops amplify the effects of an initial stimulus, reinforcing and escalating the response (Figure 2a).[68,69] This self-reinforcing mechanism is commonly

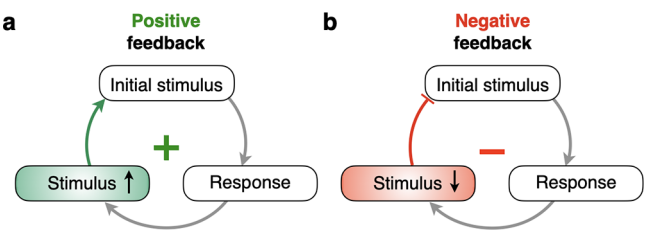

Figure 2. Schematics of (a) positive and (b) negative feedback.

observed in biological and chemical systems, such as autocatalytic reactions, where product accumulation enhances their own formation.

In contrast, negative feedback loops function as stabilizing mechanisms by reducing stimulus effects, thereby preventing excessive fluctuations and thereby maintaining system stability (Figure 2b).[70,71] Crucially, negative feedback mechanisms are

https://doi.org/10.1021/acs.chemrev.5c00358
Chem. Rev. XXXX, XXX, XXX−XXX

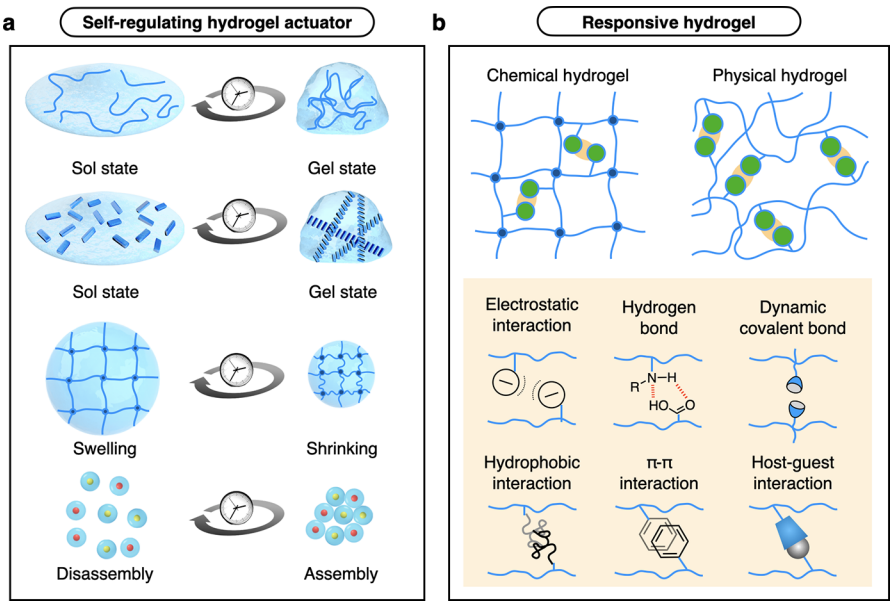

Figure 3. Various actuations of self-regulating hydrogel and dynamic interactions in responsive hydrogels. (a) Self-regulating hydrogel actuators undergo behaviors such as sol−gel transitions, swelling−shrinking, and disassembly−assembly processes. (b) Responsive hydrogels are categorized into chemical and physical types, constructed via various dynamic interactions in molecular-scale, including electrostatic interaction, hydrogen bond, dynamic covalent bond, hydrophobic interactions, $\pi-\pi$ interaction, and host−guest interaction.

central to sustaining nonequilibrium (or out-of-equilibrium) dynamics, as they enable continuous correction and adaptive modulation away from thermodynamic equilibrium or steady states. Classical thermodynamics dictates that all systems inherently progress toward equilibrium states of maximum entropy or minimum free energy.[72,73] Therefore, the realization of sustained nonequilibrium states remains fundamentally difficult, demanding mechanisms capable of actively countering these intrinsic thermodynamic tendencies.

Biological systems sustain adaptive dynamic behaviors through intricate feedback pathways that continuously modulate internal states in response to external stimuli. To replicate such self-regulating behaviors in synthetic materials, carefully engineered negative feedback mechanisms are essential. These mechanisms drive continuous internal structural changes, enabling artificial actuators to robustly maintain nonequilibrium conditions.[56,74]

Self-regulating hydrogel actuators exhibit changes across molecular, mesoscopic, and macroscopic scales, which are observed as sol−gel transitions, swelling−shrinking of hydrogels, and disassembly assembly of microgels (Figure 3a). To implement such self-regulating hydrogel actuators, responsive hydrogels are first required. As shown in Figure 3b, responsive hydrogels are categorized into chemical hydrogels, which form covalently cross-linked polymer networks, and physical hydrogels, which form networks through noncovalent interactions.[75,76] The dynamic interactions in chemical or physical hydrogels include electrostatic interactions,[77−79] hydrogen bonding,[80,81] hydrophobic interactions,[44,45,82] dynamic covalent bonds,[83−86] $\pi-\pi$ interactions,[87,88] and host−guest interactions,[89,90] enabling the reversible association and dissociation of dynamic interactions between polymers. Association−dissociation here denotes the repeated formation and rupture of those reversible interactions; depending on the system, such microscopic cycles may manifest macroscopically as reversible sol−gel transitions and volume changes. These interactions are modulated by stimuli, enabling structural changes in the hydrogels. For instance, enzyme-mediated pH changes can modulate electrostatic interactions,[77,78] and thermoresponsive hydrogels exhibit shrinkage driven by enhanced hydrophobic interactions.[44,45,82] Furthermore, peptide-based systems form reversible networks through hydrogen bonding and $\pi-\pi$ interactions.[91] Selecting specific dynamic interactions in self-regulating hydrogels can influences factors such as reversibility, mechanical strength, and responsiveness.[92,93] Moreover, accurately describing the kinetics of self-regulation demands consideration beyond dynamic interactions alone. Polymer diffusion and substrate transport in and out of the hydrogel networks often significantly influence the overall response rate.[94−96] Therefore, when self-regulating hydrogel actuators are designed, it is essential to carefully coordinate the molecular-scale dynamic interactions with the macroscopic diffusion and mass transport processes, taking into account the intended function and underlying reaction mechanisms of the system.

Building upon these regulatory principles, self-regulating hydrogel actuators integrate responsive polymer networks with negative feedback loops to achieve autonomous actuation. Depending on the type of negative feedback loop, self-regulating hydrogel actuators exhibit sustained or one-cycle regulation determined by the interplay of spatiotemporal dynamics, reaction sequences, and reaction kinetics (Figure 4). In sustained regulation, the dissociation−association cycles of dynamic interactions between polymers are continuously driven by fuel under constant environmental conditions (Figure 4a). This sustained regulation can be achieved through mechanical and optical feedback loops or oscillatory chemical reactions. Mechanical/optical feedback loops operate by inducing shape deformation of the hydrogels upon fuel injection (or exposure to stimuli such as light or chemicals), moving the system away from the stimulus, followed by shape recovery, subsequently reexposing the system to the initial fuel. This leads to cyclic dissociation−association transitions of dynamic interactions between polymers. Oscillatory chemical

https://doi.org/10.1021/acs.chemrev.5c00358
Chem. Rev. XXXX, XXX, XXX−XXX

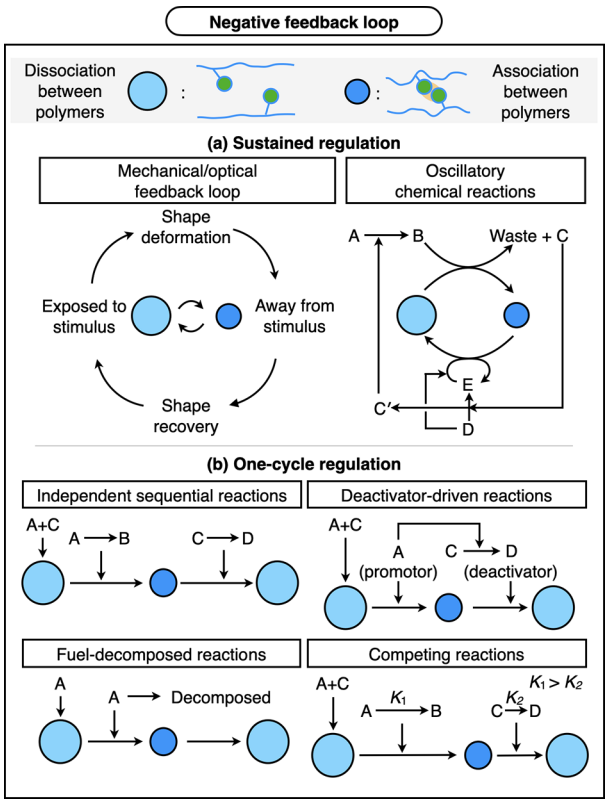

Figure 4. Negative feedback loops are implemented through two strategies. (a) Sustained regulation, such as mechanically or optically induced deformation and recovery cycles, and oscillatory chemical reactions. (b) One-cycle regulation, driven by independent sequential reactions, deactivator-driven reactions, fuel-decomposed reactions, and competing reactions. In the schematic, light blue filled circles represent dissociated states of dynamic interactions between polymers (e.g., sol, swollen, or disassembled states), whereas dark blue filled circles indicate associated states of dynamic interactions between polymers (e.g., gel, shrunken, or assembled microgel states). For the one-cycle regulation cases, "A" and "C" represent the fuels, while "B" and "D" correspond to the waste products generated during the reactions.

reactions involve chemical reaction networks composed of various chemical species, which periodically alter the pH or redox states of transition metal complexes to repeatedly regulate the dissociation−association of dynamic interactions between polymers.

In contrast, one-cycle regulation is characterized by a transient association state of dynamic interactions between polymers induced by an initial fuel, after which the system spontaneously reverts to its original dissociation state under constant conditions (Figure 4b). This regulation can be classified into four categories: Independent sequential reactions involve two separate reactions independently controlling the dissociation and association of dynamic interactions between polymers. Deactivator-driven reactions feature a promoter initially inducing an association state from a dissociation state with the subsequent production of a deactivator within the system returning it to its original state. Fuel-decomposed reactions utilize a transient association state created by fuel that upon decomposition of the fuel itself reverts to the initial dissociation state. Lastly, competing reactions comprise two reaction pathways with distinct kinetics, where the rapid first reaction induces association from dissociation, followed by a slower competing reaction, restoring the original dissociation state.

3. CLASSIFICATION OF SELF-REGULATING HYDROGEL ACTUATORS

Self-regulating hydrogel actuators can be classified along four components—fuel source, driving mechanism, change of transducer, and regulation mode—as summarized in Figure 5. It systematically describes, for each entry: (i) the type of fuel that initiates the regulation, accompanied by an illustrative schematic representing representative actuation; (ii) the driving mechanism that integrates the response to the fuel into a negative feedback loop; (iii) the principal transducer of dynamic interactions between polymers in the hydrogel; and (iv) a regulation mode depicting representative time-dependent responses during self-regulation. Thus, it presents a concise landscape enabling effective comparisons across diverse self-regulating hydrogel actuators.

4. SUSTAINED REGULATION

4.1. Design Criteria for Sustained Regulation

Sustained regulation in self-regulating hydrogel actuators can be categorized according to the origin of their negative feedback loops. In mechanical/optical feedback loops, deformation of the hydrogel causes deviations in the surrounding stimulus field (e.g., light intensity, temperature gradients, reagent diffusion, or proton flux), and these changes subsequently feed back into the hydrogel, completing a mechanically or optically mediated negative feedback loop. In contrast, sustained regulation driven by chemical oscillatory reactions (e.g., pH oscillators or Belousov−Zhabotinsky (BZ) reactions) relies on periodically modulated internal chemical variables, such as proton concentration or redox state, independent of hydrogel deformation. Each mode is governed by its own specific design criteria and inherent limitations. Mechanical/optical feedback loops critically depend on three essential factors to establish sustained out-of-equilibrium dynamics. First, the rapid responsiveness of hydrogels to external stimuli is imperative to continuously drive the system away from equilibrium. Second, the shape and geometry of the hydrogels significantly influence the establishment and maintenance of mechanical feedback loops. Lastly, precise spatial alignment between the hydrogel actuator and the stimulus field is essential for establishing and maintaining mechanical/optical regulation. Consequently, the amplitude and frequency of these regulation cycles are inherently limited, because their feedback loops depend on this fixed external setup. Nonetheless, once the regulation cycle has been initiated, the reaction kinetics and overall stability can still be modulated, within the bounds set by the predefined alignment, by tailoring the hydrogel's chemical composition and network architecture. In contrast, chemical oscillatory reactions, including pH oscillators[97−103] and the BZ reactions,[104,105] circumvent these constraints by exploiting external or internal chemical reaction networks. In pH oscillator systems, externally driven chemical oscillations are synchronized with hydrogel actuation, enabling sustained regulation. Similarly, BZ reaction-driven systems allow the hydrogel to absorb external chemical fuel and generate self-oscillations within the matrix, achieving sustained regulation. Unlike mechanical feedback loops, chemical oscillatory systems do not require rapid responsiveness, specialized hydrogel geometry, or precise

https://doi.org/10.1021/acs.chemrev.5c00358
Chem. Rev. XXXX, XXX, XXX−XXX

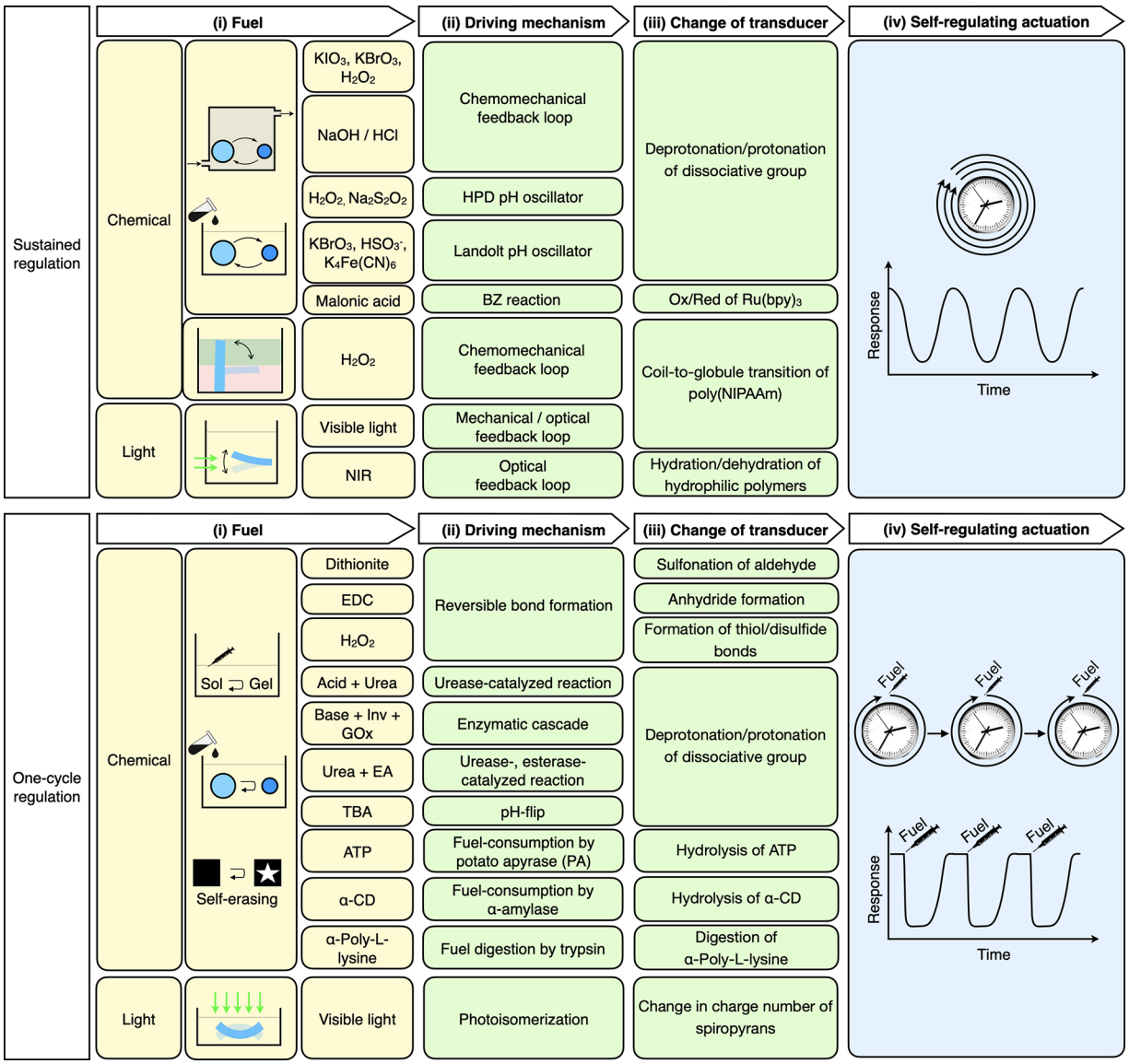

Figure 5. Classification of self-regulating hydrogel actuators. We systematically categorized the components according to fuel type, driving mechanism, change of transducer, and mode of self-regulating actuation.

spatial arrangements because the intrinsic chemical reaction network inherently sustains the system out of equilibrium. Therefore, the primary focus shifts to the design of intricate chemical reaction networks capable of sustaining robust oscillatory dynamics. However, chemical oscillatory systems present their own significant limitations. Constructing such reaction networks is inherently complex and challenging due to intricate interactions among multiple chemical species. Additionally, instead of requiring rapid response to external stimuli, these systems inherently rely on chemical reactions that typically exhibit slow intrinsic kinetics. This intrinsic slowness is further compounded by limited diffusion within the polymer network and hindered mass transport of the reactants and products. Nevertheless, these systems offer significant advantages in terms of tunability, as both the amplitude and frequency of oscillations can be effectively controlled by adjusting parameters, such as reactant concentrations and reaction conditions. Moreover, the efficiency and stability of chemically driven oscillations can be further tuned by engineering the hydrogel's porosity and microstructure, which modulate diffusion lengths, controlling both oscillation amplitude and frequency.

4.2. Mechanical Feedback Loop

A mechanical feedback loop is a closed-loop operating cycle in which spatiotemporal shape changes of hydrogels are induced by environmental inputs, such as chemical reactions, light, and heat. As illustrated in Figure 6a, it can be categorized into three representative principles depending on the mechanisms. One common approach involves placing a hydrogel actuator across liquid bilayers, each inducing opposite swelling behaviors, where time-dependent bending causes the gel to continuously switch between bilayers, resulting in periodic spatiotemporal shape changes (Figure 6a(i)).[106,107] Another strategy employs a self-shadowing effect wherein constant illumination induces localized photothermal contraction, causing the hydrogel to bend and block the incoming light. As a result, the hydrogel cools and returns to its original shape, repeatedly establishing sustained spatiotemporal feedback loop (Figure 6a(ii)).[108−114] A more sophisticated system involves a continuously stirred tank reactor (CSTR), into which chemical reactants are

https://doi.org/10.1021/acs.chemrev.5c00358
Chem. Rev. XXXX, XXX, XXX−XXX

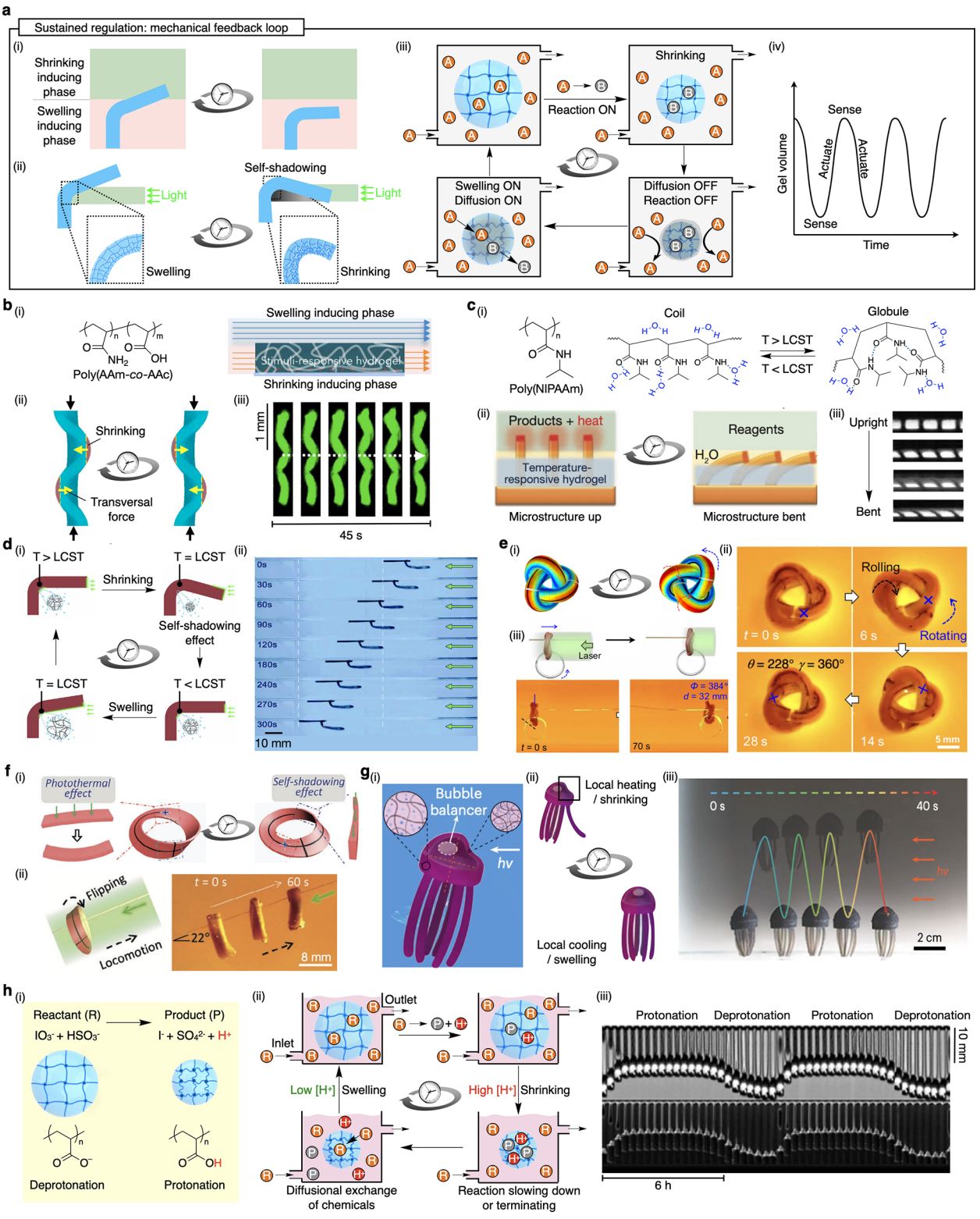

Figure 6. Self-regulating hydrogels with sustained regulation driven by mechanical feedback loop. (a) (i) Schematics of a chemomechanical feedback loop using a two-phase reactor. One phase induces shrinkage of the gel, while the other phase induces swelling of the gel. (ii) Schematics of a mechanical feedback loop using the self-shadowing effect. The gel shrinks upon light exposure and swells again when the shrunken state blocks the light. (iii) Schematics of a chemomechanical feedback loop using a continuous stirred tank reactor (CSTR). A chemical reaction induces gel shrinkage, which in turn modulates reagent diffusion and triggers reswelling, forming a self-sustained oscillation. (iv) Schematic graph showing time-dependent sustained volume changes of a self-regulating hydrogel driven by a mechanical feedback loop. (b) (i) Chemical structure of the poly(AAm-*co*-AAc) hydrogel and schematic of its spatial placement in a two-phase laminar flow system. (ii) Schematics of a mechanical feedback loop based on dynamic buckling. Local swelling and shrinking generate transversal forces that drive snap-through between bistable buckled states, forming a self-regulating cycle. (iii) Time-lapse fluorescence images showing periodic swaying motion of the hydrogel strip under continuous dual-stimuli flow. (c) (i) Chemical structure of poly(NIPAAm) and schematics of its coil-to-globule transition across the lower critical solution

https://doi.org/10.1021/acs.chemrev.5c00358
Chem. Rev. XXXX, XXX, XXX−XXX

Figure 6. continued

temperature (LCST). (ii) Schematics and time-lapse images of a chemomechanical system integrating a poly(NIPAAm) hydrogel with catalyst-tipped microstructures. (iii) Captured confocal fluorescence images showing microfin configurations during actuation in a bilayer liquid system. The white-colored bottom layer is deionized water labeled with Rhodamine B, while the top layer contains nonfluorescent reagents. (d) (i) Schematics of a light-fueled mechanical feedback loop in a poly(NIPAAm)−AuNPs hydrogel oscillator. (ii) Time-lapse images showing periodic oscillatory bending of a fishhook-shaped hydrogel under constant light illumination. (e) (i) Schematics of a topologically constrained trefoil hydrogel knotbot undergoing light-fueled deformation. (ii) Experimental demonstration of directional rolling under localized laser irradiation. (iii) Time-lapse images of the trefoil knotbot under uniform illumination. (f) (i) Schematics of a twisted hydrogel ribbon undergoing self-sustained deformation under static light. (ii) Time-lapse images showing flipping locomotion of the twisted hydrogel ring on a stretched string under constant illumination. (g) (i) Schematics of a self-regulating phototactic hydrogel vehicle. Design of the jellyfish-inspired hydrogel robot was composed of poly(NIPAAm) hydrogel embedded with AuNPs and reduced graphene oxide (r-GO). The central air-filled bubble balancer shifts under asymmetric heating. (ii) Schematic cycle of buoyancy- and deformation-mediated feedback loop driving vertical oscillation under constant light illumination. (iii) Time-lapse images of the robot's repeated jumping toward the light under solar simulator illumination. (h) (i) Reaction scheme of the pH-switch oscillator. (ii) Schematics of a chemomechanical feedback loop coupling hydrogel deformation and proton concentration. (iii) Time-lapse images of a cylindrical hydrogel actuator composed of poly(NIPAAm-*co*-AAc), suspended in a continuously stirred solution. Light background: shadowscopic image; dark background: directly photographed image. Reaction conditions: KIO_3 0.06 M, Na_2SO_3 0.18 M, H_2SO_4 0.05 M; flow rate: 240 mL/h. Panel (b) is reproduced with permission from ref 106. Copyright 2021 Elsevier. Panel (c) is reproduced with permission from ref 107. Copyright 2012 Springer Nature. Panel (d) is reproduced with permission from ref 108. Copyright 2019 American Association for the Advancement of Science. Panel (e) is reproduced with permission from ref 109. Copyright 2024 licensed under CC 4.0 Springer Nature. Panel (f) is reproduced with permission from ref 110. Copyright 2024 John Wiley and Sons. Panel (g) is reproduced with permission from ref 111. Copyright 2023 Springer Nature. Panel (h) is reproduced with permission from ref 118. Copyright 2015 John Wiley and Sons.

continuously fed.[115,116] The hydrogel positioned within this reactor undergoes contraction driven by reaction products, regulating the inward and outward diffusion of reactants and products, thereby generating chemomechanical shape changes (Figure 6a(iii)).[117−122] Finally, such mechanisms lead to sustained regulation by changing the volume over time, as depicted in the schematic graph (Figure 6a(iv)).

Hua et al. developed a chemomechanical self-regulating system in which a pH-responsive hydrogel strip undergoes dynamic buckling transitions between bistable configurations under spatially distinct chemical stimuli (Figure 6b).[106] Unlike conventional self-oscillators that rely on chemical reactions or externally applied cyclic inputs, this system integrates a built-in mechanical feedback loop that allows the material to autonomously regulate its own motion through rapid and repeated snap-through between two stable states.[123−131] The hydrogel, composed of poly(acrylamide-*co*-acrylic acid) (poly(AAm-*co*-AAc)), is anchored to a rigid substrate within a liquid bilayer (Figure 6b(i)). The liquid bilayer, crucial for maintaining spatially distinct chemical environments, was established by injecting two chemically distinct fluids into a microfluidic channel under carefully controlled laminar flow conditions.[132,133] The laminar flow effectively prevents vertical mixing, preserving a stable chemical gradient essential for sustained oscillation. Poly(acrylic acid) (poly(AAc)) hydrogels are representative pH-responsive materials whose swelling behavior is governed by the ionization state of their carboxylic acid groups.[134−136] Under alkaline conditions (pH > pK_a), deprotonation induces electrostatic repulsion, causing swelling. Conversely, acidic conditions (pH < pK_a) lead to protonation, reducing electrostatic repulsion, enhancing hydrogen bonding, and resulting in shrinking. When exposed to a vertically asymmetric chemical environments—alkaline solution (NaOH, pH 13) above (swelling) and acidic solution (HCl, pH 2) below (shrinking)—the gel experiences differential swelling across its thickness, causing it to buckle. Buckling shifts portions of the gel into the shrinking region, building transversal force until it triggers a rapid snap-through to the complementary buckled state. This rapid bistable transition restores the initial chemical asymmetry, initiating another cycle and thereby sustaining continuous oscillations (Figure 6b(ii)). Each oscillation cycle completes approximately every 30−45 s with a maximum bending angle reaching ∼52° under optimal conditions (Figure 6b(iii)).

Thermal stimuli can also be exploited to achieve sustained regulation. One representative class of thermoresponsive hydrogels is poly(*N*-isopropylacrylamide) (poly(NIPAAm)), which exhibits a well-defined lower critical solution temperature (LCST) around 32 °C (Figure 6c(i)).[137−142] Below the LCST, poly(NIPAAm) chains adopt an extended coil conformation due to favorable hydrogen bonding with water, leading to hydrogel swelling. Above the LCST, hydrophobic interactions dominate, causing the polymer network to collapse into a globular state and shrink. Leveraging this reversible thermal responsiveness, He et al. developed a self-regulating chemomechanical system termed the self-regulated mechano-chemical adaptively reconfigurable tunable system (SMARTS) (Figure 6c).[107] In this design, catalyst-functionalized microstructures are embedded within a poly(NIPAAm) hydrogel and placed within a laminar flow liquid bilayer composed of an aqueous layer and an organic reagent layer containing hydrogen peroxide (H_2O_2). The platinum-catalyzed decomposition of H_2O_2 rapidly generates localized heat, raising the temperature above the LCST and inducing an immediate hydrogel shrinkage. Due to this rapid thermomechanical response, the microstructures promptly retract from the reagent layer, halting the reaction and allowing the system to cool. Upon cooling below the LCST, the hydrogel swells again, rapidly reimmersing the catalyst into the reagent and reactivating the cycle (Figure 6c(ii)). This closed chemomechanical feedback loop results in self-sustained regulation of both microstructure position and hydrogel volume. Notably, each regulation cycle occurs approximately every 4.2 min, with the vertical coordinate of the microstructure oscillating between ∼14 and ∼10 μm under bilayer liquid conditions (Figure 6c(iii)). This system demonstrates the potential of integrating thermoresponsive hydrogels with localized catalysis to achieve homeostatic regulation without external control.[133]

Another strategy for achieving self-regulated actuation involves light-triggered mechanical feedback loops, where hydrogel deformation dynamically modulates its light absorption. The photothermal effect refers to the conversion

https://doi.org/10.1021/acs.chemrev.5c00358
Chem. Rev. XXXX, XXX, XXX−XXX

of absorbed light energy into heat, enabling local temperature elevation upon illumination.[143] Poly(NIPAAm) hydrogels incorporating photothermal agents such as gold nanoparticles (AuNPs)[55,144] and reduced graphene oxides (r-GOs)[145] have demonstrated self-sustained oscillatory behavior under constant illumination. AuNPs generate heat mainly via localized surface plasmon resonance (LSPR), whereas r-GOs achieve photothermal conversion through nonradiative electron relaxation within their $\pi-\pi$ conjugated structures.

Zhao et al. exemplified this principle by embedding AuNPs into a poly(NIPAAm) hydrogel to create a self-regulating actuator (Figure 6d).[108] The hydrogel pillar was vertically mounted on a substrate in an aqueous medium and exposed horizontally to continuous visible light from one side, enabling precise spatial alignment between the hydrogel actuator and illumination source. Under continuous visible light, localized photothermal heating raised the temperature above the LCST, causing the hydrogel to bend toward the light source. The resulting self-shadowing effect blocked illumination at the photothermal site, causing the system to cool below the LCST and recover its original shape, restarting the bending cycle (Figure 6d(i)). This cyclic deformation constitutes a negative feedback loop, resulting in regulated motion with a period of approximately 0.7 to 2.0 s and a tip displacement amplitude ranging from approximately 0.3 to 2.8 mm. Leveraging this mechanism, they developed an OsciBot, a self-sustained swimmer that achieved a locomotion speed of 1.2 mm/s in aqueous media under visible light (Figure 6d(ii)). These findings highlight how dynamic shape modulation through photothermal−mechanical feedback enables self-regulating motion without the need for internal chemical oscillators.

To achieve more complex self-regulating motion beyond simple bending, Li et al. engineered topological knotbots capable of rolling and rotational actuation based on the same photothermal−mechanical feedback principles (Figure 6e).[109] These hydrogel actuators were composed of a poly(NIPAAm) matrix embedded with AuNPs for photothermal conversion and concentrically aligned fluorohectorite nanosheets (FNSs) to induce anisotropic deformation.[45,108,146,147] Upon light exposure, the prestrained topology of the trefoil structure enabled shrinkage-induced coupled rolling and braid rotation (Figure 6e(i)).[148] Crucially, knot crossings created localized self-shadowing effects that modulated the local heating, forming a mechanical feedback loop to sustain cyclic motion. Under constant illumination, the knotbot achieved a 360° rolling and 228° braid rotation within 28 s, while traversing 32 mm over 70 s (Figure 6e(ii)). This topological approach enabled not only self-regulating motility but also advanced functions, including the transportation of a trefoil knotbot along a horizontal string and the rotation of an interlocked ring under uniform light irradiation (Figure 6e(iii)).

Expanding on topological actuation, Zhu et al. developed twisted hydrogel rings—Möbius strips and Seifert ribbons—using poly(NIPAAm) embedded with AuNPs and homogeneously aligned nanosheets (NSs) (Figure 6f).[110] Under uniform illumination, photothermal heating induced bending, while self-shadowing at the twisted junctions enabled localized cooling and swelling, forming a mechanical feedback loop (Figure 6f(i)). This sustained flipping locomotion occurred autonomously without external temporal modulation, exhibiting a periodic cycle of approximately 25−30 s, with flipping amplitudes reaching up to 360° per cycle. Such flipping enabled effective locomotion along suspended wires and inclines of up to 22°, maintaining a steady motion speed of 0.68 mm/s under visible light (Figure 6f(ii)).

To achieve self-regulating phototaxis without programmed control, Hou et al. developed a phototactic vehicle (PTV) based on a poly(NIPAAm) hydrogel embedded with AuNPs and reduced graphene oxides (r-GOs) (Figure 6g).[111] The hydrogel was fabricated into a jellyfish-inspired structure consisting of a hemispherical bell and vertically arranged tentacles, designed to maximize structural asymmetry and facilitate efficient directional deformation. This configuration was strategically chosen to leverage mechanical instability and buoyancy control for effective phototactic motion (Figure 6g(i)). Upon illumination, localized heating induced asymmetric shrinking of the hydrogel and shifted the position of an internal air bubble, creating torque that guided the robot toward the light.[143] Initially, this generated upward motion driven by a convective flow and density gradients. However, as the vehicle ascended, rapid convective cooling from ambient water caused the hydrogel to reswell, restoring the bubble to its original position and reversing the density asymmetry, subsequently resulting in downward motion (Figure 6g(ii)). This repeated cycle of upward propulsion and downward recovery manifested as a vertical hopping motion with a typical period of approximately 20 s and vertical displacement amplitudes ranging from 20 to 40 mm. This self-regulating negative feedback loop enabled the PTV to adaptively correct its trajectory. The system demonstrated phototactic motion toward a solar simulator (Figure 6g(iii)). Additionally, under both solar simulator and laser illumination, speeds reached up to 18 mm/s (approximately 1.5 body lengths per second).

Horváth demonstrated a self-regulating hydrogel actuator in which chemical reactions interact with mechanical deformation in the gel to autonomously regulate motion (Figure 6h).[118] The poly(AAc)-based hydrogel autonomously regulates its shape via a pH-switching reaction when iodate and bisulfite fuels are continuously fed into a CSTR. The reactants iodate and bisulfite are converted over time to I^-, SO_4^{2-}, and protons via chemical reactions (Figure 6h(i)). Among these products, the generated protons cause a sudden drop in pH, leading to hydrogel shrinking. This deformation reduces the gel's volume and consequently shortens the diffusion path length, limiting further influx of reactants. As a result, the reaction slows and ultimately terminates in the gel. Meanwhile, continuous reactant supply in the CSTR gradually lowers the proton concentration inside the gel through diffusional exchange, enabling the gel to slowly reswell and reactivate the regulation cycle. This chemomechanical feedback loop enables self-regulating swelling−shrinking oscillations without external stimuli or a core chemical oscillator (Figure 6h(ii)). Each full oscillation cycle occurs over approximately 6 h with an amplitude of about 6 mm, and the system maintains rhythmic behavior for over a week, capable of lifting loads ten times its own mass (Figure 6h(iii)). Horváth also extended this concept by developing a chemomechanical oscillator driven by a nonredox, nonoscillatory methylene glycol-sulfite (MGS) reaction coupled with a pH-responsive hydrogel.[121] These findings highlight how reaction−diffusion coupling can be harnessed to realize self-regulating hydrogel actuators for sustained autonomous motion.

4.3. Optical Feedback Loop

Similar to the mechanical feedback loop discussed previously, optical feedback loops enable the sustained regulation of

https://doi.org/10.1021/acs.chemrev.5c00358
Chem. Rev. XXXX, XXX, XXX−XXX

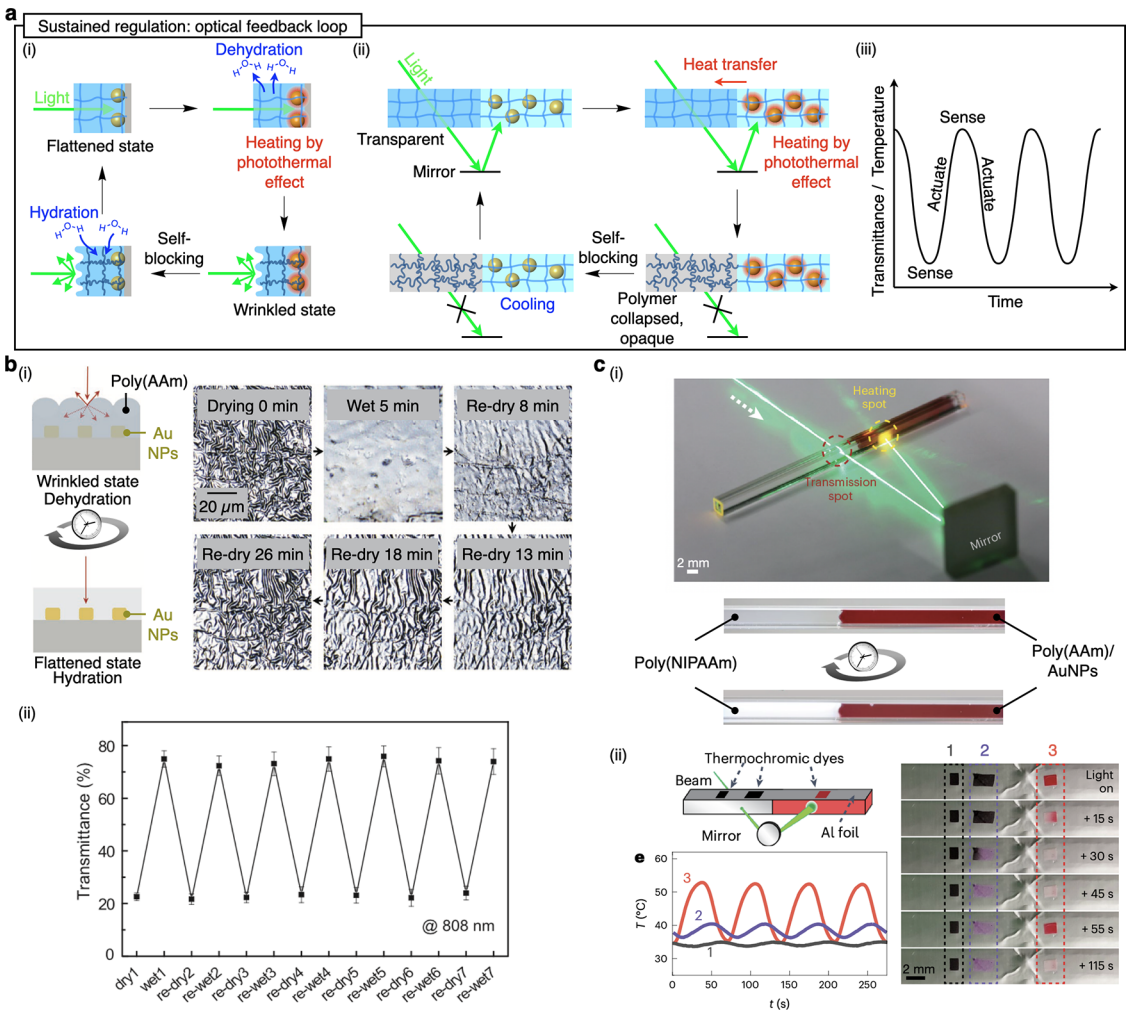

Figure 7. Self-regulating hydrogels with sustained regulation driven by optical feedback loops. (a) (i) Schematics of a morphology-mediated optical feedback loop, where moisture-induced swelling of hydrogel surfaces enhances optical transparency, enabling photothermal heating in underlying plasmonic nanoparticle arrays under constant illumination. The resulting localized heating induces dehydration-driven surface wrinkling, increasing light scattering, and achieving self-blocking. Subsequent rehydration reversibly restores the flattened, transparent state, enabling sustained self-regulation. (ii) Schematics of a phase-transition-based optical feedback loop, where photothermal heating under constant illumination triggers a coil-to-globule transition of thermoresponsive polymers, inducing opacity and achieving self-blocking. Subsequent cooling reversibly restores the transparent polymer state, allowing sustained self-regulation. (iii) Graph showing time-dependent modulation of transmittance and temperature, demonstrating reversible and sustained optical control via internal feedback mechanisms. (b) (i) Schematic and optical images of a self-regulating hydrogel actuator consisting of wrinkle-patterned poly(AAm) hydrogel on a plasmonic AuNP substrate. (ii) Transmittance plot at 808 nm showing reversible modulation through repeated hydration−dehydration-induced morphological transitions. (c) (i) Optical configuration showing beam transmission and localized photothermal heating via reflection. Schematics of a poly(NIPAAm)-poly(AAm)/AuNPs coupled hydrogel using delayed thermal feedback, enabling cyclic transparency switching through internal regulation. (ii) Temperature profiles at designated positions, visualized by spatially resolved color changes—red/white blinking (3), stable pink (2), and stable black (1)—demonstrating sustained regulation under steady illumination. Panel (b) is reproduced with permission from ref 149. Copyright 2021 John Wiley and Sons. Panel (c) is reproduced with permission from ref 150. Copyright 2022 licensed under CC 4.0 Springer Nature.

hydrogel actuators by controlling light transmittance through photothermal effects. The optical feedback loop primarily utilizes the self-blocking phenomenon, implemented through surface wrinkling (Figure 7a(i))[149] or the coil-to-globule transition of thermoresponsive polymers (Figure 7a(ii)).[150] When the hydrogel surface becomes wrinkled or opaque, self-blocking of the light can halt the photothermal effect, subsequently returning the hydrogel to the initial flattened, transparent state by adapting it to the constant humidity or temperature environment. The rapid responsiveness of hydrogels induced by the photothermal effect is imperative to continuously drive the system away from equilibrium, and a meticulous spatial arrangement between the hydrogel and the light source is essential for optimizing optical feedback. Furthermore, the region responsible for generating the photothermal effect and the region responsible for the optical feedback are spatially separated. Therefore, optical feedback loops require a more precise structural design compared with mechanical feedback loops, where deformation itself directly serves as feedback. Due to this stringent requirement, only two representative examples have been reported to date, as illustrated in Figure 7b and 7c. Ultimately, these mechanisms achieve sustained regulation through periodic changes in transmittance or temperature, as depicted schematically (Figure 7a(iii)).

https://doi.org/10.1021/acs.chemrev.5c00358
Chem. Rev. XXXX, XXX, XXX−XXX

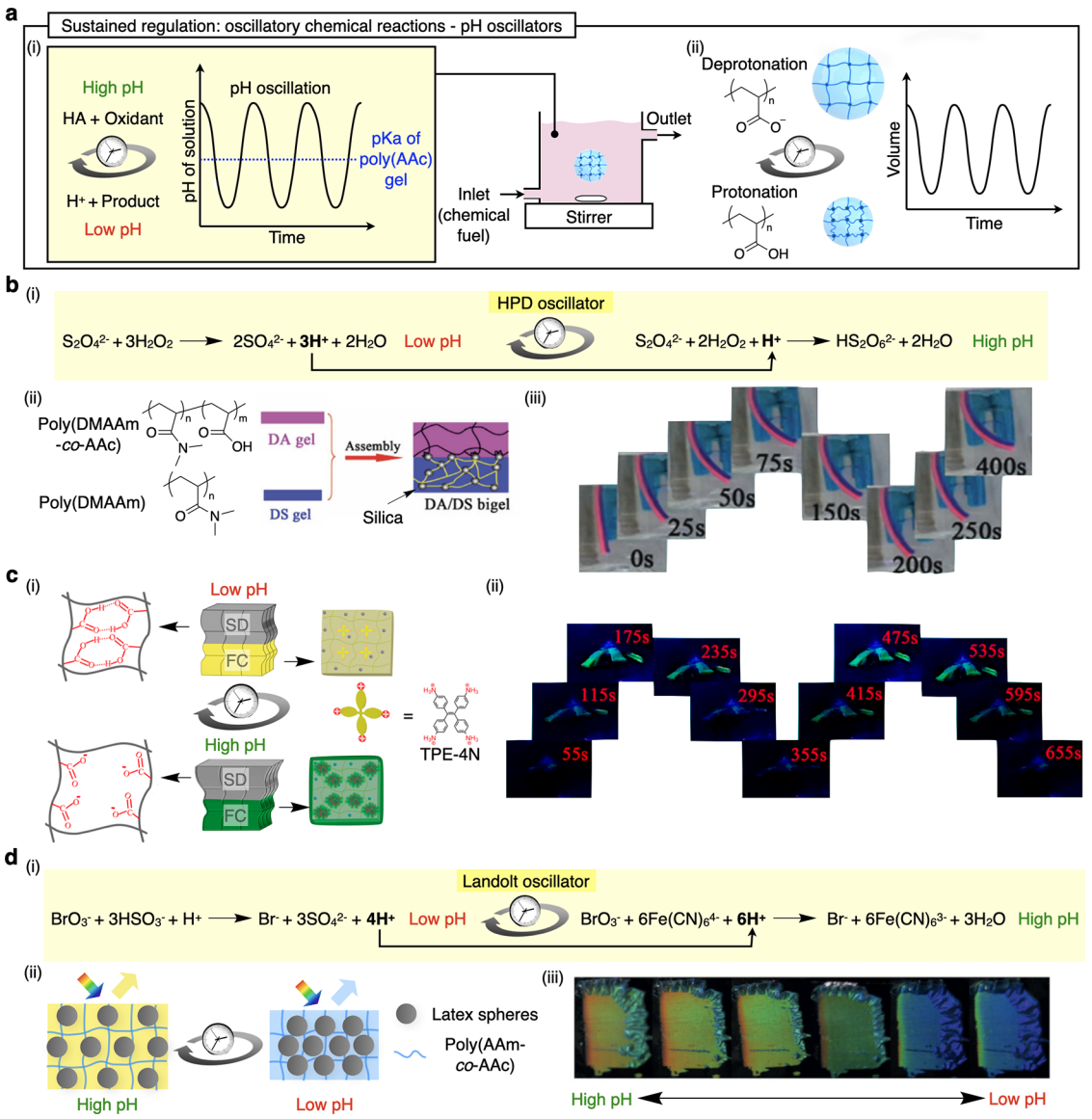

Figure 8. Self-regulating hydrogels with the oscillatory chemical reaction driven by pH oscillators. (a) (i) Schematics of a representative pH oscillator involves the oxidation of a weak acid (HA) to produce protons (H^+), resulting in periodic pH changes in solution. A continuously stirred tank reactor (CSTR) is employed to maintain steady-state conditions, ensuring stable and sustained pH oscillations that drive the chemomechanical feedback loop. (ii) Schematics of a pH-responsive hydrogel undergoing cyclic swelling and shrinking as the oscillating pH crosses the pK_a of the polymer (e.g., poly(AAc)), resulting from periodic protonation and deprotonation. Right graph plots time-dependent sustained regulation of hydrogel volume in response to periodic pH changes. (b) (i) Reaction mechanism of the HPD oscillator, where H_2O_2 and dithionite react to alternately produce and consume protons, inducing autonomous pH oscillations between pH values of ~3.5 and 9.2. (ii) Schematics of a bilayer hydrogel actuator fabricated by assembling a pH-responsive poly(DMAAm-*co*-AAc) hydrogel (DA gel) and a nonresponsive poly(DMAAm)−silica hydrogel (DS gel). (iii) Time-lapse snapshots showing reversible and periodic bending−stretching motion of the DA/DS bigel strip, synchronized with the pH oscillation ($[H_2O_2]$ = 50 mM, $[Na_2S_2O_2]$ = 12 mM in an acetate buffer = 5 mM, pH 5.5). (c) (i) Schematic illustration of the bilayer hydrogel actuator composed of a shape deformation (SD) layer containing poly(AAc) and a fluorescence color (FC) layer embedded with tetra(4-pyridylphenyl)ethylene (TPE-4N), a pH-responsive luminogen. (ii) Time-lapse images of the jellyfish-shaped actuator showing synchronized deformation and green fluorescence modulation ($[H_2O_2]$ = 50 mM, $[Na_2S_2O_2]$ = 12 mM in an acetate buffer = 5 mM, pH 5.5). (d) (i) Reaction mechanism of the Landolt oscillator, which consists of two competing reactions: proton-producing oxidation of sulfite by bromate and proton-consuming oxidation of ferrocyanide by bromate. (ii) Schematic of a photonic crystal (PC) hydrogel composed of poly(AAm-*co*-AAc), whose periodic nanostructure undergoes volume-induced modulation during pH oscillation. The resulting change in lattice spacing shifts the photonic stopband, enabling visible color oscillation. (iii) Time-lapse images showing cyclic color transitions of the PC hydrogel under Landolt-driven pH oscillation (10.86 g/L $KBrO_3$, 9.45 g/L Na_2SO_3, 8.45 g/L, $K_4Fe(CN)_6$, 0.98 g/L, H_2SO_4, flow rate: 0.3 mL/min). Panel (b) is reproduced with permission from ref 151. Copyright 2005 Royal Society of Chemistry. Panel (c) is reproduced with permission from ref 152. Copyright 2022 American Chemical Society. Panel (d) is reproduced with permission from ref 158. Copyright 2009 John Wiley and Sons.

As an example of morphology-driven optical feedback, Lee et al. developed a self-regulating hydrogel system by combining wrinkle-patterned poly(acrylamide) (poly(AAm)) hydrogels with plasmonic lattices of gold nanoparticles (AuNPs) (Figure 7b).[149] Upon exposure to moisture, poly(AAm) swells, flattening the surface and increasing the light transmittance, which induces photothermal heating by the AuNPs. The generated heat subsequently causes surface dehydration,

https://doi.org/10.1021/acs.chemrev.5c00358
Chem. Rev. XXXX, XXX, XXX−XXX

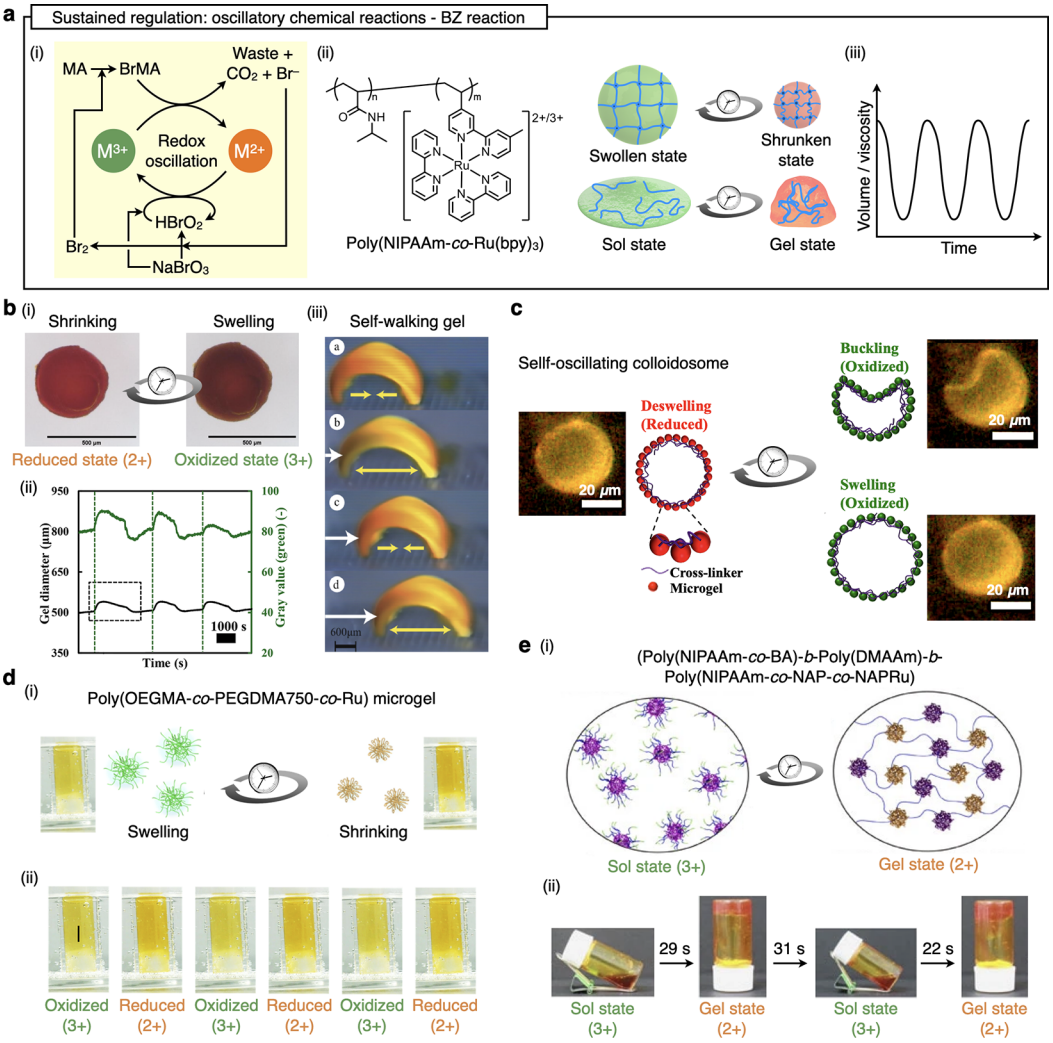

Figure 9. Self-regulating hydrogels based on BZ reactions. (a) (i) Schematics of redox oscillation via the BZ reaction. During the oxidation of malonic acid (MA) by sodium bromate ($NaBrO_3$), the redox state of the metal complex catalyst (M) undergoes periodic oscillation. Once the inhibitor bromide ion (Br^-) has been depleted, the autocatalytic production of bromous acid ($HBrO_2$) becomes active, driving M into its oxidized form. The bromine (Br_2) generated at this stage reacts with MA to form bromomalonic acid (BrMA), and BrMA reduces M and regenerates Br^-, thereby completing the cycle. (ii) Chemical structure of a typical BZ-driven self-regulating polymer, poly(*N*-isopropylacrylamide-*co*-tris(2,2′-bipyridyl)ruthenium) (poly(NIPAAm-*co*-Ru(bpy)$_3$)). (iii) Time-dependent sustained regulation of volume and viscosity driven by self-mediated BZ reaction. (b) (i) Schematics of the volumetric oscillation and (ii) the oscillation profiles of the self-oscillating gel, poly[*N*-isopropylacrylamide-*co*-*N*-(3-aminopropyl)methacrylamide-*co*-*N*-(3-aminopropyl)methacrylamide-tris(2,2′-bipyridyl)ruthenium-*co*-*N*,*N*′-methylenebis(acrylamide)] (poly(NIPAAm-*co*-NAP-*co*-NAPRu-*co*-MBAAm)) gel, in a catalyst free BZ substrate solution at 20 °C ([HNO_3] = 0.894 M, [$NaBrO_3$] = 0.84 M, [MA] = 0.064 M). (iii) Time-lapse images showing the autonomous motion of a self-walking gel in a catalyst free BZ substrate solution at 18 °C ([HNO_3] = 0.894 M, [$NaBrO_3$] = 0.84 M, and [MA] = 0.0625 M). (c) Buckling/unbuckling motion of self-oscillating colloidosomes composed of poly(*N*-isopropylacrylamide-*co*-*N*-(3-aminopropyl)methacrylamide-*co*-*N*-(3-aminopropyl)methacrylamide-tris(2,2′-bipyridyl)ruthenium) (poly(NIPAAm-*co*-NAPMAm-*co*-NAPMAmRu)) microgels and poly(NIPAAm-*co*-(*N*-acryloxysuccinimide)) (poly(NIPAAm-*co*-NAS)) cross-linker, in a catalyst free BZ substrate solution at 20 °C ([HNO_3] = 0.3 M, [$NaBrO_3$] = 0.4 M, [MA] = 0.025 M). (d) (i) Volumetric oscillation of poly[oligoethylene glycol methacrylate-*co*-tris(2,2′-bipyridyl)ruthenium)-*co*-poly(ethylene glycol) dimethacrylate] (poly(OEGMA-*co*-PEGDMA750-*co*-Ru)) microgel (OEGMA: M_n = 300, PEGDMA750: M_n = 750). (ii) Time-lapse images showing the aggregation and dissociation oscillation of a poly(OEGMA-*co*-PEGDMA750-*co*-Ru) microgel in a catalyst free BZ substrate solution at 65 °C ([HNO_3] = 2.5 M, [$NaBrO_3$] = 0.08 M, [MA] = 0.5 M). (e) (i) Schematics of the periodic sol−gel transition based on structural changes of the self-oscillating triblock terpolymer, poly(*N*-isopropylacrylamide-*co*-butyl acrylate)-*b*-poly(*N*,*N*-dimethylacrylamide)-*b*-poly[*N*-isopropylacrylamide-*co*-*N*-(3-aminopropyl)-methacrylamide-*co*-*N*-(3-aminopropyl)methacrylamide-tris(2,2′-bipyridyl)ruthenium] (poly(NIPAAm-*co*-BA)-*b*-poly(DMAAm)-*b*-poly(NIPAAm-*co*-NAP-*co*-NAPRu)). (ii) Sol−gel oscillation of the self-oscillating triblock terpolymer solution (5.0 wt %) in a catalyst free BZ substrate solution at 30 °C ([HNO_3] = 0.81 M, [$NaBrO_3$] = 0.1 M, [MA] = 0.04 M). Panels (b)(i) and (b)(ii) are reproduced with permission from ref 166. Copyright 2023 licensed under CC 3.0 Royal Society of Chemistry. Panel (b)(iii) is reproduced with permission from ref 170. Copyright 2007 John Wiley and Sons. Panel (c) is reproduced with permission from ref 171. Copyright 2016 John Wiley and Sons. Panel (d) is reproduced with permission from ref 173. Copyright 2021 American Chemical Society. Panel (e) is reproduced with permission from ref 174. Copyright 2017 licensed under CC 4.0 Springer Nature.

forming wrinkles and increasing optical scattering, thereby self-blocking further photothermal heating. Rehydration by moisture then restores the flat state, completing the optical feedback loop (Figure 7b(i)). At a constant humidity of 43%,

https://doi.org/10.1021/acs.chemrev.5c00358
Chem. Rev. XXXX, XXX, XXX−XXX

each hydration-dehydration cycle occurred approximately every 26 min, demonstrating stable oscillations with approximately 60% change in transmittance (Figure 7b(ii)).

For another optical feedback mechanism, Zhang et al. designed a self-regulating hydrogel system utilizing the phase transition of poly(NIPAAm) to modulate transparency (Figure 7c).[150] This system comprises poly(NIPAAm)−poly(AAm)/AuNPs layers, where incident light passes through the transparent poly(NIPAAm) layer and is reflected by the underlying poly(AAm)/AuNPs layer, generating heat that is transferred to the poly(NIPAAm) layer. This delayed heating triggers the coil-to-globule transition of poly(NIPAAm), increasing the opacity and blocking the incoming light. When illumination decreases, the temperature drops, the transparency of poly(NIPAAm) is restored, and light transmission resumes (Figure 7c(i)), thus completing the optical feedback loop. Under room temperature conditions, this light-driven feedback mechanism produced stable and sustained temperature oscillations, enabling dissipative color displays (Figure 7c(ii)). Specifically, the irradiated region (3) exhibited blinking between red and white every 75 s with a temperature variation exceeding 15 °C; intermediate areas (2) remained consistently pink, and cooler areas (1) maintained stable black coloration, visually demonstrating spatially resolved sustained regulation.

4.4. Oscillatory Chemical Reactions

4.4.1. pH Oscillators. The pH oscillators offer a chemical platform for achieving sustained self-regulation in hydrogels through periodic proton modulation (Figure 8a(i)). Self-regulating hydrogels driven by pH oscillators utilize autocatalytic and feedback-regulated chemical reactions, typically conducted in a continuous stirred tank reactor (CSTR), to generate cyclic pH fluctuations, which in turn trigger reversible volume transitions in pH-sensitive polymer networks.[151−162] These systems rely on the ionizable functional groups of the hydrogel—such as carboxylic acids—whose protonation and deprotonation are directly governed by the surrounding pH (Figure 8a(ii)). A key advantage of pH oscillators is their ability to produce large-amplitude pH swings across the pK_a threshold of the gel, enabling significant and tunable mechanical responses. Various pH oscillators, including the hydrogen peroxide−dithionite (HPD) oscillator[163] and the Landolt oscillator,[164] generate periodic acidification and neutralization through the dynamic interplay of oxidants and reductants, inducing swelling−shrinking cycles in hydrogels. These chemically programmed oscillators enable highly reproducible pH cycling and sustained volumetric regulation.

A representative example of a pH oscillator is the HPD system (Figure 8b). The HPD oscillator operates through alternating proton-generating and proton-consuming reactions, leading to autonomous pH fluctuations typically ranging from pH 3.5 to 9.2, with a cycle period of approximately 300 s under 50 mM H_2O_2 and 12 mM $Na_2S_2O_2$ in an acetate buffer (5 mM, pH 5.5) (Figure 8b(i)).[151] To harness this pH oscillation, a bilayer hydrogel actuator was constructed by integrating a pH-responsive poly(DMAAm-*co*-AAc) hydrogel (DA gel) with a nonresponsive poly(DMAAm)−silica hydrogel (DS gel) (Figure 8b(ii)). As the pH oscillations cyclically crossed the pK_a of the DA gel, the bilayer underwent sustained bending and unbending driven by asymmetric swelling between the layers, achieving a maximum bending degree of approximately 80%, defined as the relative length change between the two ends of the actuator compared to its initial length (Figure 8b(iii)).

Building upon the DA/DS bigel actuator design, Yang et al. advanced the system by integrating optical functionality into the hydrogel architecture, enabling simultaneous mechanical and fluorescent modulation (Figure 8c).[152] The actuator consists of a bilayer structure composed of a shape deformation (SD) layer made from pH-responsive poly(AAc) and a fluorescence color (FC) layer incorporating tetra(4-pyridylphenyl)ethylene (TPE-4N),[165] a pH-sensitive luminogen (Figure 8c(i)). Under the same HPD pH oscillator conditions, the hydrogel experiences periodic pH changes between approximately 3.5 and 9.2, with a cycle period of about 290 s. These oscillations simultaneously trigger conformational changes in the SD layer and fluorescence switching in the FC layer. As a result, the jellyfish-shaped hydrogel actuator demonstrates synchronized, reversible shape morphing and light emission under static chemical conditions, exhibiting bending angle amplitudes ranging from approximately 30° to 322° per oscillation cycle (Figure 8c(ii)).

In parallel with structural−optical coupling strategies, Tian et al. demonstrated a color-oscillating photonic crystal (PC) hydrogel actuator powered by the Landolt pH oscillator (Figure 8d).[158] The Landolt oscillator operates through alternating proton-generating and -consuming reactions, resulting in autonomous pH fluctuations typically ranging from 3.3 to 6.7 under continuous feeding of aqueous solutions containing 10.86 g/L $KBrO_3$, 9.45 g/L Na_2SO_3, 8.45 g/L $K_4Fe(CN)_6$, and 0.98 g/L H_2SO_4 at a flow rate of 0.3 mL/min (Figure 8d(i)). The system employs a poly(AAm-*co*-AAc) hydrogel containing a periodic colloidal array that produces structural coloration via Bragg diffraction (Figure 8d(ii)). Under oscillatory pH conditions, the hydrogel experiences cyclic protonation and deprotonation. These changes modulate the periodic swelling and shrinkage of the lattice spacing. Consequently, the photonic stopband shifts from approximately 510 to 590 nm, generating oscillations in structural color between blue and orange (Figure 8d(iii)). The system operates under constant flow conditions, with an oscillation period of approximately 25−40 min depending on the feed rate.

4.4.2. Belousov−Zhabotinsky (BZ) Reactions. Following the oscillatory chemical reactions driven by the pH oscillator, the Belousov−Zhabotinsky (BZ) reaction serves as an excellent driving circuit for achieving sustained regulation in hydrogels, owing to its intrinsic periodic state changes (Figure 9a).[166−184] The BZ reaction stands out as one of the most iconic examples of a chemical oscillation reaction (Figure 9a(i)).[104,105] In this reaction, a specific organic substrate, such as malonic acid, undergoes oxidation under strongly acidic conditions in the presence of an oxidizing agent and a redox-active metal complex catalyst. As the oxidation of the organic acid proceeds, the metal catalyst undergoes spontaneous, periodic redox switching between its oxidized (M^{3+}) and reduced (M^{2+}) states. A major reason the BZ reaction has found widespread interest in the field of self-regulating materials is that this periodic redox switching fundamentally alters the properties of the metal catalyst without any external on/off control. These valence changes of the metal complex catalyst lead to alterations in various physicochemical properties, such as hydrophilicity, ionic interactions, and coordination strength with ligands. For instance, when the metal complex is reduced from a 3^+ to a 2^+ state, the decreased positive charge

https://doi.org/10.1021/acs.chemrev.5c00358
Chem. Rev. XXXX, XXX, XXX−XXX

generally decreases its hydrophilicity and weakens the electrostatic attraction with surrounding anionic species. By embedding a BZ catalyst into a hydrogel framework, the built-in BZ reaction circuit regulates the spatiotemporal structure of the hydrogel, enabling various self-oscillating functions.

One of the most extensively studied approaches to self-regulating hydrogels driven by the BZ reaction involves coupling the redox oscillations of the prototypical catalyst ruthenium tris(2,2′-bipyridine) complex ($Ru(bpy)_3$) with thermoresponsive polymers (Figure 9a(ii)). Thermoresponsive polymers exhibit a sharp change in solubility or swelling behavior at a specific transition temperature, termed the LCST or the volume phase transition temperature (VPTT). When a metal complex catalyst is embedded into the polymer chain, its redox state can modulate the LCST or VPTT. Specifically, in the oxidized state, $Ru(bpy)_3$ becomes more hydrophilic than in the reduced state, resulting in a shift of the transition temperature toward higher values. In the reduced state, the opposite effect occurs. Therefore, when BZ substrates are supplied within this temperature range, the polymer actively participates in driving the BZ reaction, and the redox oscillations of the catalyst lead to self-regulation in either the gel volume or the viscosity of the polymer solution (Figure 9a(iii)).

In a pioneering study, Yoshida and co-workers introduced the $Ru(bpy)_3$ catalyst into a poly(NIPAAm) network, creating a "self-oscillating gel".[166] When this hydrogel was immersed in a catalyst-free BZ substrate solution, it autonomously drove the BZ reaction and exhibited rhythmic volume oscillations (Figure 9b(i)).[167] Under catalyst-free BZ conditions ($[HNO_3]$ = 0.894 M, $[NaBrO_3]$ = 0.84 M, [MA] = 0.0625 M, 20 °C), this hydrogel sphere undergoes volumetric swelling−deswelling oscillations that arise from redox-driven changes in the network. It exhibits a period of about 60 min, displaying a reversible diameter change of approximately 10% (Figure 9b(ii)). This principle has led to a variety of self-oscillating hydrogel actuators. For example, a self-oscillating gel sheet with asymmetric front and back structures can convert cyclic volume changes into self-regulating bending motions.[169] The curvature oscillations originate from swelling differences between the reduced and oxidized states caused by structural asymmetry. Furthermore, combining this self-bending strategy with a ratchet-shaped substrate produces a "self-walking gel" that autonomously advances over the substrate, driven by the self-mediated BZ reaction (Figure 9b(iii)).[170] This hydrogel enables directional mechanical work powered by a catalyst-free BZ substrate solution ($[HNO_3]$ = 0.894 M, $[NaBrO_3]$ = 0.84 M, [MA] = 0.0625 M, 18 °C), performing self-walking motions at a speed of 170 μm min^{-1}. Another notable example is a "self-oscillating colloidosome," constructed by cross-linking self-oscillating microgels with a polymer cross-linker (Figure 9c).[171] Upon addition of BZ substrates ($[HNO_3]$ = 0.3 M, $[NaBrO_3]$ = 0.4 M, [MA] = 0.025 M, 20 °C), the colloidosome undergoes buckling and unbuckling oscillations. These oscillations arise from the tangential stress induced during swelling of the hollow colloidosome structure with buckling occurring when the stress exceeds the yield point. The oscillation period ranges from approximately 100 to 500 s, with a projected area amplitude varying from about 500 to 600 μm^2. Using a similar strategy, a "self-oscillating polymersome," which also exhibits buckling and unbuckling oscillations, was realized by cross-linking a block copolymer composed of a self-oscillating polymer and a hydrophilic poly(ethylene glycol) (PEG) segment.

Recently, Enomoto et al. demonstrated that even hydrogel frameworks devoid of active components can be endowed with autonomous behavior by incorporating a thermoresponsive self-oscillating linear polymer as a semi-interpenetrated polymer network (semi-IPN).[172] In this approach, a hydrogel framework composed of poly(NIPAAm) or poly(*N*,*N*-dimethylacrylamide) (poly(DMAAm)) was fabricated in the presence of a thermoresponsive self-oscillating linear polymer. Despite the passive nature of the primary network, rhythmic structural changes of the semi-interpenetrated polymer drive volumetric oscillations of the gels in the presence of the BZ substrate ($[HNO_3]$ = 0.894 M, $[NaBrO_3]$ = 0.84 M, [MA] = 0.064 M, 25 °C). Such semi-IPN hydrogels offer notable advantages: they are straightforward to fabricate by simply mixing the self-oscillating polymer into the hydrogel precursor solution, and the oscillation amplitude and period can be tuned by adjusting the fraction of the self-oscillating polymer.

Although poly(NIPAAm) has become the prototypical thermoresponsive polymer for coupling with the BZ reaction, other temperature-responsive polymers have been explored to realize self-oscillating gels. Notably, Suzuki et al. reported a self-oscillating hydrogel based on poly(oligoethylene glycol methacrylate) (poly(OEGMA)), which exhibits a VPTT at a higher temperature than poly(NIPAAm) (Figure 9d(i)).[173] Operating at elevated temperatures accelerates the kinetics of the BZ reaction, thereby shortening the oscillation period of the swelling−deswelling oscillation. Indeed, in poly(OEGMA)-based self-oscillating microgels, initiation of the BZ reaction around 65 °C results in extremely rapid oscillations between aggregated and dispersed states on the order of 1 s ($[HNO_3]$ = 2.5 M, $[NaBrO_3]$ = 0.08 M, [MA] = 0.5 M) (Figure 9d(ii)). As in the examples shown here, a variety of self-regulating functions can be designed by tuning the chemical and physical structures of the thermoresponsive polymers.

Furthermore, the same principle has been extended to autonomously regulate the sol−gel state of polymers driven by the BZ reaction, specifically artificial amoeba-like polymer droplets composed of triblock terpolymers (Figure 9e(i)).[174] The triblock terpolymer consists of a hydrophobic segment, a hydrophilic linker, and a self-oscillating segment. Under BZ conditions ($[HNO_3]$ = 0.81 M, $[NaBrO_3]$ = 0.1 M, [MA] = 0.04 M, 30 °C), the oxidized state (3^+) forms micellar assemblies with a hydrophobic core, whereas the reduced state (2^+) exhibits a lower LCST, inducing physical cross-linking between the micelles and forming a transient gel state. The BZ reaction drives oscillations between these states, producing a spontaneous sol−gel cycle. This system exhibits oscillation periods ranging from 50 to 100 s, with a viscosity amplitude reaching ∼1960 mPa·s. The system demonstrates the underlying mechanism of amoeboid motion (Figure 9e(ii)).

So far, we have highlighted BZ-driven self-regulating gels based on thermoresponsive polymers; however, several other strategies have been reported to achieve self-sustaining regulation powered by the BZ reaction. One such strategy for creating BZ-driven, self-regulating hydrogels leverages changes in electrostatic interactions resulting from the redox oscillations of the metal complex catalyst. Yoshida et al. showed that even nonthermoresponsive gels, such as those based on poly(DMAAm), can display self-regulating volume changes if a sufficiently high fraction of the Ru catalyst is introduced.[175] Their results suggest that, besides the shift in

https://doi.org/10.1021/acs.chemrev.5c00358
Chem. Rev. XXXX, XXX, XXX−XXX

hydrophilicity upon Ru oxidation, changes in electrostatic repulsion between immobilized Ru complexes strongly affect the swelling−shrinking behavior of the hydrogel. One advantage of these nonthermoresponsive systems is their broader usable temperature range compared to self-oscillating systems based on thermoresponsive polymers. Additionally, the period of volumetric oscillation can be tuned by changing the reaction temperature; the poly(DMAAm)-based self-oscillating gel exhibits variable periods ranging from 100 to 500 s, depending on the temperature ($[HNO_3]$ = 0.894 M, $[NaBrO_3]$ = 0.084 M, and [MA] = 0.064 M). However, they often require a higher Ru loading than thermoresponsive gels, illustrating a trade-off between ease of actuation and catalyst concentration.

In addition to periodic changes in the hydrophilicity or ionic interactions, other types of BZ reaction systems exploit different molecular interactions for self-regulation. Ueki et al., for example, utilized a redox-dependent ligand exchange reaction of the Ru-terpyridine (terpy) catalyst to realize cross-linking−decross-linking oscillation in polymer droplets.[176] Their system comprises branched PEG derivatives bearing Ru-terpy termini mixed with terpyridine-terminated PEG lacking metal centers. In the oxidized state of Ru, the monoterpy complex is more stable, and the polymer solution retains its fluidity due to the lack of interpolymer cross-linking. Conversely, the bis-terpy complex is more favorable in the reduced state, forming a transient gel via cross-links between the PEG ends. In the presence of BZ substrates ($[HNO_3]$ = 0.3 M, $[NaBrO_3]$ = 0.4 M, [MA] = 0.1 M, 25 °C), these droplets induce the BZ reaction and undergo periodic transitions in viscosity and network structure.

Interestingly, some reports describe that poly(AAm) hydrogels bearing a Ru catalyst exhibit the opposite trend from conventional BZ-driven self-regulating hydrogels, swelling in the reduced state and shrinking in the oxidized state.[177,178] The contraction of the gel upon oxidation is presumably due to increased intra- and interchain cross-linking, which becomes more favorable in the oxidized state, whereas these cross-links break upon reduction. Although experimental findings and simulation analysis both point toward this cross-linking mechanism, the molecular-level details remain somewhat controversial, indicating that further investigation is warranted. These examples highlight the diverse design strategies for constructing self-regulated hydrogels driven by the BZ reaction, through thermoresponsive coil-to-globule transitions, electrostatic repulsion/attraction, or redox-responsive coordination bonding. In each case, the spontaneous oscillations of the metal complex catalyst serve as a powerful driving circuit for self-regulating structural changes.

Taken together, in this section, we summarize representative examples of sustained regulation, categorized according to the hydrogel matrix, hydrogel type, regulating fuels, regulating period, regulation degree, deformation type, and their applications in Table 2.

5. ONE-CYCLE REGULATION

5.1. Design Criteria for One-Cycle Regulation

One-cycle regulation in self-regulating hydrogels fundamentally relies on transient chemical reaction networks that initiate temporary structural transitions and autonomously revert to their initial states upon fuel dissipation. This mechanism universally employs chemically fueled dissipative transitions, where the system is driven away from equilibrium into a transient state through chemical reactions, subsequently returning to the equilibrium state as the fuel is consumed or chemically decomposed. Based on the nature of chemical or enzymatic reactions employed, this regulation can first be classified into four categories: Independent sequential reactions, involving two independent reactions that sequentially drive structural changes; deactivator-driven reactions, in which a promoter initially induces structural changes, followed by the internal generation of a deactivator that returns the system to its original state; fuel-decomposed reactions, where transient structural changes occur and are subsequently reversed upon decomposition of the fuel itself; and competing reactions, consisting of two pathways with distinct kinetics—an initial rapid reaction causing structural changes and a slower competing reaction restoring the original state. Furthermore, from the viewpoint of chemical responsiveness and location of chemical control, these one-cycle systems can be more broadly grouped into two categories: hydrogels that are directly responsive to external chemical stimuli, such as pH changes, and hydrogels that incorporate internal reactive species, particularly enzymatic catalysts, to drive subsequent reaction cascades internally. While externally responsive systems offer simplicity and rapid responsiveness, their operational lifetimes and autonomys are inherently limited by the external chemical environment. Conversely, enzymatically driven systems allow more sophisticated control and extended lifetimes through programmed internal catalytic reactions; however, they face limitations in terms of complexity, enzyme stability, and potential loss of catalytic activity over multiple cycles. These inherent advantages and limitations highlight the necessity for balanced design criteria, aiming to optimize the chemical robustness, autonomous recovery, and overall functionality of one-cycle hydrogel actuators.

5.2. Independent Sequential Reactions

Independent sequential reactions enable one-cycle self-regulation in hydrogel actuators by leveraging chemically programmed reaction sequences to induce transient structural changes that autonomously revert to the initial state after fuel depletion (Figure 10a(i)).[185−192] These systems are activated by a single addition of chemical fuel, initiating a cascade of reactions within a predefined lifetime. Upon addition and subsequent consumption of fuel, transient supramolecular assembly, network hydrophobization, or cross-linking are mediated by reversible bond formation, triggering sol−gel or swelling−shrinking transitions that spontaneously revert to the initial state. This one-cycle regulation is governed by independent sequential reactions. Representative strategies include transient sulfonation of aldehyde fueled by dithionite, anhydride formation fueled by 1-ethyl-3-(3-(dimethylamino)-propyl)carbodiimide hydrochloride (EDC),[193−198] and disulfide formation fueled by hydrogen peroxide (H_2O_2).[199,200] These platforms enable hydrogels to transiently modulate their viscosity, volume, stiffness, and turbidity over time (Figure 10a(ii)).

A representative example of independent sequential regulation was developed by Singh et al., who designed a supramolecular hydrogel system utilizing aldehyde sulfonation fueled by dithionite (Figure 10b).[185] Upon the addition of dithionite (DT, 191 mM), the aldehyde-functionalized SachCHO monomer is rapidly reduced to $SachSO_3^-$, disrupting hydrogen bonding, and triggering gel disassembly.

https://doi.org/10.1021/acs.chemrev.5c00358
Chem. Rev. XXXX, XXX, XXX−XXX

Table 2. Representative Examples of Self-Regulating Hydrogel Actuators Exhibiting Sustained Regulation

Category	Hydrogel matrix	Hydrogel type	Regulating fuels	Regulating period	Regulation degree	Deformation type	Applications	Ref
Mechanical Feedback Loop	Poly(AAm-*co*-AAc)	Sheet gel (2.6 mm × 150 μm × 250 μm)	NaOH, HCl solution	30−45 s	Bending angle (20 to 60°)	Swelling−shrinking	Autonomous pumping, separation, transport in microfluidics	106
	Poly(NIPAAm)	Sheet gel (thickness <70 μm)	H_2O_2	4.2 min	Height change (10 to 14 μm)	Swelling−shrinking	Microstructure bent	107
	Poly(NIPAAm) with AuNPs	Sheet gel (thickness = 0.36−1.1 mm, length: 5−10 mm)	Visible light, 120−1125 mW	0.7−2 s	Tip displacement (0.3 to 2.8 mm)	Swelling−shrinking	Soft robots, artificial phototaxis, miniaturized transportation	108
	Poly(NIPAAm) with AuNPs and FNSs	Cylindrical gel (diameter = 2 mm, length = 8−15 mm)	Visible light	28−70 s	Rolling (∼360°) braid rotation (∼228°)	Swelling−shrinking	Soft robotics, gear rotation, rod climbing, transport	109
	Poly(NIPAAm) with AuNPs and NSs	Sheet gel (thickness = 0.5, 1, 1.5, 2 mm)	Visible light	10−100 s	Rotation (∼180°) flipping (∼360°)	Swelling−shrinking	Möbius [+1] strip robots, twisted ribbon robots, cargo transport	110
	Poly(NIPAAm) with AuNPs and r-GO	Jellyfish-like gel	Visible light	20−40 s	20 mm to 4 cm	Swelling−shrinking	Full-space phototaxis, photothermotactic flow-guided movement, underwater steering	111
	Poly(NIPAAm-*co*-AAc)	Cylindrical gel (diameter = 0.5 or 1 mm)	KIO_3, $KBrO_3$, H_2O_2	∼6 h	Height change (10 to 16 mm)	Swelling−shrinking	Self-lifting	118
	Poly(NIPAAm-*co*-NTBA-*co*-DMAPrMAA)	Cylindrical gel (diameter = 1.15 mm)	methylene glycol−sulphite	40 min−4 h	Height change (14%−23%)	Swelling−shrinking	Self-lifting	121
Optical Feedback Loop	Poly(AAm)	Sheet gel (thickness = 600 μm)	Light (808 nm)	7−30 min	Transmittance change (∼60%)	Swelling−shrinking	Optical regulation, moisture sensing	149
	Poly(NIPAm)-based with AuNPs	Sheet gel (50 mm × 2 mm × 2 mm)	Light (532 nm)	40−77 s	Temperature change (20 to 41 °C)	Swelling−shrinking	Dissipative dynamic materials, signal transduction, cargo transport	150
Oscillatory Chemical Reactions - pH oscillators	Poly(DMA-*co*-AAc)	Sheet gel (40 mm × 2 mm × 1 mm)	H_2O_2, $Na_2S_2O_2$	300 s	bending angle change (∼80%)	Swelling−shrinking	Gripper	151
	Poly(DMA-*co*-AAc)	Sheet gel (30 mm × 2 mm × 1 mm)	H_2O_2, $Na_2S_2O_2$	290 s	bending angle (30° to 322°)	Swelling−shrinking, color change	Jellyfish-like biomimetic hydrogel actuator	152
	Poly(AAm-*co*-AAc)	Sheet gel (20 mm × 10 mm × 50 μm)	$KBrO_3$, HSO_3^-, $K_4Fe(CN)_6$	25−40 min	Stopbands shift (555 to 696 nm)	Swelling−shrinking, color change	-	158
	Poly(NIPAAm-*co*-Ru(bpy)$_3$)	Sheet gel (20 mm × 1 mm × 1 mm)	HNO_3, $NaBrO_3$, MA	360 s	-	Swelling−shrinking	-	166
Oscillatory Chemical Reactions - BZ reactions	poly(NIPAAm-*co*-NAP-*co*-NAPRu-*co*-MBAAm)) gel	Spherical gel (diameter = 1 mm)	HNO_3, $NaBrO_3$, MA	60 min	Diameter change (∼10%)	Swelling−shrinking	-	167
	Poly(NIPAAm-*co*-Ru(bpy)$_3$)	Cylindrical gel (diameter = 0.29 mm)	HNO_3, $NaBrO_3$, MA	5 min	Bending degree (1.6 to 1.9)	Swelling−shrinking	Autonomously moving objects, biomimetic actuators	169
	Poly(NIPAAm-*co*-Ru(bpy)$_3$-*co*-AMPS)	Sheet gel (6 mm × 3 mm × 0.5 mm)	HNO_3, $NaBrO_3$, MA	112 s	Displacement (170 μm min^{-1})	Swelling−shrinking	Bending (walking)	170
	Poly(NIPAAm-*co*-NAPMAm)-*co*-Poly (NIPAAm-*co*-NAS) colloidosome	Microgel (diameter = 26 μm)	HNO_3, $NaBrO_3$, MA	100−500 s	Projected area (500 to 600 μm^2)	Swelling−shrinking	Artificial cell-like systems	171
	Poly(NIPAAm-*co*-NAPMAm-*co*-NAPMAmRu) and poly(DMAAm), semi-IPN	Sheet gel (1 mm × 1 mm × 1 mm)	HNO_3, $NaBrO_3$, MA	∼144 s	Gel side length (∼40 μm)	Swelling−shrinking	Autonomous volumetric oscillation	172
	Poly(OEGMA-*co*-Ru)	Microgel (diameter = 272 nm)	HNO_3, $NaBrO_3$, MA	1.3 s	-	Swelling−shrinking	Biomimetic heartbeat-like motion	173
	Poly(NIPAAm-*co*-BA)-*b*-poly (DMAAm)-*b*-poly(NIP-*co*-NAP-*co*-NAPRu)	-	HNO_3, $NaBrO_3$, MA	50−100 s	Viscosity (1960 mPa·s)	Sol−gel transition	Amoeba-like autonomous droplet motion	174
	poly(DMAAm-*co*-NAPMAm-*co*-NAPMAmRu(bpy)3)	Sheet gel (thickness = 500 μm)	HNO_3, $NaBrO_3$, MA	100−500 s	Volume change ratio (∼10.8%)	Swelling−shrinking	-	175

https://doi.org/10.1021/acs.chemrev.5c00358
Chem. Rev. XXXX, XXX, XXX−XXX

Table 2. continued

Category	Hydrogel matrix	Hydrogel type	Regulating fuels	Regulating period	Regulation degree	Deformation type	Applications	Ref
	Ru^{2+}tpy-octa-PEG gel (poly(octa (2,2′:6′,2″-terpyrid-4′-yl)-PEG-Ru (II)))	-	HNO_3, $NaBrO_3$, MA	200 s	Absorbance at 485 nm (0.35 to 0.65 nm)	Sol−gel transition	-	176

This reduction step occurs independently of the regeneration mechanism, which involves formaldehyde release from hexamethylenetetramine (HMTA, 190 mM) via slow acid-catalyzed hydrolysis mediated by glucono-δ-lactone (GdL, 93.6−374 mM). The use of orthogonal chemistries for disassembly and reassembly enables a temporally ordered gel−sol−gel transition following a single fuel injection (Figure 10b(i)). These independent sequential reactions were precisely engineered: a fuel-driven activation event is followed by a kinetically delayed, chemically distinct deactivation process, facilitating autonomous recovery without feedback coupling. Under standard catalytic conditions, the complete regulation cycle occurs over approximately 75 min, reaching a maximum amplitude in G' of approximately 2100 Pa. Moreover, when formaldehyde is directly added in excess (≥50 equiv), the system undergoes rapid reassembly within approximately 1 min, as demonstrated in Figure 10b(ii).

Another compelling demonstration of independent sequential regulation was reported by Xu et al., who developed a self-resettable bilayer hydrogel actuator based on EDC-fueled modulation of polymer hydrophilicity (Figure 10c).[186] The actuator consists of a poly(AAc) hydrogel layer covalently bonded to a soft PDMS layer. Upon the addition of EDC (3.0 equiv relative to carboxylic acid groups), the hydrophilic carboxyl moieties in the poly(AAc) network are transiently converted into hydrophobic anhydrides. This conversion leads to localized dehydration and shrinking, inducing unidirectional bending of the bilayer strip. The rehydration and recovery processes are governed by spontaneous hydrolysis of the anhydrides in aqueous buffer (MES, pH 5.0), which restores the initial hydrophilic state of the swollen poly(AAc) network (Figure 10c(i)). The mechanical deformation and spontaneous reset are time-programmed by tuning the EDC concentration and ambient conditions. Each full bending−recovery regulation cycle proceeds over approximately 5 h, reaching a maximum bending angle amplitude of approximately 37° (Figure 10c(ii)).

Furthermore, Tena-Solsona et al. developed an EDC-fueled transient hydrogel system exhibiting sol−gel−sol transitions based on the transient supramolecular assembly and disassembly of dicarboxylates such as fluoren-9-ylmethoxycarbonyl-alanine-alanine-glutamate (Fmoc-AAE) via independent sequential reactions (Figure 10d).[187] Upon addition of EDC (50−300 mM), the dicarboxylates (Fmoc-AAE, 10 mM) are transiently converted into an anhydride intermediate, inducing assembly into anisotropic fibrillar networks through hydrophobic collapse and π-orbital overlap, thereby forming a hydrogel state with significantly increased G' (∼40−100 Pa). As the anhydride spontaneously hydrolyzes back to the original dicarboxylate precursor, the assemblies gradually disintegrated, and the material returns to its original sol state characterized by a modulus lower than that of G'' ($G' \sim 0.01$ Pa) (Figure 10d(i)). Importantly, this reversible assembly−disassembly process enabled precise temporal control over the gel's mechanical properties, allowing the hydrogel lifetime to be finely tuned from 40 to 152 min depending on the initial concentration of EDC (Figure 10d(ii)).

Lastly, Sarkar et al. introduced an H_2O_2-fueled one-cycle regulation governed by a redox system in hydrogels using independent sequential reactions for sol−gel−sol transitions (Figure 10e).[188] The hydrogel matrix consists of thiol-terminated four-arm poly(ethylene glycol) (sPEG-SH, 0.7 mM). Upon injection of hydrogen peroxide (H_2O_2, 17.5−18.5

https://doi.org/10.1021/acs.chemrev.5c00358
Chem. Rev. XXXX, XXX, XXX−XXX

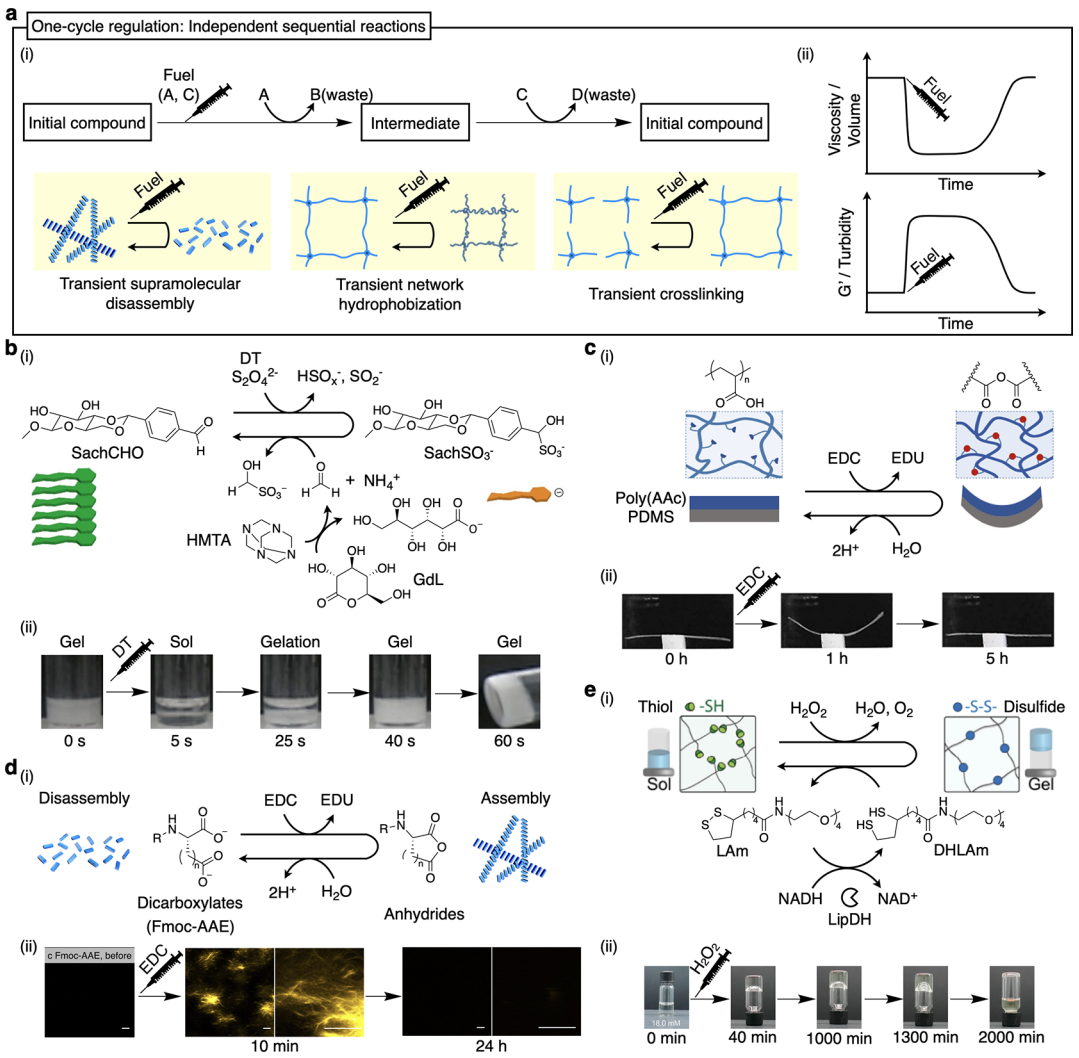

Figure 10. Self-regulating hydrogels with the one-cycle regulation driven by independent sequential reactions. (a) (i) Representative strategies for one-cycle regulation based on independent sequential reactions. Fuel-induced reversible bond formation such as transient supramolecular disassembly, network hydrophobization, and cross-linking enables a one-cycle actuation. (ii) Schematic graphs showing time-dependent one-cycle regulation of viscosity and gel volume (top), and stiffness and turbidity (bottom), triggered by chemical fuels. (b) (i) Schematics of a fuel-driven transient supramolecular hydrogel system based on SachCHO. Addition of dithionite (DT) induces sulfonation of aldehyde (from SachCHO to $SachSO_3^-$), breaking hydrogen bonds and inducing gel disassembly. Catalytic regeneration of SachCHO from hexamethylenetetramine (HMTA) via formaldehyde production is triggered by glucono-δ-lactone (GdL), enabling one-cycle regelation. (ii) Time-lapse images showing rapid gel−sol−gel transition under excess formaldehyde conditions. (c) (i) Schematics of a transient self-resettable hydrogel actuator driven by EDC-fueled anhydride formation. The bilayer structure consists of a poly(AAc) hydrogel layer adhered to a PDMS layer, enabling one-cycle of bending and recovery based on hydrophilicity modulation. (ii) Time-lapse images powered by EDC as a chemical fuel. (d) (i) Schematics of the mechanism underlying fuel-driven one-cycle assembly in a self-erasing hydrogel ink. EDC serves as a chemical fuel to induce the formation of transient anhydride bonds in dicarboxylates. (ii) Confocal micrographs of Fmoc-AAE series in response to EDC. All scale bars are 10 μm. (e) (i) Schematics of a fuel-driven one-cycle regulation in sPEG-SH hydrogels mediated by an enzymatic redox network. Upon H_2O_2 addition, thiol-terminated 4-arm polyethylene glycol (sPEG-SH) forms disulfide cross-links, inducing gelation. The sol state is restored via an enzymatic reduction cascade in which lipoamide dehydrogenase (LipDH) oxidizes NADH to generate dihydrolipoamide methyl ester (DHLAm) from lipoamide methyl ester (LAm), which reduces disulfide bonds. (ii) Time-lapse images show a one-cycle gel−sol−gel transition. Panel (b) is reproduced with permission from ref 185. Copyright 2020 American Chemical Society. Panel (c) is reproduced with permission from ref 186. Copyright 2022 American Chemical Society. Panel (d) is reproduced with permission from ref 187. Copyright 2017 licensed under CC 4.0 Springer Nature. Panel (e) is reproduced with permission from ref 188. Copyright 2024 American Chemical Society.

mM) as the chemical fuel, thiol groups are oxidized to form −S−S− bonds, resulting in gelation. To reverse this oxidation, the system employs lipoamide dehydrogenase (LipDH), NADH, and dihydrolipoic acid methyl ester (DHLAm), which together catalyze the selective reduction of disulfide bonds, restoring the sol state. LipDH acts as an oxidoreductase, transferring electrons from NADH to lipoic acid derivatives, generating DHLAm, which subsequently reduces disulfide cross-links (Figure 10e(i)).[201] This orthogonal redox pathway enables the gel to return to the sol state. Gelation typically occurs approximately 40−60 min after H_2O_2 injection, with the G' increasing significantly from ∼0.1 Pa (sol state) to ∼650 Pa (gel state). The hydrogel maintains a stable gel state before gradually transitioning back to the sol state, with G' eventually returning to ∼8 Pa after 900−1500 min, depending on the fuel concentration (Figure 10e(ii)).

https://doi.org/10.1021/acs.chemrev.5c00358
Chem. Rev. XXXX, XXX, XXX−XXX

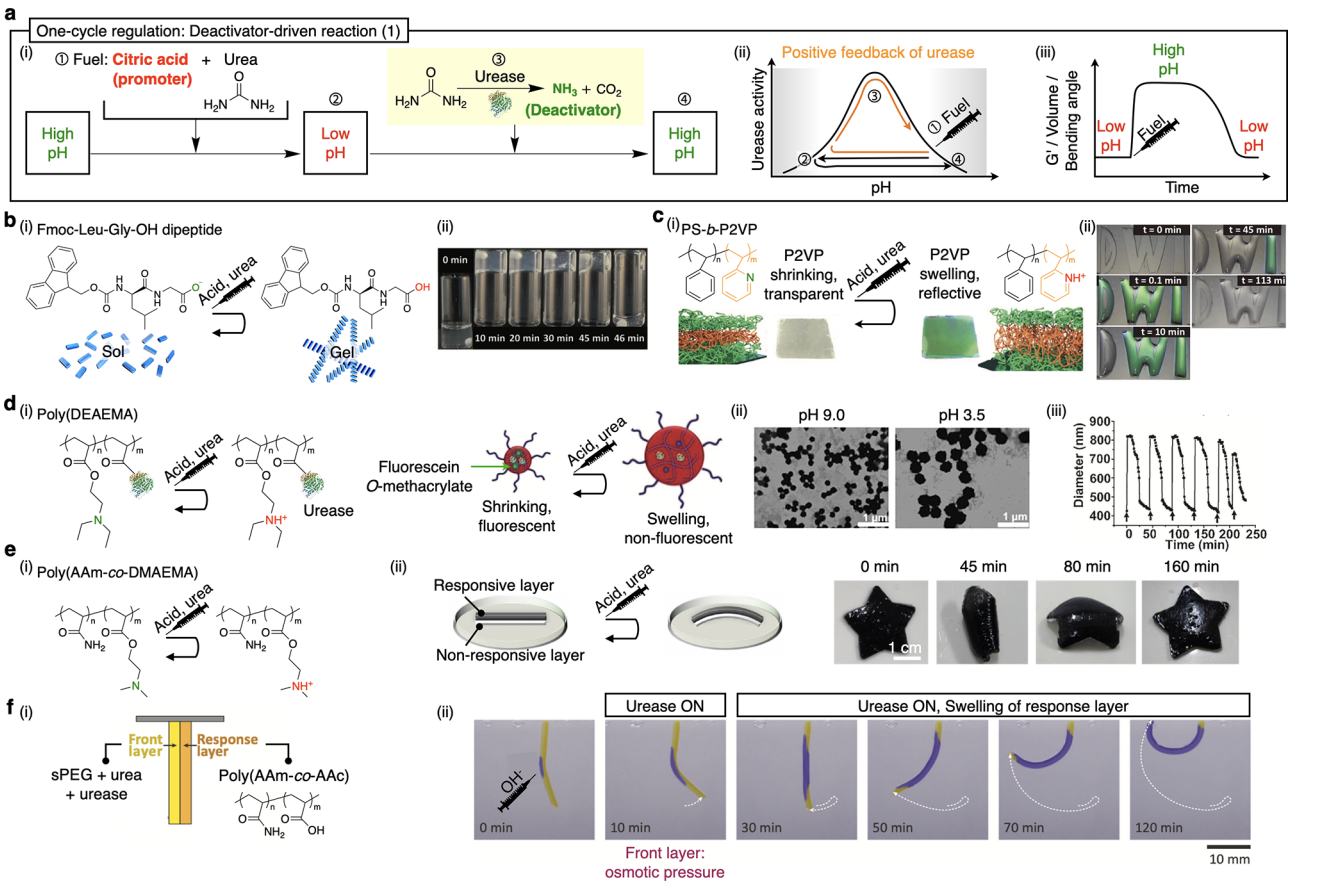

Figure 11. Self-regulating hydrogels with one-cycle reaction via deactivator-driven urease catalysis. (a) (i) Schematics of the urease-catalyzed enzymatic reaction for self-regulation. Injection of citric acid (promotor) and urea induces an initial pH drop followed by gradual pH recovery via urease-catalyzed generation of ammonia, resulting in a one-cycle transition in hydrogel structure and mechanics. (ii) Schematic graph showing time-dependent one-cycle regulation. Black curve: bell-shaped activity profile of urease, illustrating its positive feedback behavior. Black arrow: system trajectory starting from high pH, followed by acid injection and subsequent pH recovery via the urease-catalyzed reaction. Orange curve: real-time change in urease activity. (iii) Schematic graph showing time-dependent one-cycle regulation of G', layer thickness, gel volume, and bending angle. (b) (i) Molecular structure of Fmoc-L-G-OH (Fmoc = fluorenylmethoxycarbonyl, L = leucine, G = glycine) dipeptide. It can self-assemble to the gel state forming nanofibrillar hydrogels under acidic conditions through the protonation of dissociable groups. (ii) Snapshots showing a one-cycle sol−gel−sol transition in a dipeptide hydrogel, driven by sequential fueling with citric acid and urea. (c) (i) Schematic of a photonic gel film composed of polystyrene-*block*-poly(2-vinylpyridine) (PS-*b*-P2VP), where protonation of the poly(2-vinylpyridine) block induces optical reflection. (ii) Time-lapse images showing a one-cycle transient color change, governed by enzymatic pH feedback and fluorescence oscillation under repeated urea fueling. (d) (i) Structure and feedback mechanism of a breathing microgel system based on poly(*N*,*N*-diethylaminoethyl methacrylate) (poly(DEAEMA)), exhibiting reversible fluorescence switching. (ii) TEM images of the hybrid microgel at pH 9 and pH 3.5. Reversible diameter changes of the microgel in time following repeated additions of chemical fuels. (iii) Reversible diameter changes of the microgel by repeated additions of chemical fuels. (e) (i) Schematic of a bilayer actuator composed of a responsive layer based on poly(*N*,*N*-dimethylaminoethyl methacrylate) (poly(DMAEMA)) and a nonresponsive layer loaded with urease. (ii) Snapshots showing one-cycle deformation and recovery of a star-shaped actuator, programmed by citric acid and urea fueling. (f) (i) Schematic design of a bilayer meta-gel system consisting of a reaction−diffusion front layer composed of sPEG, urea, and urease, and a pH-responsive layer composed of poly(acrylamide-*co*-acrylic acid) (poly(AAm-*co*-AA)). (ii) Snapshots showing one-cycle bending behavior, triggered by internal OH^- amplification via the urea−urease reaction initiated by a high-pH hydrogel. Panel (b) is reproduced with permission from ref 202. Copyright 2015 John Wiley and Sons. Panel (c) is reproduced with permission from ref 204. Copyright 2017 John Wiley and Sons. Panel (d) is reproduced with permission from ref 205. Copyright 2017 John Wiley and Sons. Panel (e) is reproduced with permission from ref 206. Copyright 2022 American Chemical Society. Panel (f) is reproduced with permission from ref 207. Copyright 2024 licensed under CC 4.0 Springer Nature.

These approaches demonstrate how fuel consumption and regulation can be precisely controlled through the design of independent sequential reactions.

5.3. Deactivator-driven Reactions

Deactivator-driven reactions represent a subclass of one-cycle self-regulation, often utilizing enzyme-driven catalytic reactions to induce transient structural changes. Initially, a pH shift is triggered by introducing a promoter (e.g., acid or base) and placing the system into a transient activated state. Subsequently, enzymatic reactions—typically catalyzed by urease,[202−214] invertase (Inv), or glucose oxidase (GOx)[215−218]—generate deactivators such as ammonia, fructose, or gluconic acid, respectively. These deactivators gradually reverse the initial pH change, returning the system to its original state. By temporally separating the promoting and deactivating processes, deactivator-driven reactions enable precise, one-cycle self-regulation.

Urease plays a crucial role by catalyzing the hydrolysis of urea into ammonia (NH_3, the deactivator) and carbon dioxide (CO_2).[219,220] As illustrated in Figure 11a(i), the system

https://doi.org/10.1021/acs.chemrev.5c00358
Chem. Rev. XXXX, XXX, XXX−XXX

initially resides in a high-pH state, where urease remains inactive due to its pH-dependent catalytic profile (Figure 11a(ii)). Upon injection of a promoter (①), such as citric acid, the pH rapidly decreases, driving the system into a low-pH state (②). This acidic environment activates urease, bringing it into its optimal activity range near a neutral pH. The active enzyme catalyzes the hydrolysis of urea, generating NH_3 and CO_2 (③). NH_3 counteracts the effect of the promoter by gradually increasing the local pH, further enhancing urease activity and establishing a self-reinforcing positive feedback loop (Figure 11a(ii), orange line). The reaction continued until urease exited its active pH range, causing the reaction to self-limit. Consequently, the system autonomously returns to its original high-pH state (④) completing a self-regulated one-cycle transition without additional inputs. This mechanism enables dynamic modulation of material properties in hydrogel actuators, particularly observed by changes in storage modulus (G'), volume, and bending angle (Figure 11a(iii)).

Heuser et al. introduced a urease-catalyzed self-regulating sol−gel−sol transition behavior (Figure 11b).[202] They selected Fmoc-L-G-OH (Fmoc = fluorenylmethoxycarbonyl, L = leucine, G = glycine), which self-assembles into well-defined twisted ribbon-type nanofibrils and hydrogels at low pH upon removal of electrostatic repulsion at the carboxylate groups (Figure 11b(i)).[221] An initial solution containing 0.6 wt % Fmoc-L-G-OH and 0.8 g/L urease was prepared, into which a fuel mixture of 60 mM urea and 12 mM citric acid/sodium citrate (CA/Na_3C, 9:1) buffer was subsequently added. This fuel addition established a transient pH profile, rapidly dropping from pH 9.5 to 3.5 within 0.1 min and then gradually recovering to above 8.5 after approximately 20 min, triggering gel formation followed by spontaneous disassembly. The system rapidly transitions from sol to gel, forming a self-supporting hydrogel, and then reverts to the sol state within approximately 46 min. Rheological analysis revealed that G' sharply increased to above 2000 Pa within ∼3 min after fuel addition, surpassing the loss modulus (G'') and indicating the formation of a robust gel state. However, after ∼20 min, G' dropped below 1 Pa, falling beneath G'', corresponding to a return to the sol state. This behavior was confirmed by simple tube-inversion tests (Figure 11b(ii)). Analogously, transient supramolecular hydrogels were developed using benzyloxycarbonyl-L-phenylalanine (Cbz-Phe), which self-assembled into densely entangled nanofibers under acidic conditions via hydrogen bonding and $\pi-\pi$ interactions.[203] Rapid acidification induced fibrillation and gelation, while a subsequent generation of ammonia from urea led to a pH increase, resulting in defibrillation and gel collapse.

They further applied urease-catalyzed one-cycle regulation to pH-responsive photonic gels composed of polystyrene-*b*-poly(2-vinylpyridine) (PS-*b*-P2VP) diblock copolymers.[204] These copolymers self-assemble into lamellar mesophase structures, allowing selective hydrophobic/hydrophilic switching of the P2VP layers (Figure 11c). Under neutral or high pH conditions, the photonic film remained dry and transparent. However, when the pH is reduced below the apparent pK_a of P2VP (∼3.2), protonation of pyridine groups leads to anisotropic swelling of the P2VP layers, thereby inducing a photonic bandgap in the visible spectrum and a reflective color appearance at approximately 560 nm (Figure 11c(i)).[222] A film prepared by depositing a 50 mg/mL PS-*b*-P2VP solution onto a glass substrate was immersed in an aqueous solution containing urease. By fueling the system with a chemical mixture containing urea (60 mM) and citric acid/sodium citrate buffer (4 mM CA/Na_3C, CA:Na_3C = 0.95:0.05), the initial pH drops triggered swelling in the photonic layer, activating urease. This enzymatic reaction increased the pH, reversing the swelling and causing shrinkage of the P2VP layers, thus autonomously reverting the gel to its transparent state autonomously. This strategy was further extended to demonstrate the first example of patterned, self-regulating photonic displays (Figure 11c(ii)). A photonic mirror composed of PS-*b*-P2VP was selectively masked with a PDMS film patterned with three distinct letters. By immersing this device into pH-fueled solutions containing varying urease concentrations (0.30, 0.15, and 0.10 g/L), each letter exhibited a reflective state with individually programmed lifetimes of approximately 10, 45, and 113 min, respectively.

Che et al. developed a one-cycle self-regulating "breathing" microgel system composed of poly(*N*,*N*-diethylaminoethyl methacrylate) (poly(DEAEMA)) and covalently immobilized urease (Figure 11d).[205] Protonation and deprotonation of poly(DEAEMA) chains in response to pH changes enabled reversible swelling and shrinkage of the microgel particles, resulting in dynamic size modulation and fluorescence switching (Figure 11d(i)). To drive one-cycle regulation, the system was fueled with urea (60 mM) and citric acid/sodium citrate buffer (9 mM CA/Na_3C, CA:Na_3C = 9:1). Urease was covalently immobilized within the microgel at a concentration of 0.6 mg/mL. The acidic buffer initially induced the protonation and swelling of poly(DEAEMA), simultaneously activating urease to catalyze the decomposition of urea into ammonia. The resulting base generation caused the microgels to shrink (Figure 11d(ii)). Consequently, the microgel exhibited reversible swelling−shrinking and fluorescence on/off behavior. Upon repeated fuel injections, the microgel showed continuous, periodic modulation of the fluorescence intensity with a characteristic cycle period of approximately 45 min. The microgel size reversibly increased up to approximately 820 nm and subsequently decreased to about 420 nm, maintaining consistent size oscillations over multiple fuel additions (Figure 11d(iii)).

Recently, Zhang et al. explored bilayer hydrogel actuators that utilize swelling−shrinking behavior, leveraging temporally programmed responses for dynamic shape transformations (Figure 11e).[206] One such system integrated pH-responsive poly(dimethylaminoethyl methacrylate) (poly(DMAEMA))) hydrogel layer with a nonresponsive layer containing immobilized urease (4 mg/mL). Upon fueling with acidic urea solution (9.5 mM), the actuator underwent initial swelling due to acid-induced protonation, followed by enzymatic ammonia production, gradually increasing the pH and triggering shrinking (Figure 11e(i)). The curvature of the bilayer changed from 0 m^{-1} (flat) to approximately 50 m^{-1} within 40 min before gradually returning to a flat state within 220 min. Furthermore, star-shaped bilayer actuators exhibited protective folding under acidic conditions induced by the promoter, subsequently recovering their original shape as the pH returned to neutral, with complete recovery occurring after approximately 160 min (Figure 11e(ii)).

Dúzs et al. also developed self-regulating bilayer hydrogel actuators termed metagels by integrating layered hydrogels with embedded chemical circuitry for spatiotemporal feedback control (Figure 11f).[207] The system comprises a front layer of star-shaped PEG (sPEG) containing urease (1.34 g/L) and urea (55 mM) and a responsive layer composed of poly(AAm-

https://doi.org/10.1021/acs.chemrev.5c00358
Chem. Rev. XXXX, XXX, XXX−XXX

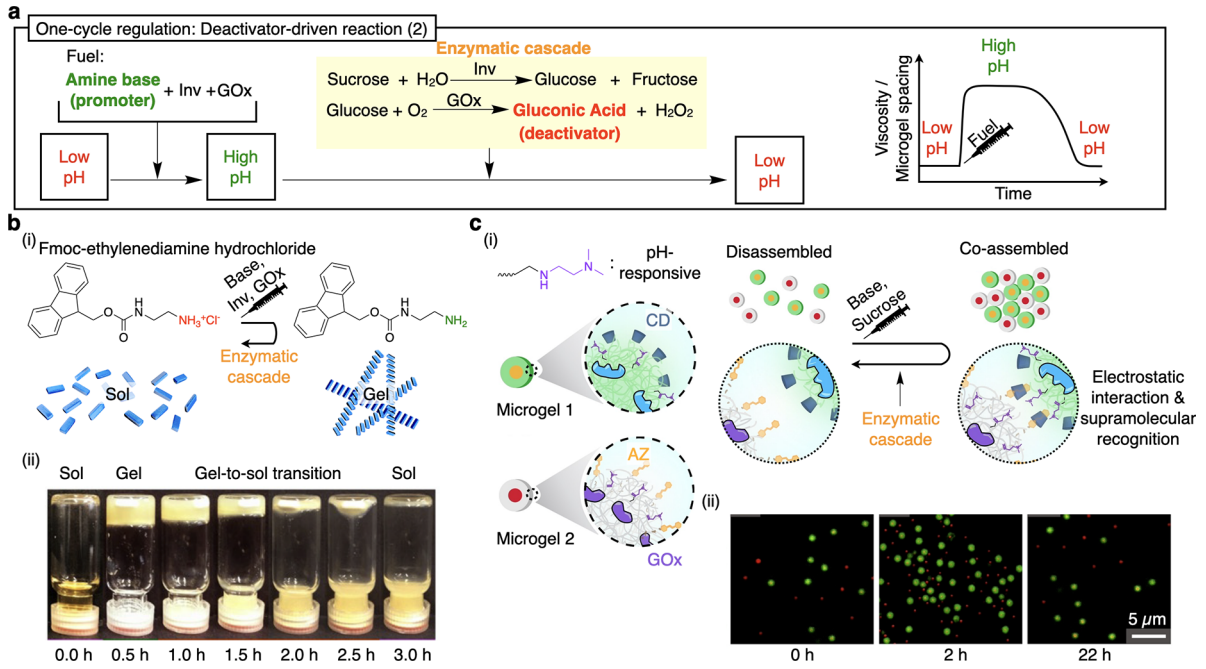

Figure 12. Self-regulating hydrogels with one-cycle reaction via deactivator-driven enzymatic cascades. (a) Schematics of the deactivator-driven enzymatic cascades composed of invertase (Inv) and glucose oxidase (GOx), enabling one-cycle regulation. Addition of an amine base (promotor), Inv, and GOx initially increases the pH, which is subsequently decreased through the enzymatic cascade, resulting in a transient pH cycle that drives reversible hydrogel transitions. Schematic graph showing time-dependent one-cycle regulation of viscosity and microgel spacing. (b) (i) Molecular structure of Fmoc-ethylenediamine hydrochloride, a pH-responsive gelator that self-assembles into nanofibrillar hydrogels under basic conditions (pH > 8.4). (ii) Snapshots showing a one-cycle sol−gel−sol transition, driven by base, Inv, and GOx fueling, highlighting sol−gel−sol transition. (c) (i) Schematic of a chemo-structural feedback system based on pH-responsive microgels, where microgel 1 (functionalized with CD) and microgel 2 (modified with AZ) undergo coassembly at high pH through host−guest interactions. The enzymatic production of gluconic acid triggers disassembly, completing one-cycle regulation. (ii) Confocal laser scanning microscopy (CLSM) images showing one-cycle reversible coassembly and disassembly, with time-dependent changes in microgel spacing visualizing the enzymatic cascade. Panel (b) is reproduced with permission from ref 215. Copyright 2021 John Wiley and Sons. Panel (c) is reproduced with permission from ref 216. Copyright 2022 John Wiley and Sons.

co-AAc) (Figure 11f(i)). Upon contact with a high-pH hydrogel piece, 2.40 mM NaOH was introduced, and OH^- diffused into the front layer, triggering autocatalytic OH^- production via the urea−urease reaction and initiating a reaction-diffusion wave across the device. This chemical amplification activated swelling in the adjacent pH-sensitive poly(AAm-*co*-AAc) hydrogel layer. Initially, osmotic pressure from ion generation caused slight rightward bending (0−10 min). As OH^- diffused further, deprotonation of AAc moieties induced substantial swelling, causing the bend to shift from rightward to leftward over 120 min (Figure 11f(ii)).

Glucose oxidase (GOx) and invertase (Inv) are widely utilized in deactivator-driven one-cycle regulation due to their capability to generate acidic byproducts (deactivator) through an enzymatic cascade. As depicted in Figure 12a, this cascade initiates from a high-pH state maintained by an amine base (promoter). Upon the introduction of sucrose as a chemical fuel, Inv catalyzes its hydrolysis into glucose and fructose. Subsequently, glucose is oxidized by GOx, yielding gluconic acid, a deactivator that progressively lowers the system's pH. This acidification eventually overrides the promoter's effect, inducing a directional pH shift. As the environment becomes increasingly acidic, enzyme activities decline as they exit their optimal pH ranges, naturally terminating the cascade. This multistep enzymatic cascade allows precise one-cycle pH modulation, driving sol−gel−sol or disassembly−assembly−disassembly transitions in hydrogels, which can be tracked via time-dependent viscosity changes or variations in microgel spacing.

Fan et al. developed an enzymatic cascade-based logic gate system to control transient pH signals and sol−gel−sol transitions (Figure 12b).[215] Their system, comprising 1 wt % Fmoc-ethylenediamine hydrochloride, initially existed in a sol state under mildly acidic conditions (pH 3.0, 1.5 mM CA/Na_3C buffer). The addition of fuel (100 mM sucrose, 20 mM Tris(hydroxymethyl)aminomethane (Tris) buffer as a pH promoter, 0.60 g/L invertase, and 1.40 g/L glucose oxidase) established a transient pH profile, rapidly increasing from pH 3.0 to 8.8 within 0.1 min, followed by a gradual decrease to around 3.5 over several hours due to gluconic acid production by enzymatic cascade reactions (Figure 12b(i)). To illustrate environmental robustness, sucrose was replaced with beet syrup, enabling the system to function effectively even in complex media, such as milk. Transient hydrogels formed exclusively in the presence of both enzymes, validating the necessity of a full enzymatic cascade for effective one-cycle regulation. The gel lifetime, approximately 3 h as shown in Figure 12b(ii), could be finely adjusted from 15 min to over 24 h by modifying enzyme concentrations. The sol−gel−sol transitions were visually confirmed using tube-inversion tests and quantitatively tracked through time-dependent viscosity changes.

Sharma et al. further developed a chemo-structural feedback system utilizing pH-responsive microgels capable of transient coassembly and spontaneous disassembly via enzyme-gener-

https://doi.org/10.1021/acs.chemrev.5c00358
Chem. Rev. XXXX, XXX, XXX−XXX

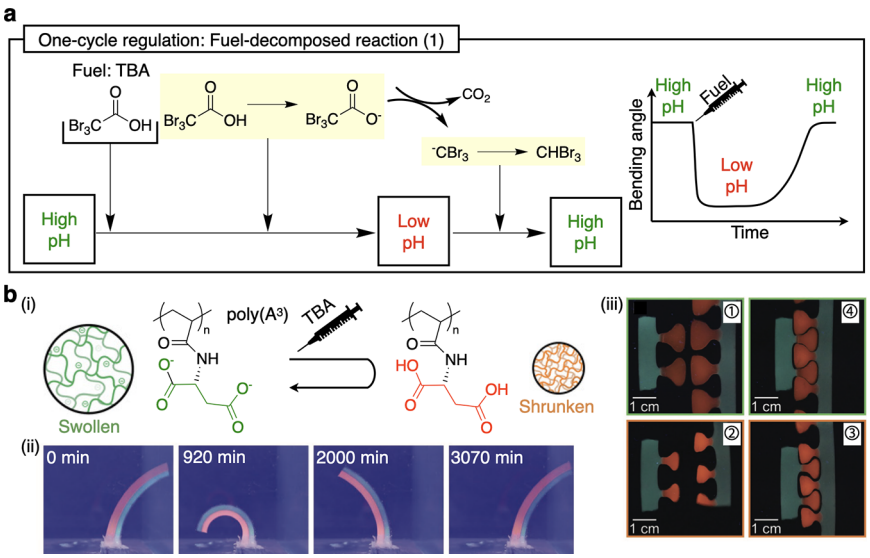

Figure 13. Self-regulating hydrogels with a one-cycle reaction via a fuel-decomposed chemical reaction. (a) Schematics of the self-decarboxylating reaction triggered by tribromoacetic acid (TBA), enabling one-cycle regulation. Upon TBA injection, transient acidification occurs through spontaneous decarboxylation, which is followed by spontaneous pH recovery, leading to time-programmed deformation of hydrogel actuators. The right graph shows the time-dependent one-cycle regulation of the bending angle of hydrogels. (b) (i) Schematic illustration of the pH-responsive behavior of poly(aspartic acid) (polyA^3) hydrogels. At high pH, deprotonated carboxylate groups induce swelling, whereas at low pH, protonation causes the hydrogel to shrink. (ii) Time-series images showing a one-cycle self-regulating behavior of a bilayer actuator composed of a polyA^3 responsive layer and a passive layer, driven by TBA-fueled transient acidification. (iii) Self-regulating interlocking of complementary hydrogel puzzle pieces through a one-cycle shrinking−swelling process. ① Unfueled pieces remain misaligned. ② TBA fueling induces contraction of hydrogel heads. ③ Contracted pieces interdigitate. ④ Reswelling irreversibly locks the interlocked structure in place. Panel (b) is reproduced with permission from ref 223. Copyright 2022 John Wiley and Sons.

ated acidification (Figure 12c).[216] Two distinct types of core−shell microgels (MGs) were synthesized: microgel 1 was functionalized with α-cyclodextrin (CD), N,N-dimethylethylenediamine, and immobilized Inv (0.2 mg/mL), whereas microgel 2 was modified with azobenzene (AZ), the same amine base, and immobilized GOx (0.2 mg/mL) (Figure 12c(i)). The complementary host−guest interactions between CD and AZ units facilitated selective coassembly. Initially, under acidic conditions (1.5 mM citric acid/sodium citrate buffer (CA/Na_3C, pH 3.5)), electrostatic repulsion among the weak cationic groups (−$N(Me)_2$) prevented the microgels from assembling, maintaining them as dispersed. Upon fueling with a chemical mixture consisting of tris buffer (20 mM, pH 8.8) and sucrose (200 mM), the resulting pH increase promoted coassembly via electrostatic attraction and host−guest interactions between CD and AZ units. In the coassembled state, spatial proximity between enzyme-loaded microgels enhanced the enzymatic cascade, where Inv converted sucrose into glucose, subsequently oxidized by GOx into gluconic acid. The resultant pH decrease disrupted the supramolecular interactions and electrostatic attraction, leading to spontaneous disassembly. This dynamic behavior was directly visualized via confocal laser scanning microscopy (CLSM), showing reversible coassembly and dispersion of labeled microgels (Figure 12c(ii)). The system exhibited a lifetime of approximately 780 min, significantly shorter than a control system lacking coassembly capabilities.

5.4. Fuel-Decomposed Reactions

Fuel-decomposed reactions represent a crucial subclass of one-cycle self-regulation, wherein transient hydrogel states are driven by chemical fuels that undergo intrinsic chemical decomposition[223] or enzymatic degradation.[224−226] The return to the original state occurs spontaneously without additional external stimuli, as it is driven by the internal consumption of the fuel itself.

A representative example is the self-decarboxylation of tribromoacetic acid (TBA) (Figure 13). Upon addition to an alkaline medium, TBA rapidly deprotonates to tribromoacetate, which subsequently undergoes spontaneous decarboxylation. This decarboxylation forms a carbanion intermediate, which quickly scavenges a proton from solution, ultimately yielding bromoform ($CHBr_3$) as a neutral product (Figure 13a).[227] During this process, the pH initially decreases sharply, inducing shrinkage of responsive hydrogels by protonation. As decarboxylation progresses and the acidic fuel is gradually consumed, the pH autonomously returns to its original alkaline state, completing a one-cycle self-regulation loop.

Fusi et al. demonstrated this mechanism using TBA to control self-regulating actuation in poly(aspartic acid) (polyA^3) hydrogels (Figure 13b).[223] PolyA^3 hydrogels swell at high pH due to ionization of carboxylate groups and shrink at lower pH through protonation (Figure 13b(i)). Upon injection of TBA, the pH rapidly decreased from an initial value of approximately 7.0 to ∼3.0, and this acidic state persisted for about 250 min (∼4 h). Subsequently, due to the decarboxylation of TBA, the pH gradually increased, enabling spontaneous recovery. Using bilayer actuators composed of a polyA^3 responsive layer and poly(2-acrylamido-2-methylpropanesulfonic acid) (poly(AMPS)), addition of TBA (5.0 mM) induced bending, a maximum deformation of approximately 140° at ∼2000 min, followed by recovery at ∼3070 min (Figure 13b(ii)). This self-regulation enabled complex functions such as interlocking hydrogel-based puzzle pieces, illustrating the system's potential for programmable actuation tasks autonomously (Figure 13b(iii)).

https://doi.org/10.1021/acs.chemrev.5c00358
Chem. Rev. XXXX, XXX, XXX−XXX

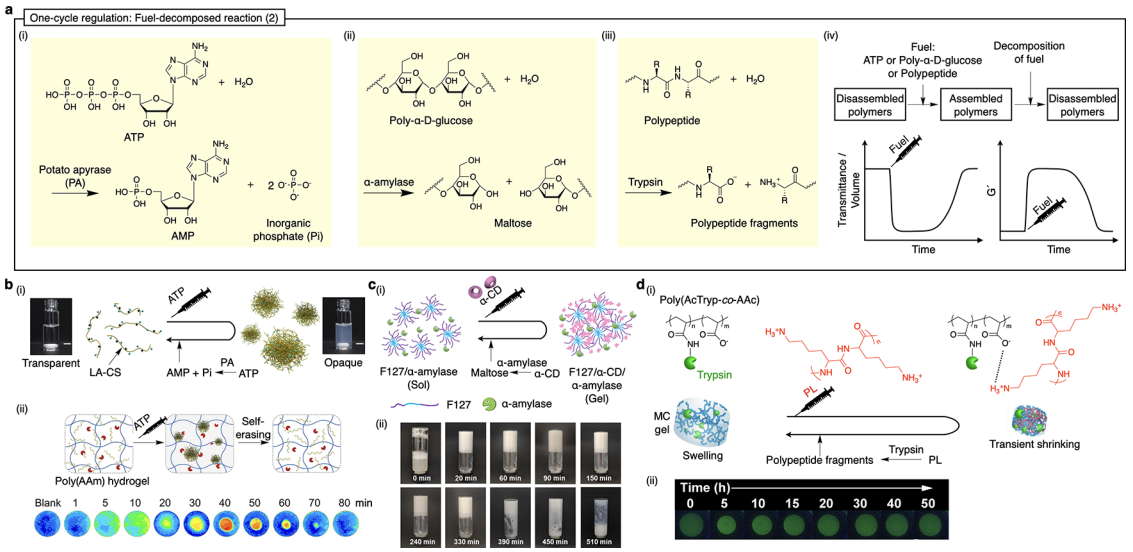

Figure 14. Self-regulating hydrogels with a one-cycle reaction via fuel-decomposed enzymatic reaction. (a) Schematics of fuel-decomposed enzymatic reactions catalyzed by (i) potato apyrase (PA), (ii) α-amylase, and (iii) trypsin, enabling one-cycle regulation. (iv) Chemical fuels such as ATP, poly-α-D-glucose, or polypeptides induce transient structural changes, which are autonomously reversed by enzymatic degradation of the fuel. The graph shows time-dependent one-cycle regulation of transmittance or volume or G'. (b) (i) Schematic of transient nanoparticle formation and disassembly driven by ATP as a fuel. ATP electrostatically complexes with lactobionic acid-modified chitosan (LA-CS), inducing turbidity. Over time, PA catalyzes ATP hydrolysis into AMP and Pi, depleting the fuel and restoring hydrogel transparency. (ii) Time-lapse images of the hydrogel labeled with pseudocolors, showing self-regulation of opaqueness. (c) (i) Schematic of transient supramolecular hydrogels based on α-CD-fueled host−guest interactions. α-CD forms inclusion complexes with the PEO chains of Pluronic F127, inducing gelation. Embedded α-amylase enzymatically degrades α-CD over time, depleting the fuel and causing gel collapse. (ii) Optical images showing the appearance of the F127/α-CD/α-amylase system at different times after fuel addition, visualizing the complete sol−gel−sol cycle. (d) (i) Schematic of one-cycle shrinking−swelling behavior in a metabolic cycle-inspired hydrogel (MC gel) composed of acrylic acid (AAc) and acrylamide−trypsin conjugate (AcTryp). Fueling with poly-L-lysine (PL) induces gel shrinking via electrostatic cross-linking, followed by autonomous reswelling triggered by enzymatic degradation of PL into short peptides by embedded trypsin. (ii) Time-dependent volume change of the MC gel, showing a full one-cycle transition from shrinkage to recovery upon PL fueling. Panel (b) is reproduced with permission from ref 224. Copyright 2023 John Wiley and Sons. Panel (c) is reproduced with permission from ref 225. Copyright 2022 John Wiley and Sons. Panel (d) is reproduced with permission from ref 226. Copyright 2022 John Wiley and Sons.

One-cycle regulation can also be achieved through enzymatic digestion of molecular or polymeric fuels (Figure 14). Representative examples include potato apyrase (PA)-mediated ATP-consuming reactions, controlling host−guest interaction by α-amylase, and enzymatic degradation of polycations using trypsin. Specifically, PA functions by gradually decomposing ATP in solution into adenosine monophosphate (AMP) and two molecules of orthophosphate (Pi), thereby reducing the multivalency and binding capacity of the fuel over time (Figure 14a(i)).[228] In an analogous mechanism, α-amylase catalyzes the hydrolysis of poly-α-D-glucose into maltose (Figure 14a(ii)).[229] Similarly, trypsin catalyzes the stepwise cleavage of polypeptide chains into short polypeptide fragments (Figure 14a(iii)).[230] These mechanisms are utilized in one-cycle self-regulating systems, where injection of ATP or polypeptide into initially disassembled polymer networks induces the rapid association and formation of assembled structures via electrostatic interactions. As the enzymatic digestion proceeds, the fuel is consumed and the system autonomously returns to its original disassembled state. This dynamic process enables time-dependent one-cycle regulation of physical properties such as transmittance or gel volume or G' (Figure 14a(iv)).

Li et al. developed a dissipative self-assembly system that couples ATP-triggered nanoparticle formation with enzymatic fuel decomposition to regulate hydrogel properties (Figure 14b).[224] In this design, lactobionic acid-modified chitosan (LA-CS, 0.16 wt %) undergoes rapid electrostatic complexation with ATP, leading to the formation of transient nanoparticles. These nanoparticles induce light scattering and opacification of the solution or hydrogel matrix. Over time, potato apyrase (PA) catalyzes the hydrolysis of ATP into AMP and Pi, thereby disassembling the nanoparticles. This one-cycle results from transparent to opaque and back to transparent (Figure 14b(i)). Upon addition of 5 μL of 60 mg/mL ATP with potato apyrase concentrations of 5 U/mL into the hydrogels, the opacity gradually increased, reaching its maximum intensity after about 40 min, followed by recovery of transparency within about 80 min (Figure 14b(ii)). The grayscale intensity changed from approximately 0 to between 40 and 100 during a single cycle. This system exemplifies precise self-regulation of hydrogel transparency mediated by enzymatically controlled transient self-assembly.

Lu et al. developed a host-fueled transient supramolecular hydrogel system in which α-cyclodextrin (α-CD) acts as a chemical fuel to drive gelation via host−guest interactions with Pluronic F127 (Figure 14c).[225] In this design, the poly(ethylene oxide) (PEO) chains of F127 thread into the hydrophobic cavity of α-CD, forming pseudopolyrotaxane structures that promote supramolecular cross-linking and induce gelation.[231] The embedded enzyme α-amylase gradually hydrolyzes α-CD into maltose, thereby depleting the fuel and disrupting the host−guest network. This process enables an autonomously timed sol−gel−sol transition (Figure 14c(i)). As shown in Figure 14c(ii), the system rapidly transitions from a transparent solution to an opaque hydrogel within 20 min

https://doi.org/10.1021/acs.chemrev.5c00358
Chem. Rev. XXXX, XXX, XXX−XXX

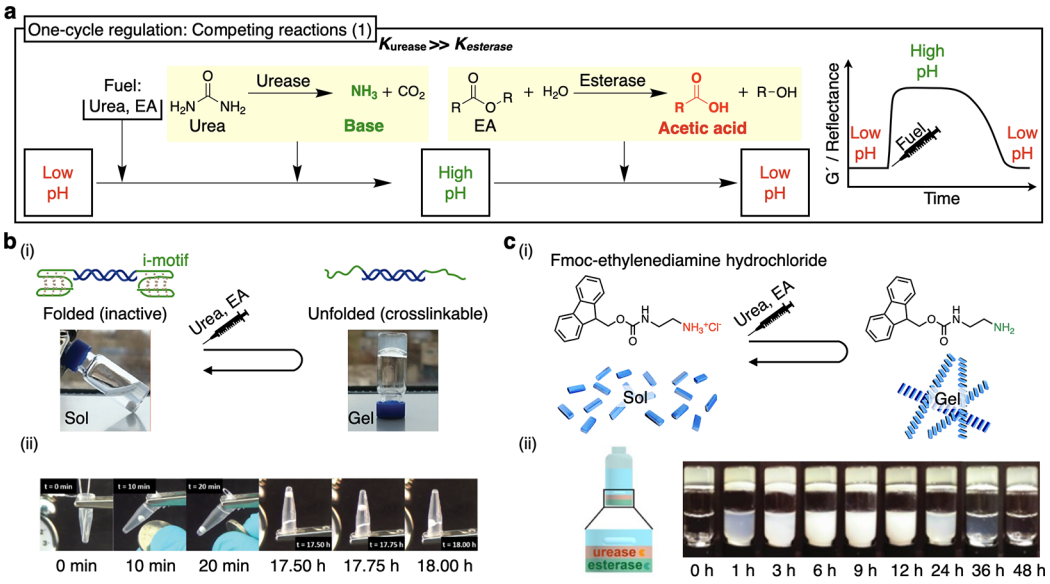

Figure 15. Self-regulating hydrogels with a one-cycle reaction via competing reactions of enzymes. (a) Schematics of the urease- and esterase-catalyzed enzymatic reactions for one-cycle self-regulation. Fueling with urea and ethyl acetate initiates opposing pH-modulating reactions, where urease produces ammonia to raise pH and esterase generates acetic acid to lower pH, enabling a temporally programmed one-cycle transition. (b) (i) Schematic of a pH-responsive DNA hydrogel cross-linked by i-motif sequences. Urea and ethyl acetate act as fuels for urease- and esterase-catalyzed reactions, respectively, inducing reversible sol–gel–sol transitions through sequential pH shifts. (ii) Tube inversion test showing a one-cycle gelation and disassembly process, driven by enzymatic fuel consumption. (c) (i) Schematic of transient Fmoc-ethylenediamine assembly controlled by a compartmentalized hydrogel containing esterase and urease in layered domains. Fueling triggers spatially modulated pH gradients, leading to temporary self-assembly in the supernatant. (ii) Time-lapse images showing turbidity changes, reflecting one-cycle peptide aggregation and disassembly regulated by enzymatic reaction timing. Panel (b) is reproduced with permission from ref 238. Copyright 2017 American Chemical Society. Panel (c) is reproduced with permission from ref 240. Copyright 2020 John Wiley and Sons.

after α-CD addition, accompanied by an increase in G' from approximately 400 to 45,000 Pa within 90 min, and returns to a sol state after approximately 390 min as the α-CD is enzymatically consumed. The gelation and degradation processes are fully reversible upon refueling with α-CD.

In another study using α-amylase, Li et al. recently reported the use of γ-cyclodextrin (γ-CD) as a biocompatible chemical fuel.[232] In this system, γ-CD forms transient host–guest complexes with the hydrophobic C18 side chains of a poly(AAc)-based hydrogel, disrupting the hydrophobic domains and inducing gel disassembly. Over time, the enzyme α-amylase gradually degrades γ-CD, allowing the hydrophobic interactions to reform and restore the gel state.[233−237]

Nakamoto et al. developed a biomacromolecule-fueled hydrogel system that undergoes a one-cycle transient volume phase transition in response to poly-L-lysine (PL) as a polymeric fuel (Figure 14d).[226] The system employs a metabolic-cycle-inspired hydrogel (MC gel) incorporating AAc (50 g/L) for PL affinity and acrylamide-functionalized trypsin (AcTryp, 1 g/L) for enzymatic digestion. Upon PL (2 g/L) fueling, the negatively charged hydrogel forms electrostatic cross-links with PL, leading to macroscopic shrinkage due to network densification (Figure 14d(i)). As embedded trypsin digests PL into oligolysine fragments that cannot maintain cross-linking, the hydrogel spontaneously reswells. This dynamic behavior proceeds with rapid shrinkage, followed by slower reswelling, determined by the fuel concentration and digestion kinetics. At a PL concentration of 2 g/L, the gel volume decreased to ∼43% within 2 h and recovered to ∼94% over ∼50 h (Figure 14d(ii)). This system demonstrates one-cycle self-regulation driven solely by the interplay between multivalent binding and enzymatic fuel decomposition.

5.5. Competing Reactions

One-cycle regulation can also be achieved by systems coupling two reactions with opposing effects and distinct kinetic profiles. These reactions broadly fall into two categories: enzyme-based systems (Figure 15)[238−240] and kinetically mismatched photoresponsive systems (Figure 16).[241] In enzyme-based systems, two enzymes with distinct kinetics act on different substrates, generating pH changes in opposite directions. Photoresponsive systems, on the other hand, employ two photoisomerizable components exhibiting different kinetic responses to the same light stimulus, resulting in time-dependent variations in net charge or hydrophilicity.

First, enzyme-based systems utilize kinetic asymmetry between enzymes to control pH dynamics. As illustrated in Figure 15a, urease hydrolyzes urea to produce ammonia (NH_3) and carbon dioxide (CO_2), causing a rapid pH increase. Subsequently, esterase hydrolyzes ethyl acetate (EA) into acetic acid and ethanol, gradually decreasing the pH and reversing the initial response. This transient behavior arises because urease acts rapidly under mildly acidic conditions, whereas esterase proceeds more slowly over a broader pH range. By adjusting enzyme ratios, fuel amounts, and buffer capacity, the duration and magnitude of the high-pH state can be finely tuned.[242] This competitive enzymatic strategy enables dynamic hydrogel transitions, trackable through time-dependent changes in G' and optical reflectance.

Heinen et al. developed a self-regulating DNA hydrogel system by integrating a biocatalytic pH-feedback network with a pH-responsive, i-motif cross-linked poly(AAm) hydrogel.[238] The i-motif DNA domains exhibit pH-dependent folding behavior; at low pH (approximately 4.5), the i-motif folds into an intramolecular quadruplex structure, preventing hybrid-

https://doi.org/10.1021/acs.chemrev.5c00358
Chem. Rev. XXXX, XXX, XXX−XXX

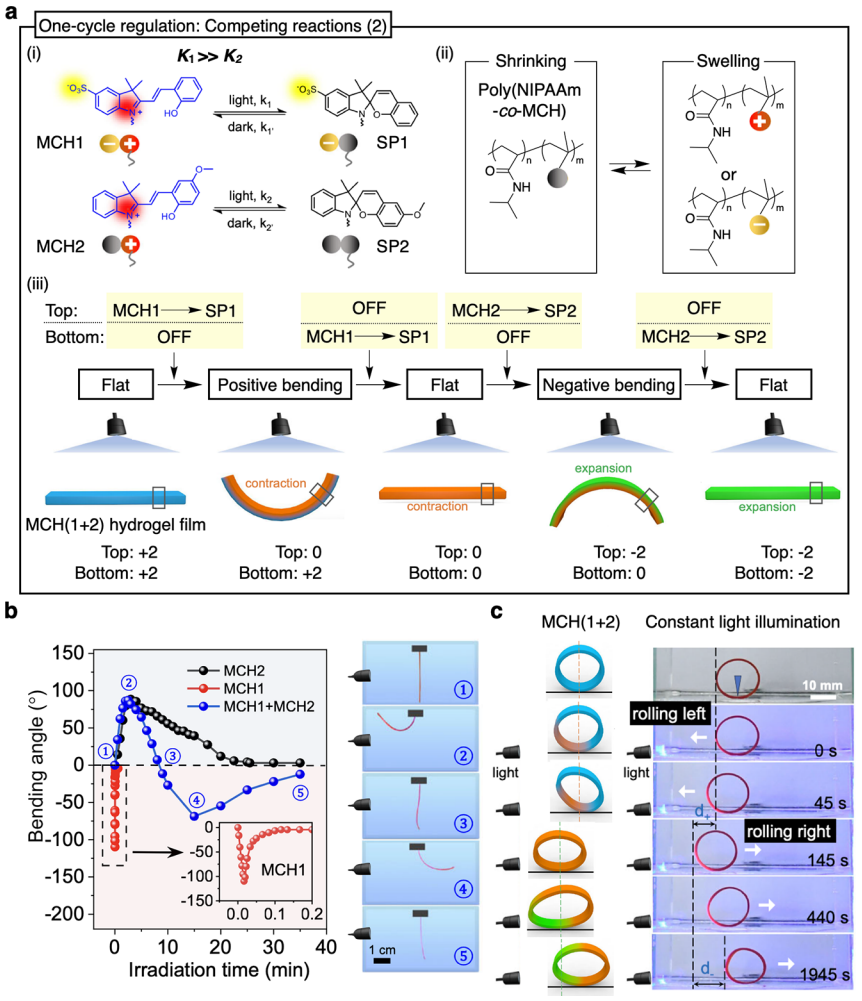

Figure 16. Self-regulating hydrogels with one-cycle reaction via competing reactions of photoisomerizations. (a) (i) Chemical structures and photoinduced charge transitions of MCH1 and MCH2. Upon visible light irradiation, MCH1 rapidly converts from a zwitterionic to a negatively charged spiropyran, while MCH2 slowly transitions from a positively charged to a neutral form. (ii) Schematic of a poly(NIPAAm-*co*-MCH), exhibiting light-driven swelling−shrinking behavior governed by net charge variation. (iii) Schematics showing asymmetric charge transitions across the MCH(1+2) hydrogel film under constant illumination, generating a transient top-to-bottom gradient and inducing bidirectional one-cycle bending deformation. (b) Bending angle plot of an MCH(1+2) hydrogel film under constant illumination, showing sequential positive and negative curvature, completing one full cycle of bidirectional actuation. (c) Rolling behavior of an O-ring-shaped MCH(1+2) hydrogel actuator, demonstrating one-cycle bidirectional locomotion under constant illumination. The actuator initially rolls in one direction and subsequently reverses, completing a full locomotion cycle. Panels (a), (b), and (c) are reproduced with permission from ref 241. Copyright 2024 licensed under CC 4.0 Springer Nature.

ization and maintaining the hydrogel in a sol state (Figure 15b(i)). Upon introduction of chemical fuels consisting of urea (60 mM) and ethyl acetate (EA, 240 mM), with enzymes urease (0.6 g/L) and esterase (0.5 g/L), the urease-driven hydrolysis of urea initially elevated the pH from 4.5 up to approximately 8.5 within ~20 min, unfolding the i-motif. This structural change enables hybridization between the i-motif DNA cross-linker and complementary strands embedded in the polyacrylamide backbone, triggering a sol-to-gel transition. Over time, the esterase-mediated hydrolysis of EA gradually decreased the pH back to around 4.75 after approximately 17.5 h, prompting the refolding of the i-motif structures and restoration of the initial sol state. Through precise tuning of buffer conditions and enzyme proportions, distinct lag times and gel durations can be programmed. A representative setup demonstrated a lag phase of approximately 20 min followed by a transient gel phase lasting about 17.5 h, during which the G' significantly increased from approximately 1 Pa (sol state) to around 60 Pa (gel state), underscoring the system's robust programmability and controlled responsiveness (Figure 15b-b(ii)). Furthermore, Bashir et al. demonstrated reversible control of sol−gel−sol transitions of PVA−borate hydrogels based on a similar mechanism.[239]

As shown in Figure 15c, Fan et al. designed a compartmentalized trilayer hydrogel system to achieve one-cycle control over Fmoc-ethylenediamine hydrochloride self-assembly similar to Figure 12b.[240] One typical setup spatially separated urease and esterase into distinct hydrogel layers: urease (0.3 mg/mL) was embedded in the top hydrogel layer and esterase (0.7 mg/mL) in the bottom layer. Upon fueling with urea (12.5 mM) and ethyl acetate (EA, 187.5 mM), urease in the upper layer rapidly converted urea into ammonia, increasing the pH and inducing peptide self-assembly and gelation. The concentration of Fmoc-ethylenediamine hydrochloride was 0.3 wt %. Subsequently, esterase-generated acetic acid diffused upward, gradually decreasing the pH and

https://doi.org/10.1021/acs.chemrev.5c00358
Chem. Rev. XXXX, XXX, XXX−XXX

Table 3. Representative Examples of Self-Regulating Hydrogel Actuators Exhibiting One-Cycle Regulation

Category	Hydrogel matrix	Hydrogel type	Regulating fuels	Regulating period	Regulation degree	Deformation type	Applications	ref
Independent Sequential Reactions	SachCHO hydrogelator	-	DT	60 s−75 min	G' change (Maximum: 2100 Pa)	Gel−sol−gel	Long distance signal transport viapropagating pH waves	185
	Poly(AAc) hydrogel/PDMS	Sheet gel (35 mm × 5 mm × 5 mm)	EDC	4−8 h	Bending angle change (0 to ∼37°)	Swelling−shrinking	Self-resettable soft robots	186
	Fmoc-AAE	-	EDC	200 min	G' change (∼0.01 to ∼40−100 Pa)	Sol−gel−sol	Self-erasing inks witha tunable lifetime	187
	sPEG-SH	-	H_2O_2	900−1500 min	G' change (∼0.1 to ∼650 Pa)	Sol−gel−sol	-	188
Deactivator-driven Reactions	Fmoc-L-G-OH	-	Acid + Urea	20 min−11 h	G' change (1 to 2000 Pa)	Sol−gel−sol	Fluidic guidance, burst release, transient prototyping	202
	Cbz-Phe	-	Acid + Urea	∼30 min	Fluorescence intensity change (∼45% decrease)	Sol−gel−sol	-	203
	PS-*b*-P2VP	Sheet gel (thickness = ∼1 μm)	Acid + Urea	10 min−4 h	λ change (490 to 590 nm)	Swelling−shrinking	Time-programmed self-erasing memories, photonic informationpatterning	204
	Poly(DEAEMA)-based hydrogel	Microgel (diameter = 420 nm)	Acid + Urea	45 min	Size change (420 to 820 nm)	Swelling−shrinking	-	205
	Poly(AAm-*co*-DMAEMA) /Poly(AAm) hydrogel	Sheet gel (40 mm × 6 mm × 4 mm)	Acid + Urea	80−220 min	Curvature change (0 to ∼60 m^{-1})	Swelling−shrinking	Pattern designing hydrogel actuators, hand-shaped hydrogel device	206
	poly(AAm-*co*-AAc)/sPEG hydrogel	Sheet gel (20 mm × 1.5 mm × 2.0 mm)	OH^-	120 min	Thickness change (22%)	Swelling−shrinking	Touching-induced bilayer actuation	207
	Fmoc-ethylenediamine	-	Sucrose or lactose + Tris buffer	15 min−24 h	-	Sol−gel−sol	Enzymatic logic gate	215
	pH-switchable microgels: functionalized CD & inv or AZ & Gox	Microgel (radius = ∼649 nm)	Sucrose + Tris buffer	22 h	-	Disassembly assembly	Transient colloidal coassemblies	216
Fuel-decomposed Reactions	Poly(A^3) hydrogel	Sheet gel (62 mm × 4 mm × 4 mm)	TBA	3070−∼5600 min	Bending angle change (0 to 150−160°)	Swelling−shrinking	Autonomous interlocking,"Fire and forget" operation	223
	Poly(AAm) hydrogel containing LA-CS	-	ATP	32.7−90.7 min	Grayscale intensity change (0 to 40−100)	Disassembly assembly	Time-and space-encoded securitylabeling	224
	Pluronic F127	-	α-CD	390 min	G' change (400 to 45000 Pa)	Sol−gel−sol	-	225
	Poly(AcTryp-*co*-AAc)-based hydrogel	Disc gel (diameter = 8 mm, thickness = 0.4 mm)	PL	50 h	Volume change (43% decrease)	Swelling−shrinking	Transient release of the payload	226
Competing Reactions	Poly(AAm) with i-motif DNA cross-linkers	-	Urea + EA	<18 h	G' change (1 to 60 Pa)	Sol−gel−sol	Transient life cycle of autonomousDNA hydrogels	238
	PVA-borate hydrogel	-	Urea + EA	∼200 min	Viscosity change (∼180 cP to 270 cP)	Sol−gel−sol	-	239
	Layered hydrogel system with Fmoc-Leu-Gly-OH	-	Urea + EA	24 h−1 week	Reflectance change (∼65 to ∼90%)	Sol−gel−sol	Time-controlled peptide self-assembly	240
	Layered hydrogel system with Fmoc-ethylenediamine hydrochloride			12 h−48 h	Reflectance change (∼50 to ∼80%)			
	Poly(NIPAAm-*co*-MCH) hydrogel	Sheet gel (30 mm × 1 mm × 0.5 mm)	Visible light	∼35 min (bending for MCH (1 + 2))	Bending angle change (90 to −75°)	Swelling−shrinking	Bidirectional bending androlling motions	241
		O-ring gel (height = 5 mm)		1945 s (O-ring)	Displacement change (80 to −50 mm)			

https://doi.org/10.1021/acs.chemrev.5c00358
Chem. Rev. XXXX, XXX, XXX−XXX

disassembling the peptide structures (Figure 15c(i)). This spatial arrangement created a time-programmed pH trajectory, resulting in the transient aggregation of amphiphilic peptides in the supernatant. The reflective state reached a maximum reflectance of approximately 80% at around 10 h after injection, decreasing back to transparent after more than 36 h (Figure 15c(ii)). Additionally, by adjustment of the order and thickness of the enzyme layers, various transient pH flips can be precisely programmed.

In addition to enzyme-based systems, one-cycle regulation can also be achieved through competing photoresponsive reactions with kinetically mismatched photoisomerization kinetics (Figure 16).[241] These systems exploit photoisomerization reactions of spiropyrans that induce time-dependent changes in the net charge of the hydrogel network.[243,244] Upon continuous light exposure, two spiropyran moieties with distinct photoisomerization kinetics undergo sequential charge transitions—one rapidly decreasing or increasing charge and the other responding more slowly. Guo et al. developed a hydrogel system incorporating two spiropyrans, MCH1 and MCH2, which exhibit opposite charge transitions upon visible light irradiation. MCH1 rapidly isomerizes from a zwitterionic merocyanine to a negatively charged spiropyran, while MCH2 slowly converts from a positively charged state to a neutral form (Figure 16a(i)). In this system, the authors used a poly(NIPAAm) hydrogel network in which two spiropyrans, MCH1 and MCH2, were uniformly copolymerized (Figure 16a(ii)). Poly(NIPAAm) hydrogel remains swollen when the network carries a net charge due to enhanced electrostatic repulsion and hydrophilicity, whereas it tends to shrink when the charge is neutralized. This kinetic mismatch leads to a sequential net charge transition from positive to neutral to negative, causing the hydrogel to first contract and then expand. This charge transition occurs asymmetrically across the hydrogel thickness due to the time-dependent penetration of light. Initially, the top layer experiences a rapid decrease in net charge (from +2 to 0) as MCH1 isomerizes, while MCH2 remains in its positively charged form. This transient neutralization leads to local contraction at the top, while the bottom layer remains positively charged, resulting in positive (upward) bending. As the illumination continues, MCH2 in the top layer slowly isomerizes to its neutral form, driving the net charge to −2. Simultaneously, the bottom layer sequentially follows the same charge transition with a delay. This reversal in the charge gradient induces negative (downward) bending, completing a full bidirectional bending cycle under constant illumination. This kinetically controlled photoisomerization strategy enables reversible one-cycle bending under constant light exposure (Figure 16a(iii)). The MCH(1+2) hydrogel exhibited clear bidirectional bending under constant illumination, with the bending angle initially reaching ∼+90° upward, then reversing direction to ∼−75° (Figure 16b). This behavior reflects the sequential contraction and expansion governed by the net charge transition across the hydrogel thickness. To further demonstrate locomotion, the hydrogel was fabricated into an O-ring shape, which showed self-regulated rolling behavior under constant light (Figure 16c). Initially, the ring rolled left due to contraction at the illuminated edge but reversed direction after 1945 s as expansion took over, completing a one-cycle bidirectional rolling motion with forward displacement of approximately 80 mm followed by backward displacement of around 50 mm.

Taken together, in this section, we summarize representative examples of one-cycle regulation, categorized according to hydrogel matrix, hydrogel type, regulating fuels, regulating period, regulation degree, deformation type, and their applications in Table 3.

6. FUTURE DIRECTIONS AND CONCLUDING REMARKS

6.1. Rebuilding Feedback Loop Architectures for Self-Regulation

Despite recent advances, significant challenges remain in improving feedback loops for self-regulating hydrogels. Mechanical and optical feedback loops rely heavily on precise spatial arrangements between the hydrogel actuator and the stimulus. They also necessitate rapid responsiveness from hydrogels, thus making the development of responsive hydrogels with fast kinetics indispensable. Furthermore, future research is essential to extend beyond traditional pH- and temperature-responsive hydrogels, enabling broader utilization of diverse responsive hydrogels. Oscillatory chemical reactions, such as Belousov−Zhabotinsky (BZ) reactions[245,246] and pH oscillators,[247] commonly involve multiple reactants and harsh reaction conditions. Moreover, their regulation typically occurs under highly specific and tightly controlled environments, severely restricting their applicability and sustainability. Systems driven by chemical oscillations often face considerable challenges when operating under physiologically or environmentally variable conditions. For instance, sustained chemical oscillations like the BZ reaction utilize highly toxic chemicals such as nitric acid, malonic acid, and sodium bromate at substantial concentrations. Similarly, pH oscillator systems (e.g., HPD and Landolt oscillators) involve hazardous chemicals, extreme pH conditions (either strongly alkaline or mildly acidic), and continuous stirred-tank reactor (CSTR) setups to maintain stable oscillations, limiting their practical deployment significantly. One-cycle regulation mechanisms are generally simpler and more biofriendly, primarily due to their reliance on enzymatic systems and biocompatible organic molecules, making them more readily adaptable to physiological conditions. However, their operation inherently necessitates repeated refueling, which constrains their long-term autonomy.

In addition to the refining feedback mechanisms, the choice of fuel is another critical consideration. Current self-regulating hydrogel systems predominantly rely on limited fuel types—primarily chemical (e.g., protons and redox agents) and optical (light). Chemical fuels are advantageous as they can store and release substantial energy through chemical reactions, effectively converted into mechanical motion or other forms of useful work. Optical fuels offer unique capabilities, including wireless signaling, remote powering, and directional control. Nevertheless, novel stimuli and alternative mechanisms for signal transduction within hydrogels should be explored. Potential stimuli include electric fields (e.g., dielectric reconfiguration), magnetic fields (e.g., paramagnetic or diamagnetic actuation), gravitational orientation (e.g., density-driven sedimentation), and buoyancy gradients (e.g., shape-dependent floating dynamics). Although these stimuli offer advantages in precise spatiotemporal control, their inherent characteristics may restrict functional diversity and long-term sustainability.

https://doi.org/10.1021/acs.chemrev.5c00358
Chem. Rev. XXXX, XXX, XXX−XXX

Integrating these alternative stimuli into hybrid systems alongside chemical or light fuels could overcome the existing limitations. Recent work shows that patterned electric fields steer photoelectroactive gels along programmed routes,[248] magnetic gradients reversibly control BZ chemical waves,[249] and buoyancy cues, combined with a chemomechanical pH oscillator in a density stratified medium, convert swelling and deswelling into spontaneous float and sink cycles.[250] These electric, magnetic, and buoyancy stimuli enhance the controllability of self-regulating systems. Additionally, integrating exothermic enzymatic reactions with mechanical feedback loops is another promising example. Such hybrid approaches could facilitate sophisticated, sustainable, and autonomous behaviors suitable for practical applications. Nonetheless, the implementation of these hybrid architectures poses significant challenges. It requires careful management of compatibility among diverse feedback mechanisms and ensuring system stability over multiple cycles, ultimately enabling versatile and practical self-regulating hydrogels. In conclusion, clearly identifying the feedback mechanisms and energy sources (fuels) is crucial in the development of self-regulating hydrogels. Ideally, the fuel should provide sufficient energy to drive reactions inducing hydrogel deformation, and well-designed feedback mechanisms should freely regulate the characteristic time scale and interactions within these out-of-equilibrium systems.

6.2. Designing Hydrogels for Enhanced Self-Regulating Actuators

Current self-regulating hydrogel actuators predominantly focus on behaviors such as locomotion through sol−gel transitions and bending via swelling−shrinking mechanisms. However, these approaches alone are insufficient to fulfill the complex requirements of life-like tasks and practical applications. Consequently, future research should aim to incorporate advanced deformation modes such as anisotropic deformation for precise directional control,[45,251] torsional actuation for rotational movements,[252] or snapping for rapid shape transformations.[253]

Moreover, optimizing the internal network topology of hydrogels represents a crucial research frontier. For instance, the design of polymer networks capable of establishing internal fuel concentration gradients is essential. Such gradients can propagate chemical oscillatory feedback loops that coordinate or temporally delay motions. Beyond external parameters like fuel concentration or light intensity, deeper investigations are required to understand how intrinsic hydrogel properties—such as shape, geometry, and internal structural heterogeneity—can autonomously modulate the cycles, directions, and dynamics of self-regulation. Leveraging 3D printing technologies will enable the creation of more complex and sophisticated self-regulating actuators. To achieve these advanced capabilities, additive manufacturing techniques—such as direct ink writing, stereolithography, and multimaterial jetting—offer exceptional promise. Recent studies have shown that these 3D printing methods can precisely impose complex geometries, internal channels, and spatially resolved functionalities within soft actuators.[254,255] Integrating such cutting-edge fabrication technologies should yield powerful strategies for designing the next generation of functionally integrated self-regulating hydrogel actuators.

In addition to self-regulating actuation, incorporating functionalities such as self-healing and recyclability can significantly broaden the functional scope of hydrogel systems.[256] These features may facilitate the development of life-like materials capable of adaptive behavior. Additionally, exploring collective regulatory behaviors among multiple interacting hydrogels could uncover fundamentally novel phenomena and functional capabilities unattainable with isolated actuators.[257−262] Moreover, methods of integrating all necessary fuels directly within hydrogels should be investigated. For instance, polymerizing substrates for enzyme reactions or BZ reactions directly into the hydrogel network could represent a promising strategy for achieving fully integrated, autonomous hydrogel actuators.[180]

6.3. Beyond Biomimetic Soft Materials: Toward New Applications of Self-Regulating Hydrogel Actuators

Currently, self-regulating hydrogels have primarily been developed to emulate biological functions, such as muscle contraction or amoeboid movement. These biomimetic approaches provide valuable insights into fundamental non-equilibrium, evolutionary, and adaptive biological processes. However, to advance beyond imitation, future research should also explore innovative, human-defined applications. To quantitatively gauge the state of these artificial systems, comparisons can be drawn to biological oscillations. Biological systems exhibit diverse oscillatory behaviors ranging from rapid muscle tremors (∼8−10 Hz),[263] moderate-frequency motions like bird wing flapping (∼3−10 Hz in typical birds, up to 80 Hz in hummingbirds),[264,265] to relatively slower movements exemplified by amoeboid cell motility (∼0.017 Hz).[266] In contrast, currently developed self-regulating hydrogel actuators exhibit substantially lower oscillation frequencies compared to biological counterparts. Typical oscillation periods observed in sustained regulation systems range approximately from 10 to 500 s (corresponding frequencies of ∼0.002−0.1 Hz). One-cycle regulation typically demonstrates even slower dynamics, often exceeding periods of 1 h (∼0.0003 Hz). Notably, studies achieving relatively faster responses have predominantly focused on sustained regulation approaches. This discrepancy underscores a significant performance gap between artificial hydrogel actuators and natural biological systems. Consequently, a critical future objective in self-regulating hydrogel actuator research is achieving independent and precise control over oscillation amplitude and frequency, free from inherent material-specific constraints. Such a control will enable tailored hydrogels to precisely match dynamic requirements for various practical applications, greatly expanding their impact beyond biomimetic systems. Toward this goal, incorporating bio-inspired polymer structural features could significantly advance the capabilities of self-regulating hydrogels. For instance, anisotropic hierarchical networks inspired by the sarcomere structures of muscle tissues[267] can promote anisotropic actuation of self-regulation.[45] Moreover, mimicking the precise network uniformity observed in biological materials such as collagen fibrils[268] and keratin filaments[269] can enable hydrogels with precision self-regulatory functionalities.[79,270] Introducing phase-separated porous structures inspired by the spongy mesophyll of plant leaves[271] and structurally colored butterfly wings or bird feathers,[272] facilitate rapid deformation kinetics, substantially enhancing the power output of actuators.[44,273] Lastly, integrating heterogeneous polymer domains modeled after the helical structures found in seedpods,[274] tendrils,[275] bacterial spirochetes,[276] and contractile *Vorticella* stalks,[277]

https://doi.org/10.1021/acs.chemrev.5c00358
Chem. Rev. XXXX, XXX, XXX−XXX

could enable large-scale shape transformations, thereby amplifying the achievable amplitude of self-regulation.[278−280]

Self-regulating hydrogels hold significant promise in environments unsuitable for conventional electronics. Because these gels can be preprogrammed to execute a single, self-terminating actuation cycle, they excel whenever follow-up intervention is impossible or undesirable. For example, self-regulating hydrogels with sustained regulation could open new avenues in autonomous robotics, energy harvesting, bistable actuators, signal generators, mechanologics, intelligent separation, and transport technologies. Artificial phototaxis offers further potential in maneuverable marine systems, miniaturized transportation, and solar sails. Meanwhile, one-cycle self-regulating hydrogels are already being explored as transient therapeutic depots that release payloads and then liquefy,[238] in situ gelling adhesives that seal wounds and subsequently degrade,[232] untethered soft actuators that autonomously grip and release cargo,[223] and programmable photonic gels that display and then erase information over time.[204] Developing soft chemical computers based on oscillatory reaction-driven logic gates could enable signal processing and actuation entirely through chemical mechanisms, eliminating the need for electronics.

Looking ahead, self-regulating hydrogel systems could evolve into adaptive metamaterials autonomously responding to environmental changes, creating novel intelligent, life-like materials. However, realizing these ambitious applications requires addressing key challenges including precise regulation under realistic operational conditions, robust material stability, and scalable fabrication methods. Overcoming these hurdles will unlock transformative capabilities across diverse fields from medicine and robotics to environmental sensing and adaptive infrastructure.

AUTHOR INFORMATION

Corresponding Author

Youn Soo Kim − *Department of Materials Science and Engineering, Pohang University of Science and Technology (POSTECH) 77 Cheongam-Ro, Pohang, Gyeongbuk 37673, South Korea;* orcid.org/0000-0003-1531-3635; Email: ysookim@postech.ac.kr

Authors

Taehun Chung − *Department of Materials Science and Engineering, Pohang University of Science and Technology (POSTECH) 77 Cheongam-Ro, Pohang, Gyeongbuk 37673, South Korea;* orcid.org/0000-0003-4760-7830

Jaewon Choi − *Department of Materials Science and Engineering, Pohang University of Science and Technology (POSTECH) 77 Cheongam-Ro, Pohang, Gyeongbuk 37673, South Korea;* orcid.org/0009-0003-0239-7240

Takafumi Enomoto − *Department of Materials Engineering, School of Engineering, The University of Tokyo, Tokyo 113-8656, Japan;* orcid.org/0000-0001-5137-6129

Soyeon Park − *Department of Materials Science and Engineering, Pohang University of Science and Technology (POSTECH) 77 Cheongam-Ro, Pohang, Gyeongbuk 37673, South Korea*

Saehyun Kim − *Department of Materials Science and Engineering, Pohang University of Science and Technology (POSTECH) 77 Cheongam-Ro, Pohang, Gyeongbuk 37673, South Korea*

Complete contact information is available at: https://pubs.acs.org/10.1021/acs.chemrev.5c00358

Author Contributions

[§]T.C. and J.C. contributed equally to this work. Conceptualization, T.C., J.C., and Y.S.K.; Investigation, T.C., T.E., S.K., and S.P.; Formal analysis, S.K. and S.P.; Visualization, T.C., J.C., and Y.S.K.; Writing—original draft preparation, T.C., J.C., T.E., and Y.S.K.; Writing—review and editing, T.C., J.C., and Y.S.K.; Supervision, Y.S.K.; Project administration, Y.S.K.; Funding acquisition, Y.S.K. All authors have read and agreed to the published version of the manuscript. CRediT: **Taehun Chung** conceptualization, investigation, visualization, writing - original draft, writing - review & editing; **Jaewon Choi** conceptualization, visualization, writing - original draft, writing - review & editing; **Takafumi Enomoto** investigation, writing - original draft; **Soyeon Park** formal analysis, investigation; **Saehyun Kim** formal analysis, investigation; **Youn Soo Kim** conceptualization, funding acquisition, project administration, supervision, validation, visualization, writing - original draft, writing - review & editing.

Notes

The authors declare no competing financial interest.

Biographies

Taehun Chung is a postdoctoral Researcher in the Department of Materials Science and Engineering at Pohang University of Science and Technology (POSTECH). He received his B.S. degree from the School of Materials Science and Engineering at Ulsan National Institute of Science and Technology (UNIST) in 2018. He earned his Ph.D. degree from the Department of Materials Science and Engineering at POSTECH in 2024 under the supervision of Prof. Youn Soo Kim. His research focuses broadly on stimuli-responsive soft materials, including the synthesis of stimuli-responsive polymers, the design of polymer networks for enhanced soft actuators, and the characterization of self-regulating hydrogels.

Jaewon Choi is a Ph.D. candidate in the Department of Materials Science and Engineering at Pohang University of Science and Technology (POSTECH). He received his B.S. degree in Polymer Science & Engineering from Pusan National University in 2022. His research focuses on the development of bioinspired actuators utilizing self-regulating systems to mimic dynamic physiological behaviors.

Takafumi Enomoto is currently an Assistant Professor in the Department of Materials Engineering at the University of Tokyo. He received his Ph.D. degree in Science from the Graduate University for Advanced Studies in 2019 under the supervision of Associate Prof. Shigeyuki Masaoka. He worked with Prof. Ryo Yoshida as a postdoctoral researcher from 2019 to 2023 at the Department of Materials Engineering from the University of Tokyo. His research mainly focuses on understanding life through creating life-like autonomous chemical systems. He is currently working on autonomous polymer materials based on marginally stable synthetic polymers and catalysis.

Soyeon Park is a M.S. candidate in the Department of Materials Science and Engineering at Pohang University of Science and Technology (POSTECH). She received her B.S. in Polymer Science & Engineering from Pusan National University in 2024. Her research explores how the internal structure of polymer gels changes when exposed to different environments, and how these microstructural changes influence the overall physical properties of the gels.

Saehyun Kim is a M.S. candidate in the Department of Materials Science and Engineering at Pohang University of Science and Technology (POSTECH). He received his B.S. in the Department of Materials Science and Engineering of the Chonnam National University (CNU) with *Summa Cum Laude* in 2024. His research is particularly focused on developing sustainable gel polymer electrolytes for energy storage devices.

Youn Soo Kim is currently an Associate Professor in the Department of Materials Science and Engineering at Pohang University of Science and Technology (POSTECH). She received her B.S. (2009) and M.S. (2011) degrees in Chemistry and Nanoscience from Ewha Womans University in Korea. She received her Ph.D. degree in Chemistry and Biotechnology from the University of Tokyo in 2015 under the supervision of Prof. Takuzo Aida and Dr. Yasuhiro Ishida. She worked with Prof. Ryo Yoshida as a postdoctoral researcher from 2015 to 2017 at the Department of Materials Engineering from the University of Tokyo. Dr. Kim's research is mainly focused on the development of new functional polymer gels based on biomimetics. Currently, her research team is working on hydrogel actuators, physical hydrogels based on block copolymers, lignogels using eco-friendly materials such as lignin, and antifreezing gels that are operable in extreme conditions. These functional hydrogels and organogels with excellent physical properties, conductivity, adhesion, and deformation speed are used in bioelectronics, tissue engineering, energy storage devices, adhesive materials, and medical devices.

ACKNOWLEDGMENTS

This work was supported by the National Research Foundation of Korea (NRF) grant funded by the Korea government (MSIT) (RS-2024-00405818, RS-2024-00408989, RS-2025-00554376, and RS-2024-00408795), KOREA TORAY SCIENCE FOUNDATION, and 2025 POSTECH International Joint Research Project.

REFERENCES

(1) Kotas, M. E.; Medzhitov, R. Homeostasis, inflammation, and disease susceptibility. *Cell* **2015**, *160* (5), 816−827.
(2) Humphrey, J. D.; Dufresne, E. R.; Schwartz, M. A. Mechanotransduction and extracellular matrix homeostasis. *Nat. Rev. Mol. Cell Biol.* **2014**, *15* (12), 802−812.
(3) Sambongi, Y.; Iko, Y.; Tanabe, M.; Omote, H.; Iwamoto-Kihara, A.; Ueda, I.; Yanagida, T.; Wada, Y.; Futai, M. Mechanical rotation of the c subunit oligomer in ATP synthase (F0F1): direct observation. *Science* **1999**, *286* (5445), 1722−1724.
(4) Fratzl, P.; Barth, F. G. Biomaterial systems for mechanosensing and actuation. *Nature* **2009**, *462* (7272), 442−448.
(5) Prosser, B. L.; Ward, C. W.; Lederer, W. X-ROS signaling: rapid mechano-chemo transduction in heart. *Science* **2011**, *333* (6048), 1440−1445.
(6) Spaet, T. H. Analytical review: hemostatic homeostasis. *Blood* **1966**, *28* (1), 112−123.
(7) Cheeseman, I. M.; Desai, A. Molecular architecture of the kinetochore-microtubule interface. *Nat. Rev. Mol. Cell Biol.* **2008**, *9* (1), 33−46.
(8) Bao, G.; Kamm, R. D.; Thomas, W.; Hwang, W.; Fletcher, D. A.; Grodzinsky, A. J.; Zhu, C.; Mofrad, M. R. Molecular biomechanics: the molecular basis of how forces regulate cellular function. *Cellular and Molecular Bioengineering* **2010**, *3*, 91−105.
(9) Hess, H. Engineering applications of biomolecular motors. *Annu. Rev. Biomed. Eng.* **2011**, *13* (1), 429−450.
(10) Takeda, S. Crystal structure of troponin and the molecular mechanism of muscle regulation. *Journal of electron microscopy* **2005**, *54* (suppl_1), i35−i41.
(11) Blanchoin, L.; Boujemaa-Paterski, R.; Sykes, C.; Plastino, J. Actin dynamics, architecture, and mechanics in cell motility. *Physiol Rev.* **2014**, *94* (1), 235−263.
(12) Kuo, I. Y.; Ehrlich, B. E. Signaling in muscle contraction. *Cold Spring Harb Perspect Biol.* **2015**, *7* (2), a006023.
(13) Fukui, Y.; Yumura, S. Actomyosin dynamics in chemotactic amoeboid movement of Dictyostelium. *Cell Motil. Cytoskeleton* **1986**, *6* (6), 662−673.
(14) Pálsson, E. A cAMP signaling model explains the benefit of maintaining two forms of phosphodiesterase in Dictyostelium. *Biophysical journal* **2009**, *97* (9), 2388−2398.
(15) De Palo, G.; Yi, D.; Endres, R. G. A critical-like collective state leads to long-range cell communication in Dictyostelium discoideum aggregation. *PLoS biology* **2017**, *15* (4), No. e1002602.
(16) Lämmermann, T.; Sixt, M. Mechanical modes of 'amoeboid'cell migration. *Curr. Opin. Cell Biol.* **2009**, *21* (5), 636−644.
(17) de Schaetzen, F.; Fan, M.; Alcolombri, U.; Peaudecerf, F. J.; Drissner, D.; Loessner, M. J.; Stocker, R.; Schuppler, M. Random encounters and amoeba locomotion drive the predation of Listeria monocytogenes by Acanthamoeba castellanii. *Proc. Natl. Acad. Sci. U. S. A.* **2022**, *119* (32), No. e2122659119.
(18) Mitchison, T.; Cramer, L. Actin-based cell motility and cell locomotion. *Cell* **1996**, *84* (3), 371−379.
(19) Yang, C.; Suo, Z. Hydrogel ionotronics. *Nature Reviews Materials* **2018**, *3* (6), 125−142.
(20) Lee, Y.; Song, W.; Sun, J.-Y. Hydrogel soft robotics. *Materials Today Physics* **2020**, *15*, 100258.
(21) Hu, L.; Chee, P. L.; Sugiarto, S.; Yu, Y.; Shi, C.; Yan, R.; Yao, Z.; Shi, X.; Zhi, J.; Kai, D.; et al. Hydrogel-based flexible electronics. *Adv. Mater.* **2023**, *35* (14), 2205326.
(22) Sakai, T. *Physics of polymer gels*; John Wiley & Sons, 2020.
(23) Na, H.; Kang, Y.-W.; Park, C. S.; Jung, S.; Kim, H.-Y.; Sun, J.-Y. Hydrogel-based strong and fast actuators by electroosmotic turgor pressure. *Science* **2022**, *376* (6590), 301−307.
(24) Kamata, H.; Li, X.; Chung, U. i.; Sakai, T. Design of hydrogels for biomedical applications. *Adv. Healthcare Mater.* **2015**, *4* (16), 2360−2374.
(25) Hawkins, K.; Patterson, A. K.; Clarke, P. A.; Smith, D. K. Catalytic gels for a prebiotically relevant asymmetric aldol reaction in water: from organocatalyst design to hydrogel discovery and back again. *J. Am. Chem. Soc.* **2020**, *142* (9), 4379−4389.
(26) Sahiner, N.; Ozay, H.; Ozay, O.; Aktas, N. A soft hydrogel reactor for cobalt nanoparticle preparation and use in the reduction of nitrophenols. *Applied Catalysis B: Environmental* **2010**, *101* (1−2), 137−143.
(27) Quan, H. C.; Kisailus, D.; Meyers, M. A. Hydration-induced reversible deformation of biological materials. *Nature Reviews Materials* **2021**, *6* (3), 264−283.
(28) Carlsson, A. E. Actin dynamics: from nanoscale to microscale. *Annual review of biophysics* **2010**, *39* (1), 91−110.
(29) Liu, X.; Steiger, C.; Lin, S.; Parada, G. A.; Liu, J.; Chan, H. F.; Yuk, H.; Phan, N. V.; Collins, J.; Tamang, S.; et al. Ingestible hydrogel device. *Nat. Commun.* **2019**, *10* (1), 493.
(30) Yuk, H.; Lin, S.; Ma, C.; Takaffoli, M.; Fang, N. X.; Zhao, X. Hydraulic hydrogel actuators and robots optically and sonically camouflaged in water. *Nat. Commun.* **2017**, *8* (1), 14230.
(31) Sydney Gladman, A.; Matsumoto, E. A.; Nuzzo, R. G.; Mahadevan, L.; Lewis, J. A. Biomimetic 4D printing. *Nat. Mater.* **2016**, *15* (4), 413−418.
(32) Must, I.; Sinibaldi, E.; Mazzolai, B. A variable-stiffness tendril-like soft robot based on reversible osmotic actuation. *Nat. Commun.* **2019**, *10* (1), 344.
(33) Onoda, M.; Ueki, T.; Shibayama, M.; Yoshida, R. Multiblock copolymers exhibiting spatio-temporal structure with autonomous viscosity oscillation. *Sci. Rep.* **2015**, *5* (1), 15792.
(34) Nonoyama, T.; Lee, Y. W.; Ota, K.; Fujioka, K.; Hong, W.; Gong, J. P. Instant thermal switching from soft hydrogel to rigid plastics inspired by thermophile proteins. *Adv. Mater.* **2020**, *32* (4), 1905878.

https://doi.org/10.1021/acs.chemrev.5c00358
Chem. Rev. XXXX, XXX, XXX−XXX

(35) Nakajima, T.; Kurokawa, T.; Ahmed, S.; Wu, W.-l.; Gong, J. P. Characterization of internal fracture process of double network hydrogels under uniaxial elongation. *Soft Matter* **2013**, *9* (6), 1955−1966.
(36) Kamata, H.; Akagi, Y.; Kayasuga-Kariya, Y.; Chung, U.-i.; Sakai, T. "Nonswellable" hydrogel without mechanical hysteresis. *Science* **2014**, *343* (6173), 873−875.
(37) Flory, P. J.; Rehner, J., Jr Statistical mechanics of cross-linked polymer networks II. Swelling. *J. Chem. Phys.* **1943**, *11* (11), 521−526.
(38) Zou, X.; Zhao, X.; Ye, L. Synthesis of cationic chitosan hydrogel with long chain alkyl and its controlled glucose-responsive drug delivery behavior. *RSC Adv.* **2015**, *5* (116), 96230−96241.
(39) Techawanitchai, P.; Ebara, M.; Idota, N.; Asoh, T.-A.; Kikuchi, A.; Aoyagi, T. Photo-switchable control of pH-responsive actuators via pH jump reaction. *Soft Matter* **2012**, *8* (10), 2844−2851.
(40) Shim, T. S.; Kim, S.-H.; Heo, C.-J.; Jeon, H. C.; Yang, S.-M. Controlled Origami Folding of Hydrogel Bilayers with Sustained Reversibility for Robust Microcarriers. *Angew. Chem., Int. Ed.* **2012**, *51* (6), 1420−1423.
(41) Bassik, N.; Abebe, B. T.; Laflin, K. E.; Gracias, D. H. Photolithographically patterned smart hydrogel based bilayer actuators. *Polymer* **2010**, *51* (26), 6093−6098.
(42) Palleau, E.; Morales, D.; Dickey, M. D.; Velev, O. D. Reversible patterning and actuation of hydrogels by electrically assisted ionoprinting. *Nat. Commun.* **2013**, *4* (1), 2257.
(43) Morales, D.; Palleau, E.; Dickey, M. D.; Velev, O. D. Electro-actuated hydrogel walkers with dual responsive legs. *Soft Matter* **2014**, *10* (9), 1337−1348.
(44) Chung, T.; Han, I. K.; Han, J.; Ahn, K.; Kim, Y. S. Fast and large shrinking of thermoresponsive hydrogels with phase-separated structures. *Gels* **2021**, *7* (1), 18.
(45) Kim, Y. S.; Liu, M.; Ishida, Y.; Ebina, Y.; Osada, M.; Sasaki, T.; Hikima, T.; Takata, M.; Aida, T. Thermoresponsive actuation enabled by permittivity switching in an electrostatically anisotropic hydrogel. *Nature materials* **2015**, *14* (10), 1002−1007.
(46) Zheng, W. J.; An, N.; Yang, J. H.; Zhou, J.; Chen, Y. M. Tough Al-alginate/Poly(N-isopropylacrylamide) Hydrogel with Tunable LCST for Soft Robotics. *ACS Appl. Mater. Interfaces* **2015**, *7* (3), 1758−1764.
(47) Sun, Z.; Yamauchi, Y.; Araoka, F.; Kim, Y. S.; Bergueiro, J.; Ishida, Y.; Ebina, Y.; Sasaki, T.; Hikima, T.; Aida, T. An anisotropic hydrogel actuator enabling earthworm-like directed peristaltic crawling. *Angew. Chem., Int. Ed.* **2018**, *57* (48), 15772−15776.
(48) Satoh, T.; Sumaru, K.; Takagi, T.; Kanamori, T. Fast-reversible light-driven hydrogels consisting of spirobenzopyran-functionalized poly(N-isopropylacrylamide). *Soft Matter* **2011**, *7* (18), 8030−8034.
(49) Tang, J.; Tong, Z.; Xia, Y.; Liu, M.; Lv, Z.; Gao, Y.; Lu, T.; Xie, S.; Pei, Y.; Fang, D.; et al. Super tough magnetic hydrogels for remotely triggered shape morphing. *J. Mater. Chem. B* **2018**, *6* (18), 2713−2722.
(50) Han, D.; Farino, C.; Yang, C.; Scott, T.; Browe, D.; Choi, W.; Freeman, J. W.; Lee, H. Soft Robotic Manipulation and Locomotion with a 3D Printed Electroactive Hydrogel. *ACS Appl. Mater. Interfaces* **2018**, *10* (21), 17512−17518.
(51) Debnath, S.; Roy, S.; Ulijn, R. V. Peptide Nanofibers with Dynamic Instability through Nonequilibrium Biocatalytic Assembly. *J. Am. Chem. Soc.* **2013**, *135* (45), 16789−16792.
(52) Jain, M.; Ravoo, B. J. Fuel-Driven and Enzyme-Regulated Redox-Responsive Supramolecular Hydrogels. *Angew. Chem., Int. Ed.* **2021**, *60* (38), 21062−21068.
(53) Murakami, Y.; Maeda, M. DNA-Responsive Hydrogels That Can Shrink or Swell. *Biomacromolecules* **2005**, *6* (6), 2927−2929.
(54) Cangialosi, A.; Yoon, C.; Liu, J.; Huang, Q.; Guo, J.; Nguyen, T. D.; Gracias, D. H.; Schulman, R. DNA sequence-directed shape change of photopatterned hydrogels via high-degree swelling. *Science* **2017**, *357* (6356), 1126−1130.
(55) Han, I. K.; Chung, T.; Han, J.; Kim, Y. S. Nanocomposite hydrogel actuators hybridized with various dimensional nanomaterials for stimuli responsiveness enhancement. *Nano Convergence* **2019**, *6*, 1−21.
(56) Li, M.; Pal, A.; Aghakhani, A.; Pena-Francesch, A.; Sitti, M. Soft actuators for real-world applications. *Nature Reviews Materials* **2022**, *7* (3), 235−249.
(57) Li, J. J.; Guo, W. J.; Zhao, W. Q.; Zhu, Y. T.; Bai, J.; Xia, Z. G.; Zhou, X.; Liu, Z. F. Recent advances in flexible self-oscillating actuators. *Escience* **2024**, *4* (5), 100250.
(58) Walther, A. Viewpoint: From Responsive to Adaptive and Interactive Materials and Materials Systems: A Roadmap. *Adv. Mater.* **2020**, *32* (20), No. e1905111.
(59) Shklyaev, O. E.; Balazs, A. C. Interlinking spatial dimensions and kinetic processes in dissipative materials to create synthetic systems with lifelike functionality. *Nat. Nanotechnol* **2024**, *19* (2), 146−159.
(60) Ghosh, S.; Baltussen, M. G.; Ivanov, N. M.; Haije, R.; Jakstaite, M.; Zhou, T.; Huck, W. T. S. Exploring Emergent Properties in Enzymatic Reaction Networks: Design and Control of Dynamic Functional Systems. *Chem. Rev.* **2024**, *124* (5), 2553−2582.
(61) Merindol, R.; Walther, A. Materials learning from life: concepts for active, adaptive and autonomous molecular systems. *Chem. Soc. Rev.* **2017**, *46* (18), 5588−5619.
(62) Deng, J.; Walther, A. ATP-Responsive and ATP-Fueled Self-Assembling Systems and Materials. *Adv. Mater.* **2020**, *32* (42), No. e2002629.
(63) Wang, Q.; Qi, Z.; Chen, M.; Qu, D. H. Out-of-equilibrium supramolecular self-assembling systems driven by chemical fuel. *Aggregate* **2021**, *2* (5), No. e110.
(64) Nie, Z. Z.; Wang, M.; Yang, H. Self-sustainable autonomous soft actuators. *Commun. Chem.* **2024**, *7* (1), 58.
(65) Shen, B.; Kang, S. H. Designing self-oscillating matter. *Matter* **2021**, *4* (3), 766−769.
(66) Sitti, M. Physical intelligence as a new paradigm. *Extreme Mechanics Letters* **2021**, *46*, 101340.
(67) Chen, C.; Shi, P.; Liu, Z.; Duan, S.; Si, M.; Zhang, C.; Du, Y.; Yan, Y.; White, T. J.; Kramer-Bottiglio, R.; et al. Advancing physical intelligence for autonomous soft robots. *Science Robotics* **2025**, *10* (102), No. eads1292.
(68) Decisions, D. R. C. Interlinked Fast and Slow Positive Feedback Loops. *New Biol.* **1972**, *237*, 244.
(69) Ansel, K. M.; Ngo, V. N.; Hyman, P. L.; Luther, S. A.; Förster, R.; Sedgwick, J. D.; Browning, J. L.; Lipp, M.; Cyster, J. G. A chemokine-driven positive feedback loop organizes lymphoid follicles. *Nature* **2000**, *406* (6793), 309−314.
(70) Tsai, T. Y.-C.; Choi, Y. S.; Ma, W.; Pomerening, J. R.; Tang, C.; Ferrell, J. E., Jr Robust, tunable biological oscillations from interlinked positive and negative feedback loops. *Science* **2008**, *321* (5885), 126−129.
(71) Harris, S. L.; Levine, A. J. The p53 pathway: positive and negative feedback loops. *Oncogene* **2005**, *24* (17), 2899−2908.
(72) Zhou, H.-X.; Gilson, M. K. Theory of free energy and entropy in noncovalent binding. *Chem. Rev.* **2009**, *109* (9), 4092−4107.
(73) De Groot, S. R.; Mazur, P. *Non-equilibrium thermodynamics*; Courier Corporation, 2013.
(74) Chen, Y.; Zhang, Y.; Li, H.; Shen, J.; Zhang, F.; He, J.; Lin, J.; Wang, B.; Niu, S.; Han, Z.; et al. Bioinspired hydrogel actuator for soft robotics: Opportunity and challenges. *Nano Today* **2023**, *49*, 101764.
(75) Zhang, Z.; Chao, T.; Jiang, S. Physical, chemical, and chemical-physical double network of zwitterionic hydrogels. *J. Phys. Chem. B* **2008**, *112* (17), 5327−5332.
(76) Maitra, J.; Shukla, V. K. Cross-linking in hydrogels-a review. *Am. J. Polym. Sci.* **2014**, *4* (2), 25−31.
(77) Hu, J.; Zhang, G.; Liu, S. Enzyme-responsive polymeric assemblies, nanoparticles and hydrogels. *Chem. Soc. Rev.* **2012**, *41* (18), 5933−5949.
(78) Ulijn, R. V. Enzyme-responsive materials: a new class of smart biomaterials. *J. Mater. Chem.* **2006**, *16* (23), 2217−2225.
(79) Han, J.; Najafi, S.; Byun, Y.; Geonzon, L.; Oh, S.-H.; Park, J.; Koo, J. M.; Kim, J.; Chung, T.; Han, I. K.; et al. Bridge-rich and loop-

https://doi.org/10.1021/acs.chemrev.5c00358
Chem. Rev. XXXX, XXX, XXX−XXX

less hydrogel networks through suppressed micellization of multiblock polyelectrolytes. *Nat. Commun.* **2024**, *15* (1), 6553.
(80) Zhou, J.; Lin, S.; Zeng, H.; Liu, J.; Li, B.; Xu, Y.; Zhao, X.; Chen, G. Dynamic intermolecular interactions through hydrogen bonding of water promote heat conduction in hydrogels. *Materials Horizons* **2020**, *7* (11), 2936−2943.
(81) Han, Z.; Wang, P.; Lu, Y.; Jia, Z.; Qu, S.; Yang, W. A versatile hydrogel network-repairing strategy achieved by the covalent-like hydrogen bond interaction. *Science advances* **2022**, *8* (8), No. eabl5066.
(82) Tang, L.; Wang, L.; Yang, X.; Feng, Y.; Li, Y.; Feng, W. Poly (N-isopropylacrylamide)-based smart hydrogels: Design, properties and applications. *Prog. Mater. Sci.* **2021**, *115*, 100702.
(83) Zheng, N.; Xu, Y.; Zhao, Q.; Xie, T. Dynamic covalent polymer networks: a molecular platform for designing functions beyond chemical recycling and self-healing. *Chem. Rev.* **2021**, *121* (3), 1716−1745.
(84) Sun, P.; Huang, T.; Wang, X.; Wang, G.; Liu, Z.; Chen, G.; Fan, Q. Dynamic-covalent hydrogel with NIR-triggered drug delivery for localized chemo-photothermal combination therapy. *Biomacromolecules* **2020**, *21* (2), 556−565.
(85) Roberts, M. C.; Hanson, M. C.; Massey, A. P.; Karren, E. A.; Kiser, P. F. Dynamically restructuring hydrogel networks formed with reversible covalent crosslinks. *Adv. Mater.* **2007**, *19* (18), 2503−2507.
(86) Whitaker, D. E.; Mahon, C. S.; Fulton, D. A. Thermoresponsive Dynamic Covalent Single-Chain Polymer Nanoparticles Reversibly Transform into a Hydrogel. *Angew. Chem. Int. Edit* **2013**, *52* (3), 956−959.
(87) Zhou, X.; Wu, T.; Ding, K.; Hu, B.; Hou, M.; Han, B. Dispersion of graphene sheets in ionic liquid [bmim][PF6] stabilized by an ionic liquid polymer. *Chem. Commun.* **2010**, *46* (3), 386−388.
(88) Zhou, X.; Wu, T.; Hu, B.; Yang, G.; Han, B. Synthesis of graphene/polyaniline composite nanosheets mediated by polymerized ionic liquid. *Chem. Commun.* **2010**, *46* (21), 3663−3665.
(89) Sinawang, G.; Osaki, M.; Takashima, Y.; Yamaguchi, H.; Harada, A. Biofunctional hydrogels based on host-guest interactions. *Polym. J.* **2020**, *52* (8), 839−859.
(90) Nakahata, M.; Takashima, Y.; Yamaguchi, H.; Harada, A. Redox-responsive self-healing materials formed from host-guest polymers. *Nat. Commun.* **2011**, *2* (1), 511.
(91) Ulijn, R. V.; Smith, A. M. Designing peptide based nanomaterials. *Chem. Soc. Rev.* **2008**, *37* (4), 664−675.
(92) Du, X.; Zhou, J.; Shi, J.; Xu, B. Supramolecular hydrogelators and hydrogels: from soft matter to molecular biomaterials. *Chem. Rev.* **2015**, *115* (24), 13165−13307.
(93) Rowan, S. J.; Cantrill, S. J.; Cousins, G. R.; Sanders, J. K.; Stoddart, J. F. Dynamic covalent chemistry. *Angew. Chem., Int. Ed.* **2002**, *41* (6), 898−952.
(94) Tanaka, T.; Fillmore, D. J. Kinetics of swelling of gels. *J. Chem. Phys.* **1979**, *70* (3), 1214−1218.
(95) Yoshida, R.; Uchida, K.; Kaneko, Y.; Sakai, K.; Kikuchi, A.; Sakurai, Y.; Okano, T. Comb-type grafted hydrogels with rapid deswelling response to temperature changes. *Nature* **1995**, *374* (6519), 240−242.
(96) Zhang, V.; Accardo, J. V.; Kevlishvili, I.; Woods, E. F.; Chapman, S. J.; Eckdahl, C. T.; Stern, C. L.; Kulik, H. J.; Kalow, J. A. Tailoring dynamic hydrogels by controlling associative exchange rates. *Chem.* **2023**, *9* (8), 2298−2317.
(97) Orbán, M. s.; Kurin-Csörgei, K.; Epstein, I. R. pH-regulated chemical oscillators. *Acc. Chem. Res.* **2015**, *48* (3), 593−601.
(98) Orban, M.; Epstein, I. R. A new type of oxyhalogen oscillator: the bromite-iodide reaction in a continuous flow reactor. *J. Am. Chem. Soc.* **1992**, *114* (4), 1252−1256.
(99) Rabai, G.; Epstein, I. R. Oxidation of hydroxylamine by periodate in a continuous-flow stirred tank reactor: a new pH oscillator. *J. Phys. Chem.* **1989**, *93* (22), 7556−7559.
(100) Orban, M.; Epstein, I. R. Systematic design of chemical oscillators. 26. A new halogen-free chemical oscillator: the reaction between sulfide ion and hydrogen peroxide in a CSTR. *J. Am. Chem. Soc.* **1985**, *107* (8), 2302−2305.
(101) Okazaki, N.; Rábai, G.; Hanazaki, I. Discovery of novel bromate- sulfite pH oscillators with Mn2+ or MnO4-as a negative-feedback species. *J. Phys. Chem. A* **1999**, *103* (50), 10915−10920.
(102) Kovács, K. M.; Rábai, G. Large Amplitude pH Oscillations in the Hydrogen Peroxide- Dithionite Reaction in a Flow Reactor. *J. Phys. Chem. A* **2001**, *105* (40), 9183−9187.
(103) Orban, M.; Epstein, I. R. Systematic design of chemical oscillators. 39. Chemical oscillators in group VIA: the copper (II)-catalyzed reaction between hydrogen peroxide and thiosulfate ion. *J. Am. Chem. Soc.* **1987**, *109* (1), 101−106.
(104) Toth, R.; Taylor, A. F. The Tris (2, 2'-Bipyridyl) Ruthenium-Catalysed Belousov-Zhabotinsky Reaction. *Progress in Reaction Kinetics and Mechanism* **2006**, *31* (2), 59−115.
(105) Zaikin, A. N.; Zhabotinsky, A. M. Concentration Wave Propagation in Two-dimensional Liquid-phase Self-oscillating System. *Nature* **1970**, *225* (5232), 535−537.
(106) Hua, M.; Kim, C.; Du, Y.; Wu, D.; Bai, R.; He, X. Swaying gel: chemo-mechanical self-oscillation based on dynamic buckling. *Matter* **2021**, *4* (3), 1029−1041.
(107) He, X.; Aizenberg, M.; Kuksenok, O.; Zarzar, L. D.; Shastri, A.; Balazs, A. C.; Aizenberg, J. Synthetic homeostatic materials with chemo-mechano-chemical self-regulation. *Nature* **2012**, *487* (7406), 214−218.
(108) Zhao, Y.; Xuan, C.; Qian, X.; Alsaid, Y.; Hua, M.; Jin, L.; He, X. Soft phototactic swimmer based on self-sustained hydrogel oscillator. *Science Robotics* **2019**, *4* (33), No. eaax7112.
(109) Zhu, Q. L.; Liu, W.; Khoruzhenko, O.; Breu, J.; Hong, W.; Zheng, Q.; Wu, Z. L. Animating hydrogel knotbots with topology-invoked self-regulation. *Nat. Commun.* **2024**, *15* (1), 300.
(110) Zhu, Q. L.; Liu, W.; Khoruzhenko, O.; Breu, J.; Bai, H.; Hong, W.; Zheng, Q.; Wu, Z. L. Closed Twisted Hydrogel Ribbons with Self-Sustained Motions under Static Light Irradiation. *Adv. Mater.* **2024**, *36* (28), 2314152.
(111) Hou, G.; Zhang, X.; Du, F.; Wu, Y.; Zhang, X.; Lei, Z.; Lu, W.; Zhang, F.; Yang, G.; Wang, H.; et al. Self-regulated underwater phototaxis of a photoresponsive hydrogel-based phototactic vehicle. *Nat. Nanotechnol.* **2024**, *19* (1), 77−84.
(112) Li, Z.; Myung, N. V.; Yin, Y. Light-powered soft steam engines for self-adaptive oscillation and biomimetic swimming. *Science Robotics* **2021**, *6* (61), No. eabi4523.
(113) Nakamura, S.; Yamanaka, M.; Oishi, Y.; Narita, T. Light-driven autonomous swing of multi-layered hydrogel. *RSC Adv.* **2022**, *12* (52), 33612−33616.
(114) Zhang, H.; Zeng, H.; Eklund, A.; Guo, H.; Priimagi, A.; Ikkala, O. Feedback-controlled hydrogels with homeostatic oscillations and dissipative signal transduction. *Nat. Nanotechnol.* **2022**, *17* (12), 1303−1310.
(115) Dolnik, M.; Banks, A. S.; Epstein, I. R. Oscillatory chemical reaction in a CSTR with feedback control of flow rate. *J. Phys. Chem. A* **1997**, *101* (28), 5148−5154.
(116) Cherkasov, N.; Adams, S. J.; Bainbridge, E. G.; Thornton, J. A. Continuous stirred tank reactors in fine chemical synthesis for efficient mixing, solids-handling, and rapid scale-up. *Reaction Chemistry & Engineering* **2023**, *8* (2), 266−277.
(117) Labrot, V.; De Kepper, P.; Boissonade, J.; Szalai, I.; Gauffre, F. Wave patterns driven by chemomechanical instabilities in responsive gels. *J. Phys. Chem. B* **2005**, *109* (46), 21476−21480.
(118) Horváth, J. Synergistic Chemomechanical Oscillators: Periodic Gel Actuators without Oscillatory Chemical Reaction. *Macromol. Symp.* **2015**, *358* (1), 217−224.
(119) Horváth, J. Peristaltic waves in a responsive gel sustained by a halogen-free non-oscillatory chemical reaction. *Polymer* **2015**, *79*, 243−254.
(120) Horvath, J. Sustained large-amplitude chemomechanical oscillations induced by the Landolt clock reaction. *J. Phys. Chem. B* **2014**, *118* (29), 8891−8900.

https://doi.org/10.1021/acs.chemrev.5c00358
Chem. Rev. XXXX, XXX, XXX−XXX

(121) Horváth, J. Chemomechanical oscillations with a non-redox non-oscillatory reaction. *Chem. Commun.* **2017**, *53* (36), 4973−4976.
(122) Horváth, J.; Szalai, I.; Boissonade, J.; De Kepper, P. Oscillatory dynamics induced in a responsive gel by a non-oscillatory chemical reaction: experimental evidence. *Soft Matter* **2011**, *7* (18), 8462−8472.
(123) Preston, D. J.; Rothemund, P.; Jiang, H. J.; Nemitz, M. P.; Rawson, J.; Suo, Z.; Whitesides, G. M. Digital logic for soft devices. *Proc. Natl. Acad. Sci. U. S. A.* **2019**, *116* (16), 7750−7759.
(124) Jiang, R.; Xiao, J.; Song, J. Buckling of thin gel strip under swelling. *Theoretical and Applied Mechanics Letters* **2017**, *7* (3), 134−137.
(125) Rothemund, P.; Ainla, A.; Belding, L.; Preston, D. J.; Kurihara, S.; Suo, Z.; Whitesides, G. M. A soft, bistable valve for autonomous control of soft actuators. *Science Robotics* **2018**, *3* (16), No. eaar7986.
(126) Gelebart, A. H.; Jan Mulder, D.; Varga, M.; Konya, A.; Vantomme, G.; Meijer, E.; Selinger, R. L.; Broer, D. J. Making waves in a photoactive polymer film. *Nature* **2017**, *546* (7660), 632−636.
(127) Coulais, C.; Sabbadini, A.; Vink, F.; van Hecke, M. Multi-step self-guided pathways for shape-changing metamaterials. *Nature* **2018**, *561* (7724), 512−515.
(128) Rafsanjani, A.; Zhang, Y.; Liu, B.; Rubinstein, S. M.; Bertoldi, K. Kirigami skins make a simple soft actuator crawl. *Science Robotics* **2018**, *3* (15), No. eaar7555.
(129) Rafsanjani, A.; Bertoldi, K.; Studart, A. R. Programming soft robots with flexible mechanical metamaterials. *Science Robotics* **2019**, *4* (29), No. eaav7874.
(130) Kang, S. H.; Shan, S.; Košmrlj, A.; Noorduin, W. L.; Shian, S.; Weaver, J. C.; Clarke, D. R.; Bertoldi, K. Complex ordered patterns in mechanical instability induced geometrically frustrated triangular cellular structures. *Physical Review Letters* **2014**, *112* (9), 098701.
(131) Kang, S. H.; Shan, S.; Noorduin, W. L.; Khan, M.; Aizenberg, J.; Bertoldi, K. Buckling-Induced Reversible Symmetry Breaking and Amplification of Chirality Using Supported Cellular Structures. *Adv. Mater.* **2013**, *25* (24), 3380−3385.
(132) Shastri, A.; McGregor, L. M.; Liu, Y.; Harris, V.; Nan, H.; Mujica, M.; Vasquez, Y.; Bhattacharya, A.; Ma, Y.; Aizenberg, M.; et al. An aptamer-functionalized chemomechanically modulated biomolecule catch-and-release system. *Nat. Chem.* **2015**, *7* (5), 447−454.
(133) He, X.; Friedlander, R. S.; Zarzar, L. D.; Aizenberg, J. Chemo-mechanically regulated oscillation of an enzymatic reaction. *Chem. Mater.* **2013**, *25* (4), 521−523.
(134) Swift, T.; Swanson, L.; Geoghegan, M.; Rimmer, S. The pH-responsive behaviour of poly (acrylic acid) in aqueous solution is dependent on molar mass. *Soft Matter* **2016**, *12* (9), 2542−2549.
(135) Philippova, O. E.; Hourdet, D.; Audebert, R.; Khokhlov, A. R. pH-responsive gels of hydrophobically modified poly (acrylic acid). *Macromolecules* **1997**, *30* (26), 8278−8285.
(136) Elliott, J. E.; Macdonald, M.; Nie, J.; Bowman, C. N. Structure and swelling of poly (acrylic acid) hydrogels: effect of pH, ionic strength, and dilution on the crosslinked polymer structure. *Polymer* **2004**, *45* (5), 1503−1510.
(137) Schild, H. G. Poly (N-isopropylacrylamide): experiment, theory and application. *Prog. Polym. Sci.* **1992**, *17* (2), 163−249.
(138) Fujishige, S.; Kubota, K.; Ando, I. Phase transition of aqueous solutions of poly (N-isopropylacrylamide) and poly (N-isopropylmethacrylamide). *J. Phys. Chem.* **1989**, *93* (8), 3311−3313.
(139) Maeda, Y.; Higuchi, T.; Ikeda, I. Change in Hydration State during the Coil-Globule Transition of Aqueous Solutions of Poly(N-isopropylacrylamide) as Evidenced by FTIR Spectroscopy. *Langmuir* **2000**, *16* (19), 7503−7509.
(140) Halperin, A.; Kröger, M.; Winnik, F. M. Poly(N-isopropylacrylamide) Phase Diagrams: Fifty Years of Research. *Angew. Chem., Int. Ed.* **2015**, *54* (51), 15342−15367.
(141) Binkert, T.; Oberreich, J.; Meewes, M.; Nyffenegger, R.; Ricka, J. Coil-globule transition of poly (N-isopropylacrylamide): a study of segment mobility by fluorescence depolarization. *Macromolecules* **1991**, *24* (21), 5806−5810.
(142) Das, A.; Babu, A.; Chakraborty, S.; Van Guyse, J. F. R.; Hoogenboom, R.; Maji, S. Poly(N-isopropylacrylamide) and Its Copolymers: A Review on Recent Advances in the Areas of Sensing and Biosensing. *Adv. Funct. Mater.* **2024**, *34* (37), 2402432.
(143) Gao, M.; Zhu, L.; Peh, C. K.; Ho, G. W. Solar absorber material and system designs for photothermal water vaporization towards clean water and energy production. *Energy Environ. Sci.* **2019**, *12* (3), 841−864.
(144) Waitkus, J.; Chang, Y.; Liu, L.; Puttaswamy, S. V.; Chung, T.; Molina Vargas, A. M.; Dollery, S. J.; O'Connell, M. R.; Cai, H.; Tobin, G. J.; et al. Gold Nanoparticle Enabled Localized Surface Plasmon Resonance on Unique Gold Nanomushroom Structures for On-Chip CRISPR-Cas13a Sensing. *Adv. Mater. Interfaces* **2023**, *10* (1), 2201261.
(145) Chen, X.; Yang, N.; Wang, Y.; He, H.; Wang, J.; Wan, J.; Jiang, H.; Xu, B.; Wang, L.; Yu, R.; et al. Highly efficient photothermal conversion and water transport during solar evaporation enabled by amorphous hollow multishelled nanocomposites. *Adv. Mater.* **2022**, *34* (7), 2107400.
(146) Kim, H.; Kang, J. H.; Zhou, Y.; Kuenstler, A. S.; Kim, Y.; Chen, C.; Emrick, T.; Hayward, R. C. Light-driven shape morphing, assembly, and motion of nanocomposite gel surfers. *Adv. Mater.* **2019**, *31* (27), 1900932.
(147) Liu, M.; Ishida, Y.; Ebina, Y.; Sasaki, T.; Hikima, T.; Takata, M.; Aida, T. An anisotropic hydrogel with electrostatic repulsion between cofacially aligned nanosheets. *Nature* **2015**, *517* (7532), 68−72.
(148) Gruziel, M.; Thyagarajan, K.; Dietler, G.; Stasiak, A.; Ekiel-Jezewska, M. L.; Szymczak, P. Periodic motion of sedimenting flexible knots. *Physical Review Letters* **2018**, *121* (12), 127801.
(149) Lee, Y. A. L.; Mousavikhamene, Z.; Amrithanath, A. K.; Neidhart, S. M.; Krishnaswamy, S.; Schatz, G. C.; Odom, T. W. Programmable Self-Regulation with Wrinkled Hydrogels and Plasmonic Nanoparticle Lattices. *Small* **2022**, *18* (1), 2103865.
(150) Zhang, H.; Zeng, H.; Eklund, A.; Guo, H.; Priimagi, A.; Ikkala, O. Feedback-controlled hydrogels with homeostatic oscillations and dissipative signal transduction. *Nat. Nanotechnol.* **2022**, *17* (12), 1303−1310.
(151) Yang, C.; Su, F.; Liang, Y.; Xu, W.; Li, S.; Liang, E.; Wang, G.; Zhou, N.; Wan, Q.; Ma, X. Fabrication of a biomimetic hydrogel actuator with rhythmic deformation driven by a pH oscillator. *Soft Matter* **2020**, *16* (12), 2928−2932.
(152) Yang, C.; Su, F.; Xu, Y.; Ma, Y.; Tang, L.; Zhou, N.; Liang, E.; Wang, G.; Tang, J. pH Oscillator-Driven Jellyfish-like Hydrogel Actuator with Dissipative Synergy between Deformation and Fluorescence Color Change. *ACS Macro Lett.* **2022**, *11* (3), 347−353.
(153) Varga, I.; Szalai, I.; Mészaros, R.; Gilányi, T. Pulsating pH-responsive nanogels. *J. Phys. Chem. B* **2006**, *110* (41), 20297−20301.
(154) Huber, M. C.; Jonas, U.; Schiller, S. M. An autonomous chemically fueled artificial protein muscle. *Advanced Intelligent Systems* **2022**, *4* (4), 2100189.
(155) Yang, X.; Zhou, Y.; Ji, L.; Ding, Y.; Wang, J.; Liang, X. Experimental evidence of large amplitude pH mediated autonomous chemomechanical oscillation. *Polymers* **2017**, *9* (11), 554.
(156) Kim, J. K.; Kim, K. I.; Basavaraja, C.; Rabai, G.; Huh, D. S. Reversible adsorption-desorption oscillations of nanoparticles on a patterned hydrogel surface induced by a pH oscillator in a closed chemical system. *J. Phys. Chem. B* **2013**, *117* (20), 6294−6303.
(157) Crook, C. J.; Smith, A.; Jones, R. A.; Ryan, A. J. Chemically induced oscillations in a pH-responsive hydrogel. *Phys. Chem. Chem. Phys.* **2002**, *4* (8), 1367−1369.
(158) Tian, E.; Ma, Y.; Cui, L.; Wang, J.; Song, Y.; Jiang, L. Color-Oscillating Photonic Crystal Hydrogel. *Macromol. Rapid Commun.* **2009**, *30* (20), 1719−1724.
(159) Nakagawa, H.; Hara, Y.; Maeda, S.; Hasimoto, S. A pendulum-like motion of nanofiber gel actuator synchronized with external periodic pH oscillation. *Polymers* **2011**, *3* (1), 405−412.
(160) Bilici, C.; Karayel, S.; Demir, T. T.; Okay, O. Self-oscillating pH-responsive cryogels as possible candidates of soft materials for

https://doi.org/10.1021/acs.chemrev.5c00358
Chem. Rev. XXXX, XXX, XXX−XXX

generating mechanical energy. *J. Appl. Polym. Sci.* **2010**, *118* (5), 2981−2988.
(161) Liang, E.; Zhou, H.; Ding, X.; Zheng, Z.; Peng, Y. Fabrication of a rhythmic assembly system based on reversible formation of dynamic covalent bonds in a chemical oscillator. *Chem. Commun.* **2013**, *49* (47), 5384−5386.
(162) Howse, J. R.; Topham, P.; Crook, C. J.; Gleeson, A. J.; Bras, W.; Jones, R. A.; Ryan, A. J. Reciprocating power generation in a chemically driven synthetic muscle. *Nano Lett.* **2006**, *6* (1), 73−77.
(163) Kovács, K. M.; Rábai, G. Large amplitude pH oscillations in the hydrogen peroxide-dithionite reaction in a flow reactor. *J. Phys. Chem. A* **2001**, *105* (40), 9183−9187.
(164) Rabai, G.; Orban, M.; Epstein, I. R. Systematic design of chemical oscillators. 64. Design of pH-regulated oscillators. *Acc. Chem. Res.* **1990**, *23* (8), 258−263.
(165) Liang, E.; Su, F.; Liang, Y.; Wang, G.; Xu, W.; Li, S.; Yang, C.; Tang, J.; Zhou, N. Dissipative aggregation-induced emission behaviour of an amino-functionalized tetraphenylethene using a pH oscillator. *Chem. Commun.* **2020**, *56* (96), 15169−15172.
(166) Yoshida, R.; Takahashi, T.; Yamaguchi, T.; Ichijo, H. Self-oscillating gel. *J. Am. Chem. Soc.* **1996**, *118* (21), 5134−5135.
(167) Lee, W. S.; Enomoto, T.; Akimoto, A. M.; Yoshida, R. Fabrication of submillimeter-sized spherical self-oscillating gels and control of their isotropic volumetric oscillatory behaviors. *Soft Matter* **2023**, *19* (9), 1772−1781.
(168) Yamada, Y.; Ito, H.; Maeda, S. Artificial temperature-compensated biological clock using temperature-sensitive Belousov-Zhabotinsky gels. *Sci. Rep.* **2022**, *12* (1), 22436.
(169) Kuksenok, O.; Yashin, V. V.; Kinoshita, M.; Sakai, T.; Yoshida, R.; Balazs, A. C. Exploiting gradients in cross-link density to control the bending and self-propelled motion of active gels. *J. Mater. Chem.* **2011**, *21* (23), 8360−8371.
(170) Maeda, S.; Hara, Y.; Sakai, T.; Yoshida, R.; Hashimoto, S. Self-Walking Gel. *Adv. Mater.* **2007**, *19* (21), 3480−3484.
(171) Tamate, R.; Ueki, T.; Yoshida, R. Evolved Colloidosomes Undergoing Cell-like Autonomous Shape Oscillations with Buckling. *Angew. Chem.* **2016**, *128* (17), 5265−5269.
(172) Sun, H.; Enomoto, T.; Lee, W. S.; Akimoto, A. M.; Yoshida, R. Autonomous Motion of Hydrogels Driven by Semi-Interpenetrating Chemical Processing Systems. *ACS Macro Lett.* **2024**, *13* (11), 1503−1508.
(173) Inui, K.; Saito, I.; Yoshida, R.; Minato, H.; Suzuki, D. High-frequency swelling/deswelling oscillation of poly (oligoethylene glycol) methacrylate-based hydrogel microspheres with a tris (2, 2′-bipyridyl) ruthenium catalyst. *ACS Applied Polymer Materials* **2021**, *3* (7), 3298−3306.
(174) Onoda, M.; Ueki, T.; Tamate, R.; Shibayama, M.; Yoshida, R. Amoeba-like self-oscillating polymeric fluids with autonomous sol-gel transition. *Nat. Commun.* **2017**, *8* (1), 15862.
(175) Lee, W. S.; Enomoto, T.; Akimoto, A. M.; Yoshida, R. Temperature-Adaptative Self-Oscillating Gels: Toward Autonomous Biomimetic Soft Actuators with Broad Operating Temperature Region. *Macromol. Rapid Commun.* **2024**, *45* (13), No. e2400038.
(176) Ueki, T.; Takasaki, Y.; Bundo, K.; Ueno, T.; Sakai, T.; Akagi, Y.; Yoshida, R. Autonomous viscosity oscillation via metallo-supramolecular terpyridine chemistry of branched poly(ethylene glycol) driven by the Belousov-Zhabotinsky reaction. *Soft Matter* **2014**, *10* (9), 1349−1355.
(177) Yuan, P.; Kuksenok, O.; Gross, D. E.; Balazs, A. C.; Moore, J. S.; Nuzzo, R. G. UV patternable thin film chemistry for shape and functionally versatile self-oscillating gels. *Soft Matter* **2013**, *9* (4), 1231−1243.
(178) Wang, J.; Ren, L.; Yu, Z.; Teng, R.; Pan, C.; Yuan, L.; Epstein, I. R.; Gao, Q. Nanogel Crosslinking-Based Belousov-Zhabotinsky Self-Oscillating Polyacrylamide Gel with Improved Mechanical Properties and Fast Oscillatory Response. *J. Phys. Chem. B* **2022**, *126* (5), 1108−1114.
(179) Inui, K.; Saito, I.; Yoshida, R.; Minato, H.; Suzuki, D. High-Frequency Swelling/Deswelling Oscillation of Poly(Oligoethylene Glycol) Methacrylate-Based Hydrogel Microspheres with a Tris(2,2′-bipyridyl)ruthenium Catalyst. *ACS Applied Polymer Materials* **2021**, *3* (7), 3298−3306.
(180) Yoshizawa, T.; Onoda, M.; Ueki, T.; Tamate, R.; Enomoto, T.; Akimoto, A. M.; Yoshida, R. Self-Oscillating Triblock Terpolymer Exhibiting an Autonomous Sol-Gel Oscillation with a Built-In Oxidizing Agent. *Chem. Mater.* **2022**, *34* (14), 6460−6467.
(181) Lee, W. S.; Enomoto, T.; Mizutani Akimoto, A.; Yoshida, R. Anisotropically Deforming Sandwich-Type Self-Oscillating Gels: A Hierarchical Model Platform of Cardiac Tissue. *Chem. Mater.* **2024**, *36* (4), 2007−2017.
(182) Li, G.; Cortes, W.; Zhang, Q.; Zhang, Y. Chemical Oscillation and Morphological Oscillation in Catalyst-Embedded Lyotropic Liquid Crystalline Gels. *Front Chem.* **2020**, *8*, 583165.
(183) Lee, W. S.; Enomoto, T.; Akimoto, A. M.; Yoshida, R. Capsule self-oscillating gels showing cell-like nonthermal membrane/shape fluctuations. *Mater. Horiz* **2023**, *10* (4), 1332−1341.
(184) Masuda, T.; Ueki, T.; Tamate, R.; Matsukawa, K.; Yoshida, R. Chemomechanical Motion of a Self-Oscillating Gel in a Protic Ionic Liquid. *Angew. Chem., Int. Ed. Engl.* **2018**, *57* (51), 16693−16697.
(185) Singh, N.; Lainer, B.; Formon, G. J. M.; De Piccoli, S.; Hermans, T. M. Re-programming Hydrogel Properties Using a Fuel-Driven Reaction Cycle. *J. Am. Chem. Soc.* **2020**, *142* (9), 4083−4087.
(186) Xu, H.; Bai, S. Y.; Gu, G. Y.; Gao, Y. L.; Sun, X.; Guo, X. H.; Xuan, F. Z.; Wang, Y. M. Bioinspired Self-Resettable Hydrogel Actuators Powered by a Chemical Fuel. *ACS Appl. Mater. Interfaces* **2022**, *14* (38), 43825−43832.
(187) Tena-Solsona, M.; Rieß, B.; Grötsch, R. K.; Löhrer, F. C.; Wanzke, C.; Käsdorf, B.; Bausch, A. R.; Müller-Buschbaum, P.; Lieleg, O.; Boekhoven, J. Non-equilibrium dissipative supramolecular materials with a tunable lifetime. *Nat. Commun.* **2017**, *8* (1), 15895.
(188) Sarkar, A.; Dúzs, B.; Walther, A. Fuel-Driven Enzymatic Reaction Networks to Program Autonomous Thiol/Disulfide Redox Systems. *J. Am. Chem. Soc.* **2024**, *146* (15), 10281−10285.
(189) Guo, K. L.; Sun, H.; Nan, M. M.; Sun, T. D.; Wang, G. T.; Liu, S. Q. An iodine-driven muscle-mimicking self-resetting bilayer hydrogel actuator. *Materials Horizons* **2025**, *12* (6), 1938−1943.
(190) Cheng, M.; Qian, C.; Ding, Y. H.; Chen, Y.; Xiao, T. X.; Lu, X. C.; Jiang, J. L.; Wang, L. Y. Writable and Self-Erasable Hydrogel Based on Dissipative Assembly Process from Multiple Carboxyl Tetraphenylethylene Derivative. *ACS Materials Letters* **2020**, *2* (4), 425−429.
(191) Heckel, J.; Loescher, S.; Mathers, R. T.; Walther, A. Chemically Fueled Volume Phase Transition of Polyacid Microgels. *Angew. Chem. Int. Edit* **2021**, *60* (13), 7117−7125.
(192) Hermans, T. M.; Singh, N. Chemically Fueled Autonomous Sol→Gel→Sol→Gel→Sol Transitions. *Angew. Chem. Int. Edit* **2023**, *62* (23), No. e202301529.
(193) Nakajima, N.; Ikada, Y. Mechanism of amide formation by carbodiimide for bioconjugation in aqueous media. *Bioconjugate Chem.* **1995**, *6* (1), 123−130.
(194) Kriebisch, C. M.; Bergmann, A. M.; Boekhoven, J. Fuel-driven dynamic combinatorial libraries. *J. Am. Chem. Soc.* **2021**, *143* (20), 7719−7725.
(195) Heckel, J.; Batti, F.; Mathers, R. T.; Walther, A. Spinodal decomposition of chemically fueled polymer solutions. *Soft Matter* **2021**, *17* (21), 5401−5409.
(196) Schnitter, F.; Bergmann, A. M.; Winkeljann, B.; Rodon Fores, J.; Lieleg, O.; Boekhoven, J. Synthesis and characterization of chemically fueled supramolecular materials driven by carbodiimide-based fuels. *Nat. Protoc.* **2021**, *16* (8), 3901−3932.
(197) Hossain, M. M.; Atkinson, J. L.; Hartley, C. S. Dissipative assembly of macrocycles comprising multiple transient bonds. *Angew. Chem., Int. Ed.* **2020**, *59* (33), 13807−13813.
(198) Kariyawasam, L. S.; Hartley, C. S. Dissipative assembly of aqueous carboxylic acid anhydrides fueled by carbodiimides. *J. Am. Chem. Soc.* **2017**, *139* (34), 11949−11955.
(199) Åslund, F.; Beckwith, J. Bridge over troubled waters:: Sensing stress by disulfide bond formation. *Cell* **1999**, *96* (6), 751−753.

https://doi.org/10.1021/acs.chemrev.5c00358
Chem. Rev. XXXX, XXX, XXX−XXX

(200) Cremers, C. M.; Jakob, U. Oxidant Sensing by Reversible Disulfide Bond Formation. *J. Biol. Chem.* **2013**, *288* (37), 26489−26496.
(201) Marcinkeviciene, J.; Blanchard, J. S. Catalytic Properties of Lipoamide Dehydrogenase fromMycobacterium smegmatis. *Archives of biochemistry and biophysics* **1997**, *340* (2), 168−176.
(202) Heuser, T.; Weyandt, E.; Walther, A. Biocatalytic Feedback-Driven Temporal Programming of Self-Regulating Peptide Hydrogels. *Angew. Chem., Int. Ed.* **2015**, *54* (45), 13258−13262.
(203) Mondal, S.; Podder, D.; Nandi, S. K.; Roy Chowdhury, S.; Haldar, D. Acid-responsive fibrillation and urease-assisted defibrillation of phenylalanine: a transient supramolecular hydrogel. *Soft Matter* **2020**, *16* (44), 10115−10121.
(204) Heuser, T.; Merindol, R.; Loescher, S.; Klaus, A.; Walther, A. Photonic Devices Out of Equilibrium: Transient Memory, Signal Propagation, and Sensing. *Adv. Mater.* **2017**, *29* (17), 1606842.
(205) Che, H.; Buddingh, B. C.; van Hest, J. C. M. Self-Regulated and Temporal Control of a "Breathing" Microgel Mediated by Enzymatic Reaction. *Angew. Chem., Int. Ed.* **2017**, *56* (41), 12581−12585.
(206) Zhang, Y.; Li, P.; Zhang, K.; Wang, X. Temporary Actuation of Bilayer Polymer Hydrogels Mediated by the Enzymatic Reaction. *Langmuir* **2022**, *38* (49), 15433−15441.
(207) Dúzs, B.; Skarsetz, O.; Fusi, G.; Lupfer, C.; Walther, A. Mechano-adaptive meta-gels through synergistic chemical and physical information-processing. *Nat. Commun.* **2024**, *15* (1), 8957.
(208) Heuser, T.; Steppert, A. K.; Lopez, C. M.; Zhu, B. L.; Walther, A. Generic Concept to Program the Time Domain of Self-Assemblies with a Self-Regulation Mechanism. *Nano Lett.* **2015**, *15* (4), 2213−2219.
(209) Panja, S.; Adams, D. J. Gel to gel transitions by dynamic self-assembly. *Chem. Commun.* **2019**, *55* (68), 10154−10157.
(210) Jee, E.; Bánsági, T.; Taylor, A. F.; Pojman, J. A. Temporal Control of Gelation and Polymerization Fronts Driven by an Autocatalytic Enzyme Reaction. *Angew. Chem. Int. Edit* **2016**, *55* (6), 2127−2131.
(211) Panja, S.; Fuentes-Caparrós, A. M.; Cross, E. R.; Cavalcanti, L.; Adams, D. J. Annealing Supramolecular Gels by a Reaction Relay. *Chem. Mater.* **2020**, *32* (12), 5264−5271.
(212) Zhong, Y. B.; Li, P. P.; Hao, J. C.; Wang, X. Bioinspired Self-Healing of Kinetically Inert Hydrogels Mediated by Chemical Nutrient Supply. *ACS Appl. Mater. Interfaces* **2020**, *12* (5), 6471−6478.
(213) Li, M.; Tian, G.; Jiang, X.; Qi, D.; Yang, B.; Li, Y. An Autonomously Liquefied Hydrogel Adhesive for Programmable Bioelectronic Interface. *Angew. Chem.* **2025**, *137*, No. e202503010.
(214) van den Akker, W. P.; van Benthem, R. A.; Voets, I. K.; van Hest, J. C. Dampened Transient Actuation of Hydrogels Autonomously Controlled by pH-Responsive Bicontinuous Nanospheres. *ACS Appl. Mater. Interfaces* **2024**, *16* (15), 19642−19650.
(215) Fan, X.; Walther, A. pH Feedback Lifecycles Programmed by Enzymatic Logic Gates Using Common Foods as Fuels. *Angew. Chem., Int. Ed.* **2021**, *60* (20), 11398−11405.
(216) Sharma, C.; Walther, A. Self-Regulating Colloidal Co-Assemblies That Accelerate Their Own Destruction via Chemo-Structural Feedback. *Angew. Chem., Int. Ed.* **2022**, *61* (19), No. e202201573.
(217) Dhanarajan, A. P.; Misra, G. P.; Siegel, R. A. Autonomous chemomechanical oscillations in a hydrogel/enzyme system driven by glucose. *J. Phys. Chem. A* **2002**, *106* (38), 8835−8838.
(218) Bell, D. J.; Felder, D.; von Westarp, W. G.; Wessling, M. Towards synergistic oscillations in enzymatically active hydrogel spheres. *Soft Matter* **2021**, *17* (3), 592−599.
(219) Sharma, C.; Maity, I.; Walther, A. pH-feedback systems to program autonomous self-assembly and material lifecycles. *Chem. Commun.* **2023**, *59* (9), 1125−1144.
(220) Cheng, E.; Xing, Y.; Chen, P.; Yang, Y.; Sun, Y.; Zhou, D.; Xu, L.; Fan, Q.; Liu, D. A pH-triggered, fast-responding DNA hydrogel. *Angew. Chem., Int. Ed.* **2009**, *48* (41), 7660−7663.
(221) Tang, C.; Ulijn, R. V.; Saiani, A. Effect of glycine substitution on Fmoc-diphenylalanine self-assembly and gelation properties. *Langmuir* **2011**, *27* (23), 14438−14449.
(222) Kim, E.; Kang, C.; Baek, H.; Hwang, K.; Kwak, D.; Lee, E.; Kang, Y.; Thomas, E. L. Control of optical hysteresis in block copolymer photonic gels: a step towards wet photonic memory films. *Adv. Funct. Mater.* **2010**, *20* (11), 1728−1732.
(223) Fusi, G.; Del Giudice, D.; Skarsetz, O.; Di Stefano, S.; Walther, A. Autonomous Soft Robots Empowered by Chemical Reaction Networks. *Adv. Mater.* **2023**, *35* (7), 2209870.
(224) Li, J.; Wang, L.; Pan, C.; Yang, B.; Li, Y. Transient Biomacromolecular Nanoparticles for Labels with Self-Erasable and Rewritable Ability. *ChemSystemsChem.* **2023**, *5* (4), No. e202200036.
(225) Lu, H.; Hao, J.; Wang, X. Host-fueled transient supramolecular hydrogels. *ChemSystemsChem.* **2022**, *4* (3), No. e202100050.
(226) Nakamoto, M.; Kitano, S.; Matsusaki, M. Biomacromolecule-Fueled Transient Volume Phase Transition of a Hydrogel. *Angew. Chem., Int. Ed.* **2022**, *61* (33), No. e202205125.
(227) Liyana Gunawardana, V. W.; Finnegan, T. J.; Ward, C. E.; Moore, C. E.; Badjić, J. D. Dissipative Formation of Covalent Basket Cages. *Angew. Chem., Int. Ed.* **2022**, *61* (33), No. e202207418.
(228) Lomakina, G. Y.; Konik, P.; Ugarova, N. The Kinetics of Hydrolysis of ATP by Apyrase A from Solanum tuberosum. *Moscow University Chemistry Bulletin* **2020**, *75*, 374−381.
(229) Sundarram, A.; Murthy, T. P. K. α-amylase production and applications: a review. *Journal of Applied & Environmental Microbiology* **2014**, *2* (4), 166−175.
(230) Waley, S. G.; Watson, J. The action of trypsin on polylysine. *Biochem. J.* **1953**, *55* (2), 328.
(231) Li, J.; Ni, X.; Zhou, Z.; Leong, K. W. Preparation and characterization of polypseudorotaxanes based on block-selected inclusion complexation between poly (propylene oxide)-poly (ethylene oxide)-poly (propylene oxide) triblock copolymers and α-cyclodextrin. *J. Am. Chem. Soc.* **2003**, *125* (7), 1788−1795.
(232) Li, J. X.; Yan, C. H.; Wang, H. C.; Lu, E. R.; Wang, Y. M.; Guo, X. H.; Wang, J. Smart Hydrogels Bearing Transient Gel-Sol-Gel Transition Behavior Driven by a Biocompatible Chemical Fuel. *ACS Applied Polymer Materials* **2023**, *5* (1), 1067−1074.
(233) Li, L.; Guo, X.; Fu, L.; Prud'homme, R. K.; Lincoln, S. F. Complexation Behavior of α-, β-, and γ-Cyclodextrin in Modulating and Constructing Polymer Networks. *Langmuir* **2008**, *24* (15), 8290−8296.
(234) Jiang, L.; Yan, Y.; Drechsler, M.; Huang, J. Enzyme-triggered model self-assembly in surfactant-cyclodextrin systems. *Chem. Commun.* **2012**, *48* (59), 7347−7349.
(235) Wang, Q.; Zhang, Q.; Zhang, Q.-W.; Li, X.; Zhao, C.-X.; Xu, T.-Y.; Qu, D.-H.; Tian, H. Color-tunable single-fluorophore supramolecular system with assembly-encoded emission. *Nat. Commun.* **2020**, *11* (1), 158.
(236) Wang, J.; Li, L.; Guo, X.; Zheng, L.; Pham, D.-T.; Lincoln, S. F.; Ngo, H. T.; Clements, P.; May, B. L.; Prud'homme, R. K.; et al. Aggregation of hydrophobic substituents of poly (acrylate) s and their competitive complexation by β-and γ-cyclodextrins and their linked dimers in aqueous solution. *Industrial & engineering chemistry research* **2011**, *50* (12), 7566−7571.
(237) Hao, Q.; Kang, Y.; Xu, J.-F.; Zhang, X. Fluorescence "Turn-On" Enzyme-Responsive Supra-Amphiphile Fabricated by Host-Guest Recognition between γ-Cyclodextrin and a Tetraphenylethylene-Sodium Glycyrrhetinate Conjugate. *Langmuir* **2021**, *37* (19), 6062−6068.
(238) Heinen, L.; Heuser, T.; Steinschulte, A.; Walther, A. Antagonistic Enzymes in a Biocatalytic pH Feedback System Program Autonomous DNA Hydrogel Life Cycles. *Nano Lett.* **2017**, *17* (8), 4989−4995.
(239) Bashir, N.; Leathard, A. S.; McHugh, M.; Hoffman, I.; Shaon, F.; Belgodere, J. A.; Taylor, A. F.; Pojman, J. A. On the use of modelling antagonistic enzymes to aid in temporal programming of

https://doi.org/10.1021/acs.chemrev.5c00358
Chem. Rev. XXXX, XXX, XXX−XXX

pH and PVA-borate gelation. *Molecular Systems Design & Engineering* **2024**, *9* (4), 372−381.
(240) Fan, X.; Walther, A. Autonomous Transient pH Flips Shaped by Layered Compartmentalization of Antagonistic Enzymatic Reactions. *Angew. Chem., Int. Ed.* **2021**, *60* (7), 3619−3624.
(241) Guo, K.; Yang, X.; Zhou, C.; Li, C. Self-regulated reversal deformation and locomotion of structurally homogenous hydrogels subjected to constant light illumination. *Nat. Commun.* **2024**, *15* (1), 1694.
(242) Heinen, L.; Walther, A. Temporal control of i-motif switch lifetimes for autonomous operation of transient DNA nanostructures. *Chem. Sci.* **2017**, *8* (5), 4100−4107.
(243) Li, C.; Iscen, A.; Palmer, L. C.; Schatz, G. C.; Stupp, S. I. Light-Driven Expansion of Spiropyran Hydrogels. *J. Am. Chem. Soc.* **2020**, *142* (18), 8447−8453.
(244) Kortekaas, L.; Browne, W. R. The evolution of spiropyran: fundamentals and progress of an extraordinarily versatile photochrome. *Chem. Soc. Rev.* **2019**, *48* (12), 3406−3424.
(245) Masuda, T.; Ueki, T.; Tamate, R.; Matsukawa, K.; Yoshida, R. Chemomechanical Motion of a Self-Oscillating Gel in a Protic Ionic Liquid. *Angew. Chem.* **2018**, *130* (51), 16935−16939.
(246) Ueki, T.; Watanabe, M.; Yoshida, R. Belousov-Zhabotinsky reaction in protic ionic liquids. *Angew. Chem., Int. Ed.* **2012**, *51* (48), 11991−11994.
(247) Lawson, H. S.; Holló, G.; Német, N.; Teraji, S.; Nakanishi, H.; Horvath, R.; Lagzi, I. Design of non-autonomous pH oscillators and the existence of chemical beat phenomenon in a neutralization reaction. *Sci. Rep.* **2021**, *11* (1), 11011.
(248) Yang, Y.; Li, C.; Palmer, L. C.; Stupp, S. I. Autonomous hydrogel locomotion regulated by light and electric fields. *Science Advances* **2023**, *9* (31), No. eadi4566.
(249) Lee, E.; Kim, Y. S.; Akimoto, A. M.; Yoshida, R. Reversible and directional control of chemical wave propagation in a hydrogel by magnetic migration through liquid interfaces. *Chem. Mater.* **2018**, *30* (17), 5841−5845.
(250) Patwal, P.; Mann, S.; Kumar, B. P. Chemomechanical Self-Oscillatory Microgel Motility in Stratified Chemical Media. *Adv. Mater.* **2025**, *37* (6), 2415568.
(251) Zhu, Q. L.; Du, C.; Dai, Y.; Daab, M.; Matejdes, M.; Breu, J.; Hong, W.; Zheng, Q.; Wu, Z. L. Light-steered locomotion of muscle-like hydrogel by self-coordinated shape change and friction modulation. *Nat. Commun.* **2020**, *11* (1), 5166.
(252) Hu, Z.; Li, Y.; Lv, J.-a. Phototunable self-oscillating system driven by a self-winding fiber actuator. *Nat. Commun.* **2021**, *12* (1), 3211.
(253) Kim, Y.; van den Berg, J.; Crosby, A. J. Autonomous snapping and jumping polymer gels. *Nat. Mater.* **2021**, *20* (12), 1695−1701.
(254) Stano, G.; Percoco, G. Additive manufacturing aimed to soft robots fabrication: A review. *Extreme Mechanics Letters* **2021**, *42*, 101079.
(255) Zhang, S.; Ke, X.; Jiang, Q.; Chai, Z.; Wu, Z.; Ding, H. Fabrication and functionality integration technologies for small-scale soft robots. *Adv. Mater.* **2022**, *34* (52), 2200671.
(256) Taylor, D. L.; in het Panhuis, M. Self-healing hydrogels. *Adv. Mater.* **2016**, *28* (41), 9060−9093.
(257) Dayal, P.; Kuksenok, O.; Balazs, A. C. Reconfigurable assemblies of active, autochemotactic gels. *P Natl. Acad. Sci. USA* **2013**, *110* (2), 431−436.
(258) Toiya, M.; González-Ochoa, H. O.; Vanag, V. K.; Fraden, S.; Epstein, I. R. Synchronization of Chemical Micro-oscillators. *J. Phys. Chem. Lett.* **2010**, *1* (8), 1241−1246.
(259) Tateyama, S.; Shibuta, Y.; Yoshida, R. Direction control of chemical wave propagation in self-oscillating gel array. *J. Phys. Chem. B* **2008**, *112* (6), 1777−1782.
(260) Kuksenok, O.; Dayal, P.; Bhattacharya, A.; Yashin, V. V.; Deb, D.; Chen, I. C.; Van Vliet, K. J.; Balazs, A. C. Chemo-responsive, self-oscillating gels that undergo biomimetic communication. *Chem. Soc. Rev.* **2013**, *42* (17), 7257−7277.
(261) Agladze, K.; Aliev, R. R.; Yamaguchi, T.; Yoshikawa, K. Chemical diode. *J. Phys. Chem-Us* **1996**, *100* (33), 13895−13897.
(262) Chen, I. C.; Kuksenok, O.; Yashin, V. V.; Balazs, A. C.; Van Vliet, K. J. Mechanical Resuscitation of Chemical Oscillations in Belousov-Zhabotinsky Gels. *Adv. Funct. Mater.* **2012**, *22* (12), 2535−2541.
(263) Lakie, M.; Vernooij, C. A.; Osborne, T. M.; Reynolds, R. F. The resonant component of human physiological hand tremor is altered by slow voluntary movements. *Journal of physiology* **2012**, *590* (10), 2471−2483.
(264) Rahman, S.; Robertson, D. A. Radar micro-Doppler signatures of drones and birds at K-band and W-band. *Sci. Rep.* **2018**, *8* (1), 17396.
(265) Warrick, D.; Hedrick, T.; Fernández, M. J.; Tobalske, B.; Biewener, A. Hummingbird flight. *Curr. Biol.* **2012**, *22* (12), R472−R477.
(266) Fache, S.; Dalous, J.; Engelund, M.; Hansen, C.; Chamaraux, F.; Fourcade, B.; Satre, M.; Devreotes, P.; Bruckert, F. Calcium mobilization stimulates Dictyostelium discoideum shear-flow-induced cell motility. *Journal of Cell Science* **2005**, *118* (15), 3445−3458.
(267) Sugi, H.; Iwamoto, H.; Akimoto, T.; Ushitani, H. Evidence for the load-dependent mechanical efficiency of individual myosin heads in skeletal muscle fibers activated by laser flash photolysis of caged calcium in the presence of a limited amount of ATP. *Proc. Natl. Acad. Sci. U. S. A.* **1998**, *95* (5), 2273−2278.
(268) Chen, J.; Ahn, T.; Colón-Bernal, I. D.; Kim, J.; Banaszak Holl, M. M. The relationship of collagen structural and compositional heterogeneity to tissue mechanical properties: a chemical perspective. *ACS Nano* **2017**, *11* (11), 10665−10671.
(269) Rouse, J. G.; Van Dyke, M. E. A Review of Keratin-Based Biomaterials for Biomedical Applications. *Materials* **2010**, *3* (2), 999−1014.
(270) Shibayama, M.; Li, X.; Sakai, T. Precision polymer network science with tetra-PEG gels—a decade history and future. *Colloid Polym. Sci.* **2019**, *297*, 1−12.
(271) Lee, S. J.; Kim, H.; Ahn, S. Water transport in porous hydrogel structures analogous to leaf mesophyll cells. *Microfluid. Nanofluid.* **2015**, *18* (5), 775−784.
(272) Saranathan, V.; Forster, J. D.; Noh, H.; Liew, S.-F.; Mochrie, S. G.; Cao, H.; Dufresne, E. R.; Prum, R. O. Structure and optical function of amorphous photonic nanostructures from avian feather barbs: a comparative small angle X-ray scattering (SAXS) analysis of 230 bird species. *Journal of The Royal Society Interface* **2012**, *9* (75), 2563−2580.
(273) Alsaid, Y.; Wu, S.; Wu, D.; Du, Y.; Shi, L.; Khodambashi, R.; Rico, R.; Hua, M.; Yan, Y.; Zhao, Y.; et al. Tunable sponge-like hierarchically porous hydrogels with simultaneously enhanced diffusivity and mechanical properties. *Adv. Mater.* **2021**, *33* (20), 2008235.
(274) Armon, S.; Efrati, E.; Kupferman, R.; Sharon, E. Geometry and mechanics in the opening of chiral seed pods. *Science* **2011**, *333* (6050), 1726−1730.
(275) Smyth, D. R. Helical growth in plant organs: mechanisms and significance. *Development* **2016**, *143* (18), 3272−3282.
(276) Tahara, H.; Takabe, K.; Sasaki, Y.; Kasuga, K.; Kawamoto, A.; Koizumi, N.; Nakamura, S. The mechanism of two-phase motility in the spirochete Leptospira: Swimming and crawling. *Science Advances* **2018**, *4* (5), No. eaar7975.
(277) Misra, G.; Dickinson, R. B.; Ladd, A. J. Mechanics of Vorticella contraction. *Biophysical Journal* **2010**, *98* (12), 2923−2932.
(278) Zhang, H.; Mourran, A.; Möller, M. Dynamic switching of helical microgel ribbons. *Nano Lett.* **2017**, *17* (3), 2010−2014.
(279) Mourran, A.; Zhang, H.; Vinokur, R.; Möller, M. Soft microrobots employing nonequilibrium actuation via plasmonic heating. *Adv. Mater.* **2017**, *29* (2), 1604825.
(280) Shin, B.; Ha, J.; Lee, M.; Park, K.; Park, G. H.; Choi, T. H.; Cho, K.-J.; Kim, H.-Y. Hygrobot: A self-locomotive ratcheted actuator powered by environmental humidity. *Science Robotics* **2018**, *3* (14), No. eaar2629.

https://doi.org/10.1021/acs.chemrev.5c00358
Chem. Rev. XXXX, XXX, XXX−XXX